QUANTITATIVE MEASUREMENT OF NONLINEAR WAVE INTERACTIONS CHARACTERIZING THE TRANSITION OF A PLANAR TURBULENT JET

By

HUAN-CHANG CHU

Bachelor of Science in Mechanical Engineering

Chung Yuan Christian University

The Republic of China

1982

Submitted to the Faculty of the Graduate College
of the Oklahoma State University
in partial fulfillment of the requirements
for the Degree of
MASTER OF SCIENCE
December, 1987

QUANTITATIVE MEASUREMENT OF NONLINEAR WAVE INTERACTIONS CHARACTERIZING THE TRANSITION OF A PLANAR TURBULENT JET

Thesis Approved:

Elmer O. Thorna
Thesis Adviser

A. J. Ghajar

Ronald L. Daugherty

Norman N. Durham
Dean of the Graduate College

PREFACE

I would like to take this opportunity to express my deep appreciation to my adviser, Dr. F. O. Thomas, for his patience, guidance and the invaluable help he has given me during my time at Oklahoma State University. I also thank him for helping me to analyze the experimental data and in writing the thesis irrespective of time and place. Further, I thank him for helping me to get the teaching and research assistantships which helped me in my studies to a great extent. Also, I am deeply indebted to my friend, Mrs. Lynn Creager, for her timely assitance in this work and to Mrs. Daleene Caldwell for typing and correcting the final draft of my thesis.

Finally, I will express my special gratitude to my parents, Mr. and Mrs. Chu, and my brother and sisters for their encouragement and moral support which made all this possible in my academic career at Oklahoma State University.

TABLE OF CONTENTS

LIST OF TABLES

LIST OF FIGURES

NOMENCLATURE

A	constant in Eq. 2.1
a_o	amplitude of model signals
$A_1(t)$	modeled anemometer signal
$A_2(t)$	modeled anemometer signal
B	constant in Eq. 2.1
$B[i,j]$	bicoherence spectrum
b	mean velocity half-width
$b[i,j]$	the normalized version of bicoherence spectrum
C_1	virtual origin based on mean flow widening
C_2	virtual origin based on mean velocity decay
C_{xy}	coincident spectral density function
D	nozzle slot width
E	mean voltage of anemometer
$E[\ ]$	an expected (or mean) value
f_c	jet column mode (Passage frequency of vortical structures near end of potential core)
f_e	acoustic excitation frequency
f_i, f_j, f_k	frequencies
f_N	Nyquist frequency
G_{xy}	cross-spectral density function
K_1	jet widening rate
K_2	mean velocity decay rate

$n(t)$	a small amplitude random noise
P_x	power spectral density function of signal x(t)
P_y	power spectral density function of signal y(t)
Q_{xy}	quadrature spectral density function
Re_D	Reynolds number based on nozzle exit
t	time variable
T	total time period
U	mean longitudinal velocity
U_m	local mean centerline velocity
U_o	nozzle exit mean velocity
x	longitudinal spatial coordinate
$x(t)$	a stationary time series
y	lateral spatial coordinate
z	vertical spatial coordinate
θ	momentum thickness of free shear layer
ϕ	phase shift of the low frequency mode
θ_{xy}	phase angle spectrum between two signals
γ^2_{xy}	spectral coherence function
Δf	a narrow frequency interval
$*$	complex conjugate
$\omega_{1...6}$	angular frequencies

CHAPTER I

INTRODUCTION

The work to be reported involves quantitative measurement of the nonlinear interactions which characterize the transition of the planar turbulent jet. Particular emphasis is placed upon understanding the detailed dynamics of a global reasonance mechanism which operates in the jet. A review of literature dealing with both global resonance effects in free shear flows and quantitative measurements of nonlinear wave interactions follows.

1.1 Global Resonance Effects in Free Shear Flows

The existence of a global resonance mechanism in free shear flows was first demonstrated experimentally by Ho and Nossier (1981) in an axisymmetric jet impinging on a flat plate placed normal to the mean flow direction. They noted that for proper separation between nozzle exit and plate, a strong resonance developed in the flow. This resonance took the form of upstream propagating pressure disturbances related to the impingement of coherent structures on the plate. These pressure perturbations excited the nascent jet shear layer and modified its development to complete the feedback loop. As a natural extension of this work, Laufer (1981) questioned whether a similar resonance mechanism occurs in free jets as well. Preliminary evidence of resonance effects in the axisymmetric jet was found by Laufer and

Monkewitz (1980) and Monkewitz (1983). These studies found that velocity fluctuations near the nozzle exit are modulated and that the frequency of modulation corresponds to the passage frequency of structures near the end of the potential core (i.e. the jet column mode). Monkewitz (1983) found that the amplitude modulation is due to a modulation of the receptivity of the nascent shear layer.

Ho and Huang (1982) indicate that both the local shear layer instability and the requirements for global resonance play important roles in determining the dynamics of the planar mixing layer. Furthermore, the requirements for global resonance essentially determine the location of vortex pairing events which have been shown by Winant and Browand (1974) to be responsible for mixing layer growth. Earlier related work by Dimotakis and Brown (1976) indicated that the mixing layer dynamics at any streamwise location is coupled to flow structures farther downstream. Aspects of the effects of global resonance on the dynamic mechanisms involved in the development of the mixing layer are concisely reviewed by Ho (1982).

Thomas and Goldschmidt (1985) found preliminary evidence that global resonance effects play an important role in the development of planar turbulent jets. More recently, experimental data for the transition of an unexcited two-dimensional jet at moderate Reynolds number obtained by Thomas and Prakash (1986) showed in detail the effect which global resonance plays in the initial jet development. This study showed that the initial jet shear layer roll-up location and frequency as well as subsequent merging locations could be predicted from a simple analytical model of global resonance requirements. The transition of the planar jet was thus found to be governed by both the initial thin

shear layer instability and the requirements for global resonance. The global resonance was found to take the form of near exit perturbations which are each related to subsequent downstream vortex interaction events. Particularly important was the first large-scale structural interaction event beyond the jet potential core involving large-scale vorticity of opposite sign.

1.2 Quantitative Measurement of Nonlinear Interactions in Free Shear Layer Flow

A review of the works described above will indicate that of central concern in each are the inherently nonlinear dynamic processes involved. In spite of this, none of the above studies has made an attempt to quantify the relevant nonlinear interactions involved. This is despite the fact that digital signal processing techniques are now readily available which allow quantitative information regarding aspects of nonlinear transition to be obtained. In this section a brief review of these techniques is now presented.

1.2.1 Bispectral Analysis

One of the important characteristics in the transition of free shear layers is the continual redistribution of energy among both existing and newly created spectral modes. Experiments by Sato (1970) and Sato and Saito (1975) in the plane wake indicated that transition is characterized by the formation of modes at sum and difference frequencies which result from nonlinear interactions between the dominant instability modes. The authors also noted the importance of low frequency amplitude modulation of the primary instability waves which

results from the nonlinear formation of modulating difference modes. Detailed power spectral measurements were used by Miksad (1972,1973) to qualitatively study the transition of the planar mixing layer. Similar techniques were employed by Thomas and Goldschmidt (1986) in the developing shear layers of the planar turbulent jet. These studies showed that nonlinear interactions between the dominant instability modes will generate the sum and difference frequencies, harmonics and subharmonics that characterize the shear layer transition process. However, as noted by Kim and Powers (1979), linear spectral analysis techniques are of limited value when various spectral components interact with one another due to some nonlinear process. In such cases, power spectra are not able to differentiate between modes that arise due to nonlinear interactions and those due to spontaneously excited instabilities.

In order to distinguish between nonlinear coupled waves and linear independent waves, a higher order spectrum is required. Kim and Powers (1979) and Kim et al (1980) describe in detail the third order spectrum known as the bispectrum, which is a cube spectral density function. A nonzero bispectrum is indicative of nonlinear interactions between instability waves.

Consider a stationary time series x(t) with zero mean whose Fourier representation may be written as

$$x(t) = \sum_{k=-\infty}^{\infty} X_k \, e^{-i\omega_k t} \tag{1.1a}$$

$$X_k = \lim_{T\to\infty} \frac{1}{T} \int_{-\frac{T}{2}}^{\frac{T}{2}} x(t) \, e^{i\omega_k t} \, dt \tag{1.1b}$$

where $\omega_k = 2\pi k\ \Delta f$, Δf is the frequency resolution and T is the total record length of x(t). The power spectrum may be written as

$$P(k) = E[X_k X_k^*] \tag{1.2}$$

where E denotes an expected (or mean value), and the superscript denotes * the complex conjugate. In a similar manner the bispectrum is defined as

$$B(i,j) = E[X_i X_j X^*_{i+j}] \tag{1.3}$$

The bicoherence spectrum is the normalized version of the bispectrum and will be defined for this study as in Kim and Powers (1979),

$$b^2(i,j) = \frac{|B(i,j)|^2}{E[|X_i X_j|^2]E[|X_{i+j}|^2]} \tag{1.4}$$

where B and P are the bispectrum and power spectrum, respectively, and i and j are integers representing the frequencies $f_i = (i-1)\Delta f$ and $f_j = (j-1)\Delta f$. The bicoherence essentially measures the phase coherence among a wave triad. The value of the bicoherence is expected to lie between zero and unity. For example, a value of the bicoherence spectrum near unity indicates that the wave at frequency $f_k = f_i + f_j$ is excited by nonlinear wave coupling (i.e. interaction between the waves at f_i and f_j). A value near zero implies an absence of phase coherence between the waves, indicating that even though the wave at f_k may satisfy the resonant condition $f_k = f_i + f_j$, the fluctuation at f_k is not related to those at f_i and f_j.

The bispectrum has been applied in a variety of studies; Van Atta and Yeh (1973) and Lii et al (1976) utilized bispectral analysis techniques to investigate nonlinear energy transfer mechanisms in turbulent flow. Miksad et al (1982) used the bispectrum to study the influence of acoustic excitation on the transition of the two-dimensional wake. Miksad et al (1982) show that both amplitude and phase modulation play important roles in the transition process, with the dominant amplitude and phase modulation frequencies produced by the nonlinear difference interaction between two artificially excited instabilities. Recently, an investigation of the natural transition of the two-dimensional wake was performed using bispectral techniques by Miksad et al (1983) which provided quantitative information regarding the nonlinear dynamics involved. This work clearly showed the importance of difference interactions in producing the continuous array of sideband fluctuations whose subsequent nonlinear interactions are largely responsible for the spectral broadening that characterizes the transition to turbulence. Solis et al (1986) investigated the influence of mean flow unsteadiness on the laminar-turbulent transition by application of bicoherence techniques. The mean flow unsteadiness was found to induce amplitude and phase modulations which act to accelerate the redistribution of spectral energy as the flow evolves. Knisely and Rockwell (1982) investigated the instabilities which characterize an impinging cavity shear layer. Bicoherence measurements revealed the interaction of low-frequency modes with the fundamental. These were found to result in either amplification of the interacting low-frequency mode or the creation of a related subharmonic.

The experimental work reviewed above indicates that the digital

bispectral analysis technique is a higher order diagnostic tool which can be quite powerful for investigating nonlinear wave-wave interactions characterizing transition. The emphasis of this thesis is the application of this technique to study the transition of the planar turbulent jet.

CHAPTER II

FLOWFIELD AND MEASUREMENT APPARATUS

2.1 The Planar Turbulent Jet

A schematic of the two-dimensional turbulent jet flow field is shown in Figure 1. Fluid discharges at velocity U_o from a two-dimensional slot of width "D" into a quiescent environment. The resulting flow field can be divided into three principal regions: the initial region, the interaction region, and the similarity region. In the initial region two thin, nominally self-preserving free shear layers develop from each nozzle lip and bound a core of irrotational fluid known as the "potential core". The two shear layers widen with downstream distance to eventually engulf the potential core at approximately x/D = 5. The actual length of the potential core depends on initial conditions and will typically vary somewhat for different flow field facilities. Values quoted here are designed to give the reader an idea of the approximate location of the different regions and are to a certain extent quite subjective. Beyond x/D = 5 the two shear layers merge and are forced to interact to eventually reach a state of dynamic equilibrium. This "interaction region" extends from approximately x/D = 5 to x/D = 11. For streamwise locations greater than x/D = 11, the flow exhibits self-similar behavior such that mean velocity profiles at various streamwise locations will collapse to a

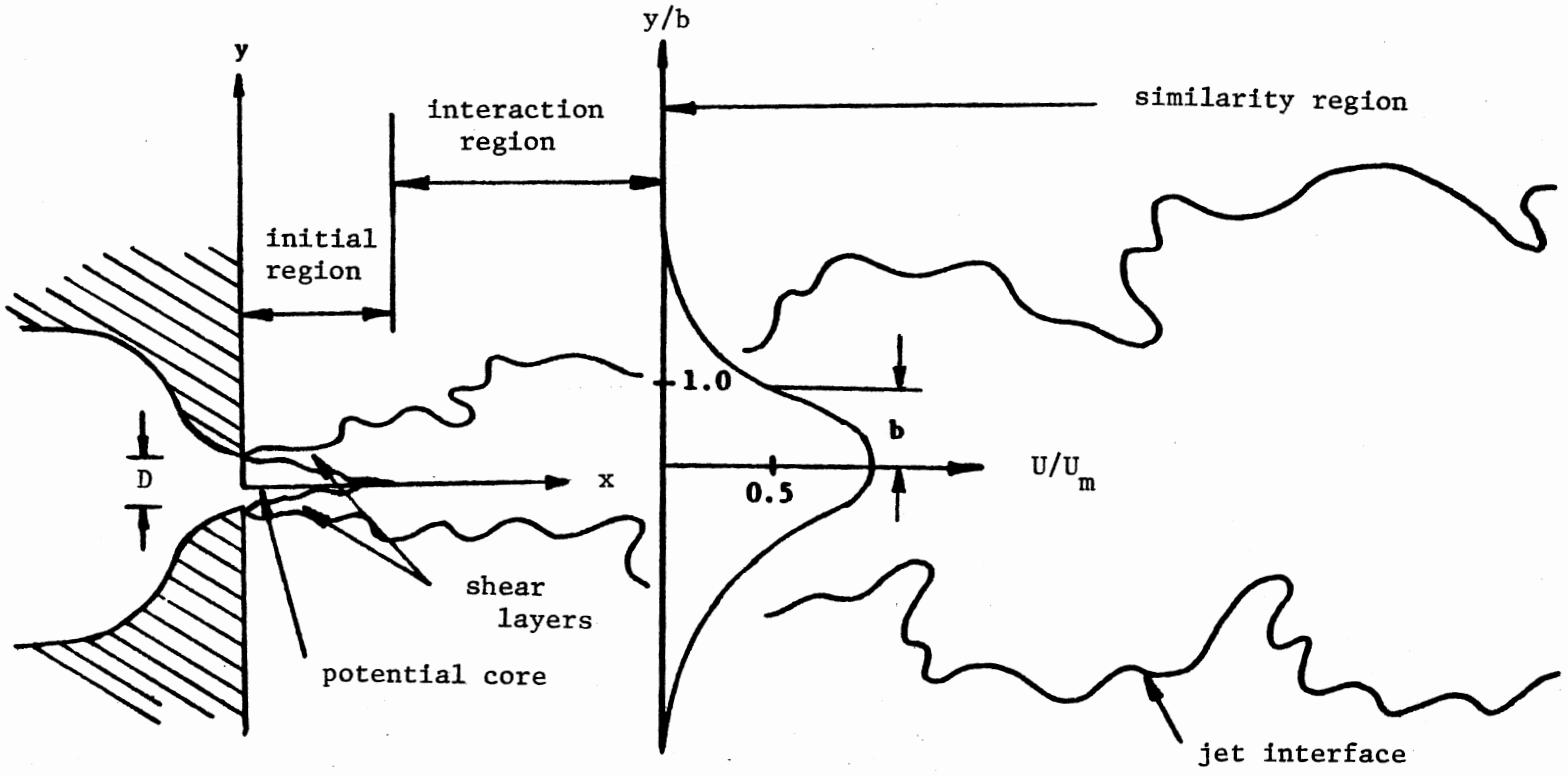

Figure 1. Two-dimensional Turbulent Jet

single profile shape when normalized by the proper local velocity and length scales. The proper velocity scale is the local mean centerline velocity, U_m, and the length scale is the mean velocity half-width, b. This is the lateral distance "y" required for the local mean velocity to drop to one half its centerline value. Profiles of turbulence quantities also show self-preserving characteristics but typically require larger downstream distances to develop this behavior. In the similarity region the jet widens in a linear fashion given by

$$b/D = k_1(x/D - C_1) \tag{2.1}$$

where $K_1 = d(b/D)/d(x/D)$ = the non-dimensional widening rate and C_1 = the virtual origin based on mean flow widening. The mean velocity decay is given by

$$(U_m/U_o)^{-2} = K_2(x/D - C_2) \tag{2.2}$$

where $K_2 = d((U_m/U_o)^{-2})/d(x/D)$ = the non-dimensional velocity decay rate and C_2 = is a virtual origin based on mean velocity decay. Near the exit the centerline velocity remains essentially constant until the developing jet shear layers engulf the potential core, after which a gradual approach to the self-similar form is noted.

Many experimental investigations have considered the planar jet flow field and a substantial body of experimental data is available which defines the basic characteristics of the this flow; some examples are: Everitt and Robins (1978), Gutmark and Wygnanski (1976), and Bradbury (1965).

2.2 Flow Field Facility and Related Measurement Apparatus

A schematic of the experimental flow field facility used for this study is shown in Figure 2. A three-stage centrifugal blower initiates the air flow through the system. It is powered by a 3 HP variable speed transmission motor. A large cubic plenum chamber with dimensions of 4 feet on each side is used for flow settling. The blower and plenum are connected by means of a flexible rubber duct which prevents motor vibration from being transmitted to the flow field. A 5 inch thick slab of fiberglass insulation material contained within the plenum is used both to filter the air and decouple the air stream from any blower pulsation. A rectangular duct which is 2.5 feet in length, 1.5 feet in height, and 8 inches in width connects the plenum chamber to the nozzle assembly. The duct contains a section of flow straighteners and three turbulence reducing screens which provide a clean inlet flow to the nozzle assembly. The two-dimensional nozzle has a contraction ratio of 16:1 and ends in a slot that is 0.5 inches in width and 18 inches in height. The nozzle contour is based on a design by Jordinson (1961).

The air discharges from the nozzle exit into the flow field which is formed by two 5 ft. by 7 ft. horizontal plywood confining plates parallel to each other and separated by an 18 inch air gap. These plates were required in order to keep the base flow two-dimensional in nature. The inner surfaces of the plywood were sanded and waxed to create a smooth surface. Twin stainless steel face plates are contained in the nozzle exit plane and extend laterally to the edge of the flow field. These plates merged smoothly to the nozzle assembly. All other sides of the jet flow field remained open. The entire set-up was

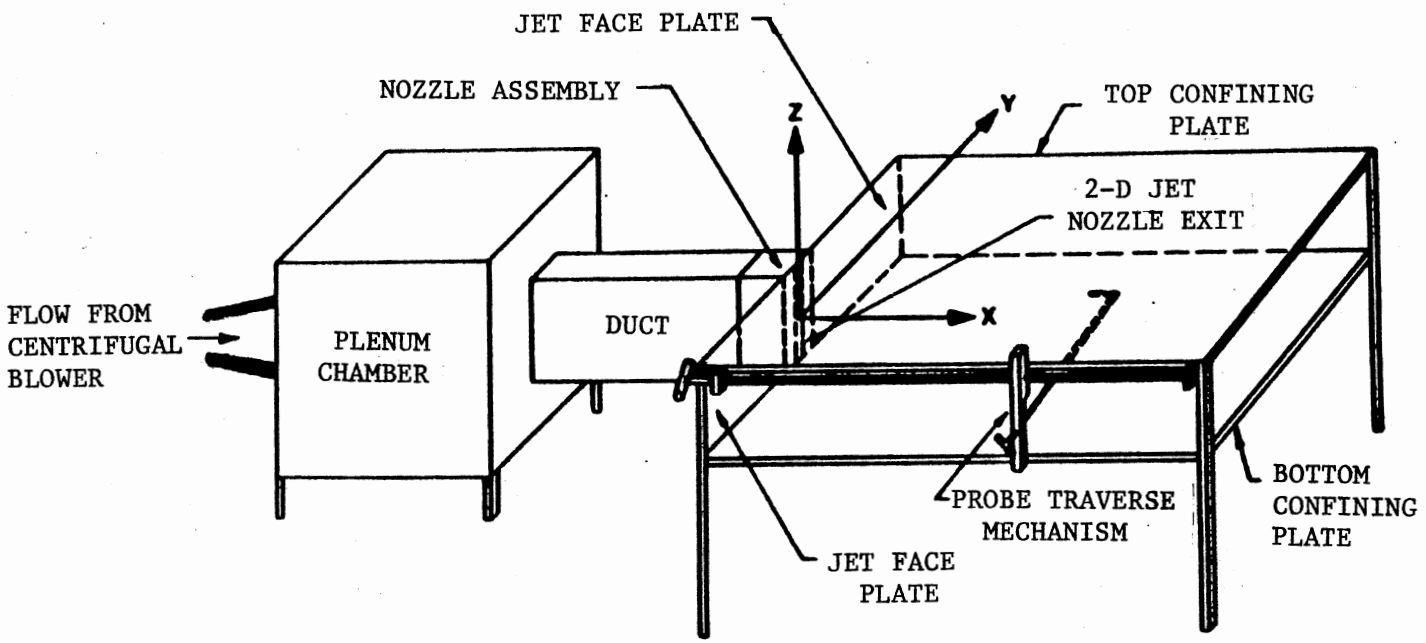

Figure 2. Schematic of Experimental Arrangement

supported by a sturdy angle-iron frame to which a precision probe supporting mechanism is mounted which allows probe positioning in three dimensions accurate to 0.03 inch. An optional micrometer assembly allowed for lateral probe positioning accurate to 0.001 inch.

A pitot static probe is mounted in the nozzle exit plane near the top plywood plate in order to monitor the jet exit velocity. The resolution of the pressure reading was 0.01 inch of water.

In order to introduce controlled sinusoidal perturbations into the flow acoustic excitation was used. The sound was generated by a loudspeaker mounted in the rectangular duct upstream from the nozzle assembly. The loudspeaker was sinusoidally driven by an audio-oscillator with the frequency monitored by a digital frequency counter. The rms amplitude of the excitation was monitored by a digital true rms voltmeter. The excitation amplitude was set at a low level; on the order of naturally occurring background disturbance modes. Subsquent disturbance amplification was provided by the jet shear layer instability mechanism. This aspect is addressed further in Chapter 3.

All measurements to be reported involved digital data acquisition with on-line processing of hot-wire anemometer signals and for this purpose DISA 56C01 anemometers operated in the constant temperature mode were used in conjunction with DISA 56C17 CTA bridges. Figure 3. shows the principal components of the data acquisition system. For measurements of the instantaneous longitudinal fluctuating component, DISA 55P01 straight wire probes were used. An operating temperature of 220 °C was selected which corresponds to an overheat ratio of approximately 1.6. The analog signals from the probes were passed through anti-alias filters and were digitized with an HP-98640A A/D board. The

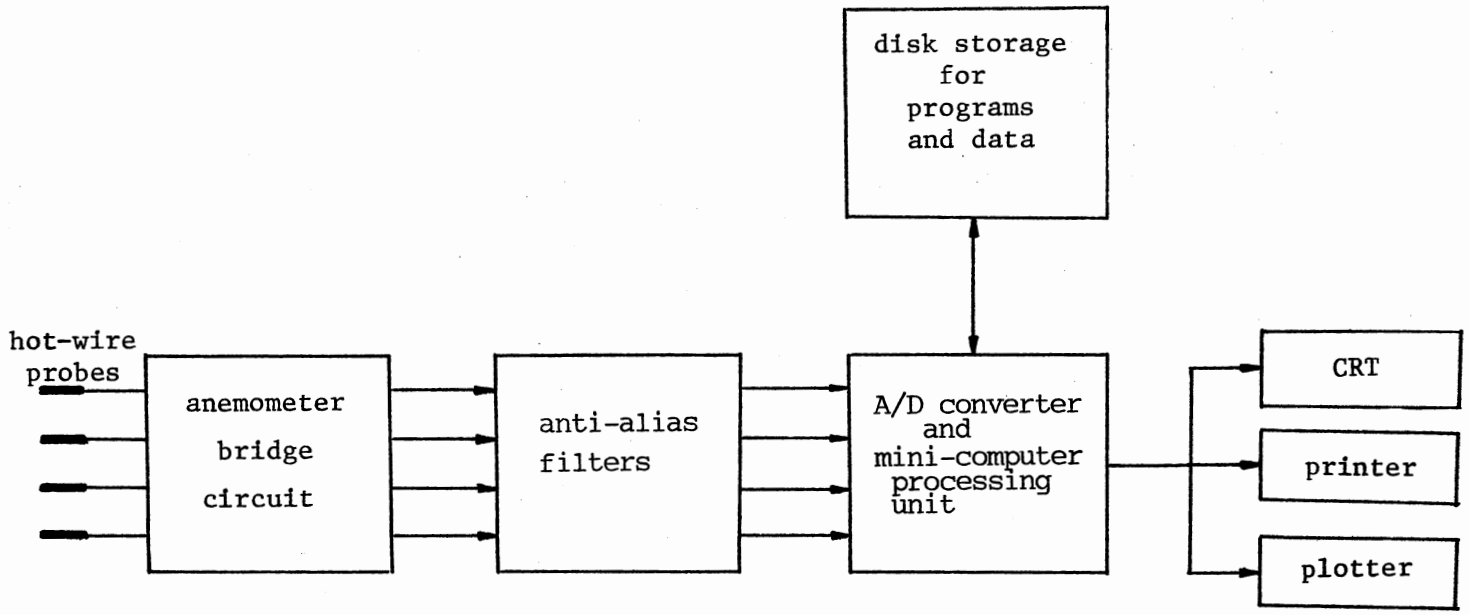

Figure 3. Schematic of Data Acquisition System

A/D board is able to sample up to seven channels of data and has a maximum sampling rate of 18 microseconds on a single channel. The digital signals were processed on line with an HP-9920S minicomputer which performed all data reduction. A 15 Mbyte hard disk was used for data storage. A high resolution CRT display, a printer, and a HP-7470A pen plotter are all available as output devices.

Calibration of the hot wires was performed by using an axisymmetric calibration jet facility. The axisymmetric jet was powered by compressed air and had an exit diameter of 0.6 inches. A valve on the calibrator was used in conjunction with a manometer to set the calibration jet velocity to any desired value. The anemometer D.C. bridge voltage was then recorded for each velocity setting of the calibration jet. A King's law calibration was utilized. This relation can be written as

$$E^2 = A + BU^{0.45} \tag{2.3}$$

where E is the mean anemometer D.C. bridge voltage, and U is the mean velocity. A least squares method was employed to determine the calibration constants A and B.

2.3 Validation Of The Flow Field

This section will present experimental results which document the general development of the planar jet. The purpose of these data is to validate the flow field in order to insure no unusual behavior that might jeopardize the generality of the conclusions to be drawn from this study.

All experimental data to be presented were obtained at a Reynolds

number (based on exit mean velocity and nozzle slot width) of 8200. This corresponds to an exit velocity of 9.45 m/s. The exit velocity was monitored with a pitot static tube connected to a Dwyer micromanometer which has a least count of 0.01 inches of water. The exit fluctuation intensity (defined as the rms longitudinal velocity fluctuation divided by the local mean centerline velocity) was measured to be 0.0028. The initial free shear layer momentum thickness was measured to be 0.00742 inch. The downstream variation of shear layer momentum thickness, θ, is documented in Figure 4. The initial development of the planar jet shear layer is characterized by localized increases in θ at approximately $x/D = 2$ and $x/D = 4$ which will be shown to correspond to large-scale vortex formation and interaction events. Farther downstream, a linear variation is noted with $d\theta/dx = 0.016$ for $x/D > 7$.

The development of planar jet mean velocity profiles is presented in Figures 5-10. Figure 5 clearly shows that the jet profile is initially flat except for two thin free shear layers that bound a core of irrotational fluid. Such "top hat" shaped profiles are characteristic of nozzles with large contraction ratio. The initial mean velocity development is characterized by the widening of the two shear layers resulting in a "shearing down" of the initially flat profile, and the jet potential core is completely engulfed by $x/D = 4.5$, as shown in Figure 8. Approximate mean velocity similarity is noted to be reached for $x/D > 11$ as seen in Figure 10.

Figure 11 documents the widening of the jet. Localized increases in widening are noted near $x/D = 2.5$ and $x/D = 5$. For $x/D > 10$ a linear variation is noted which is characteristic of the similarity region of planar jets as described in section 2.1. The non-dimensional widening

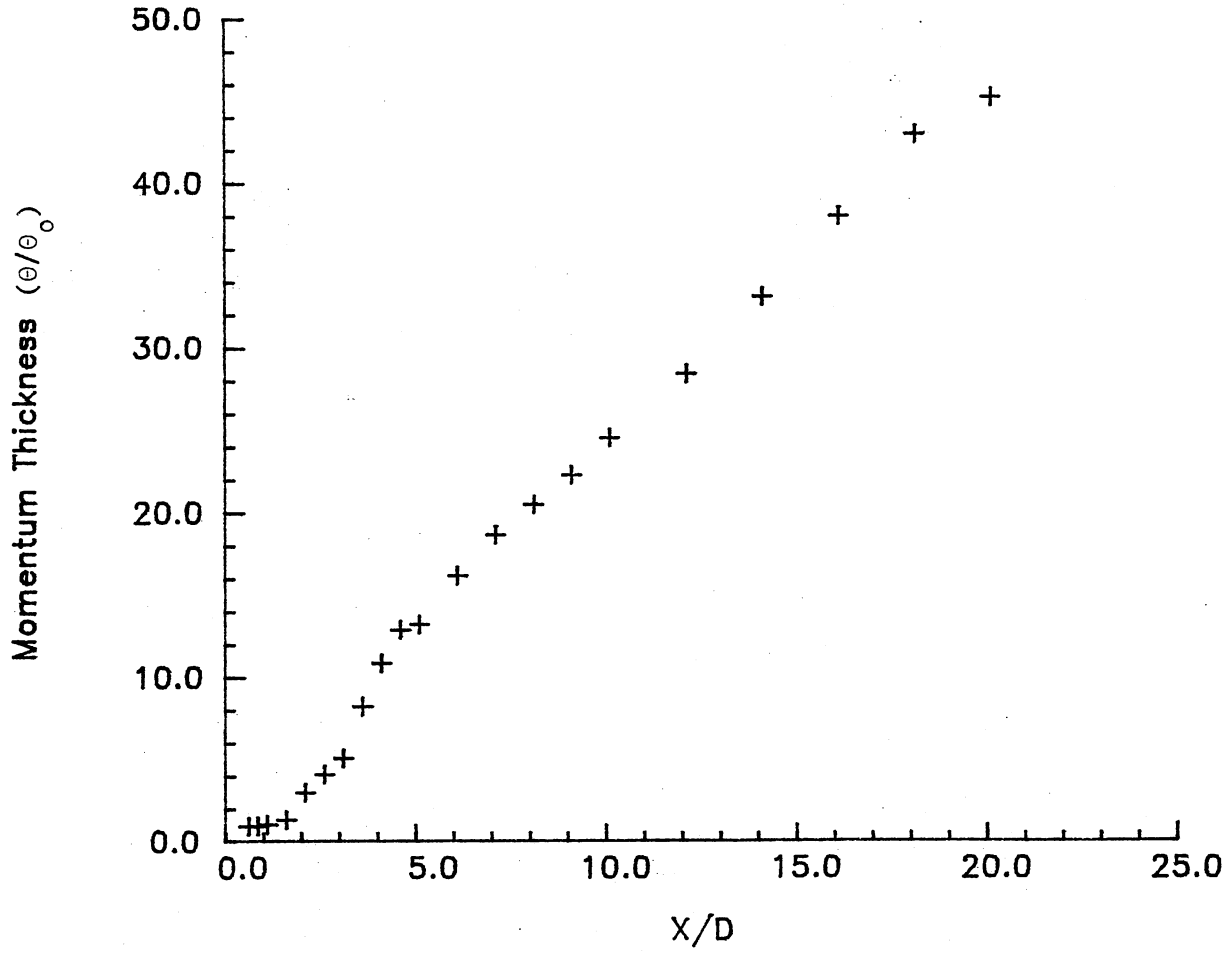

Figure 4. Variation of Momentum Thickness with Downstream Distance

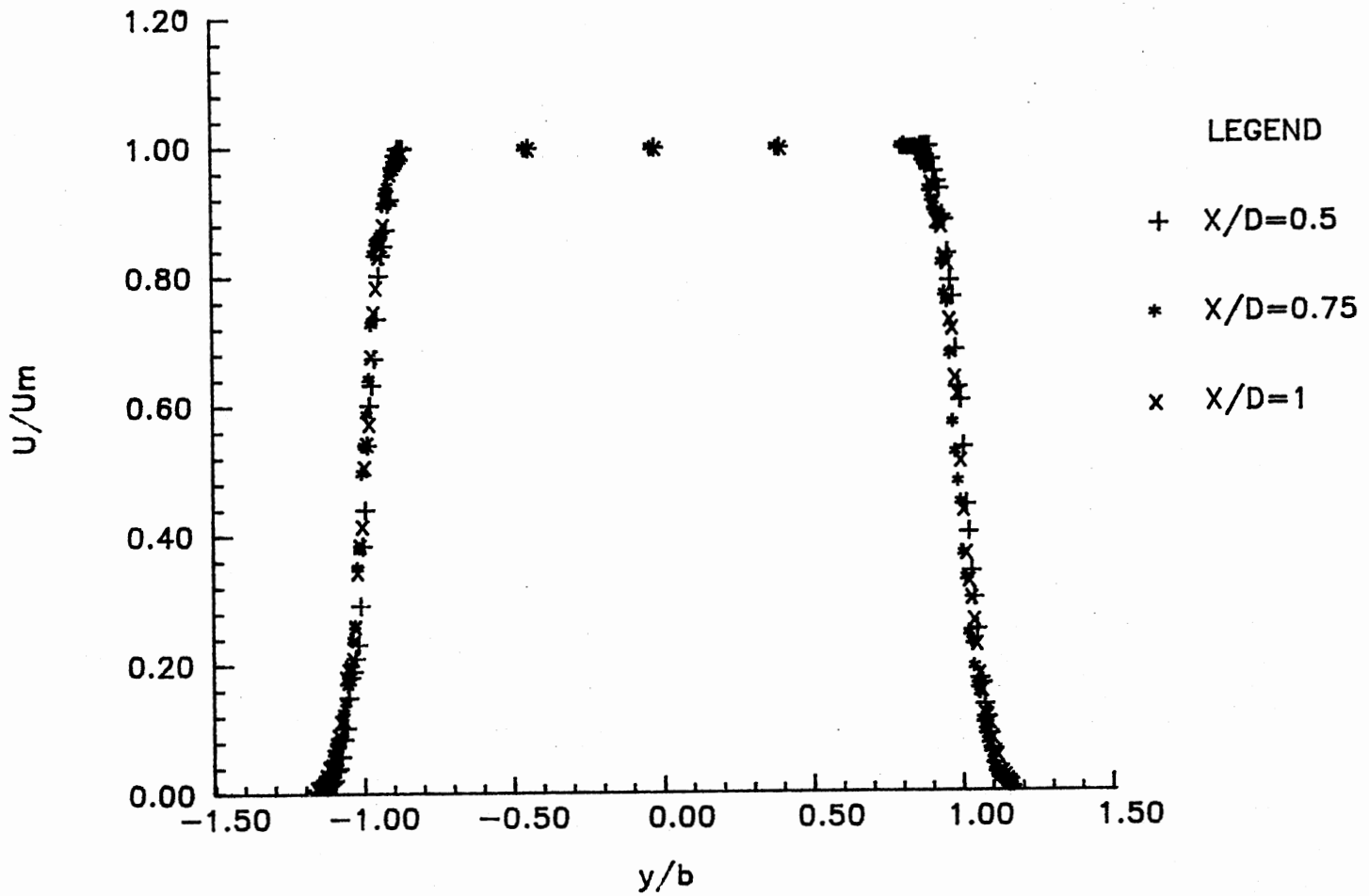

Figure 5. Mean Flow Velocity Profile at x/D = 0.5, 0.75 and 1.0

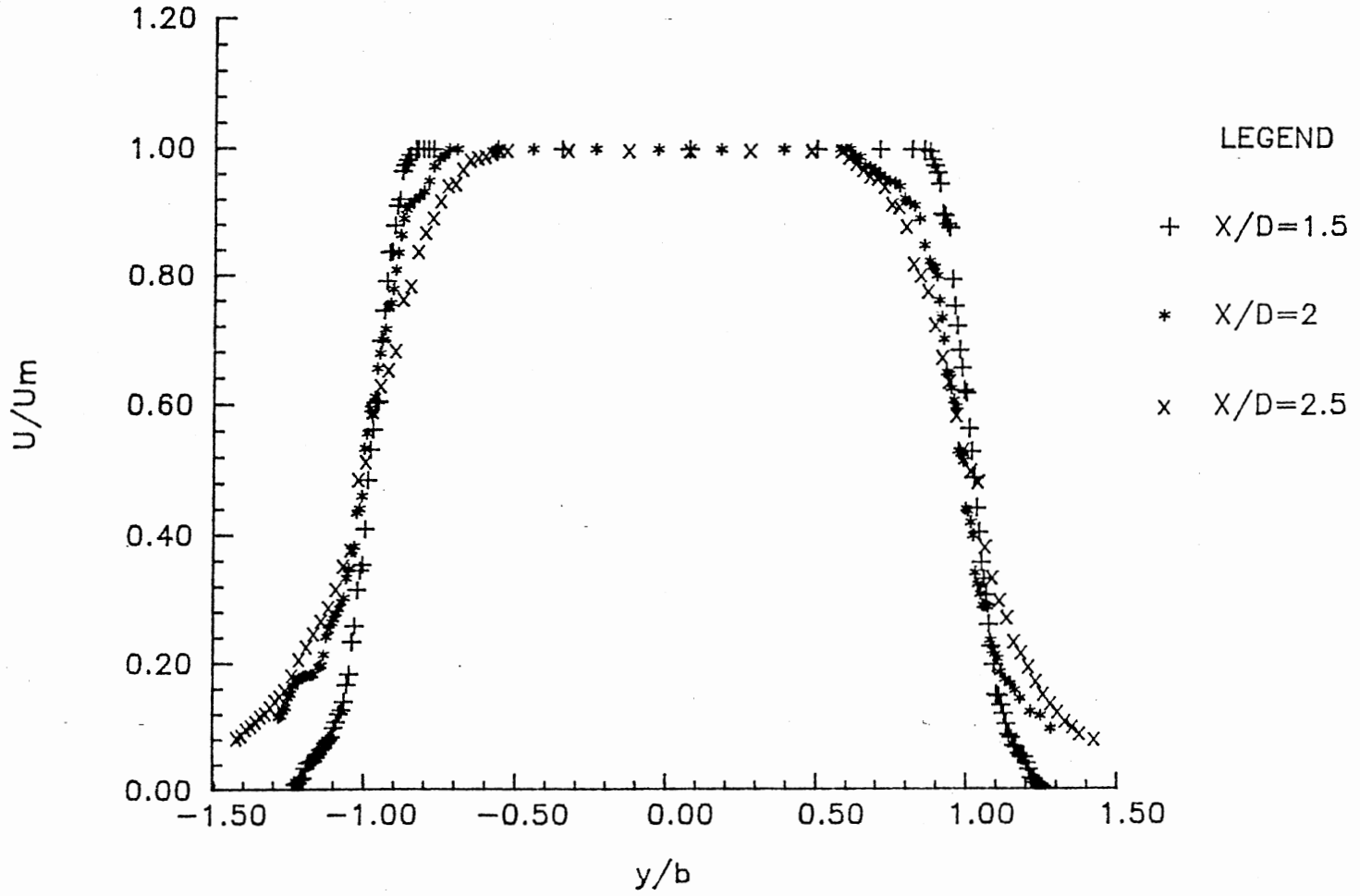

Figure 6. Mean Flow Velocity Profile at x/D = 1.5, 2.0 and 2.5

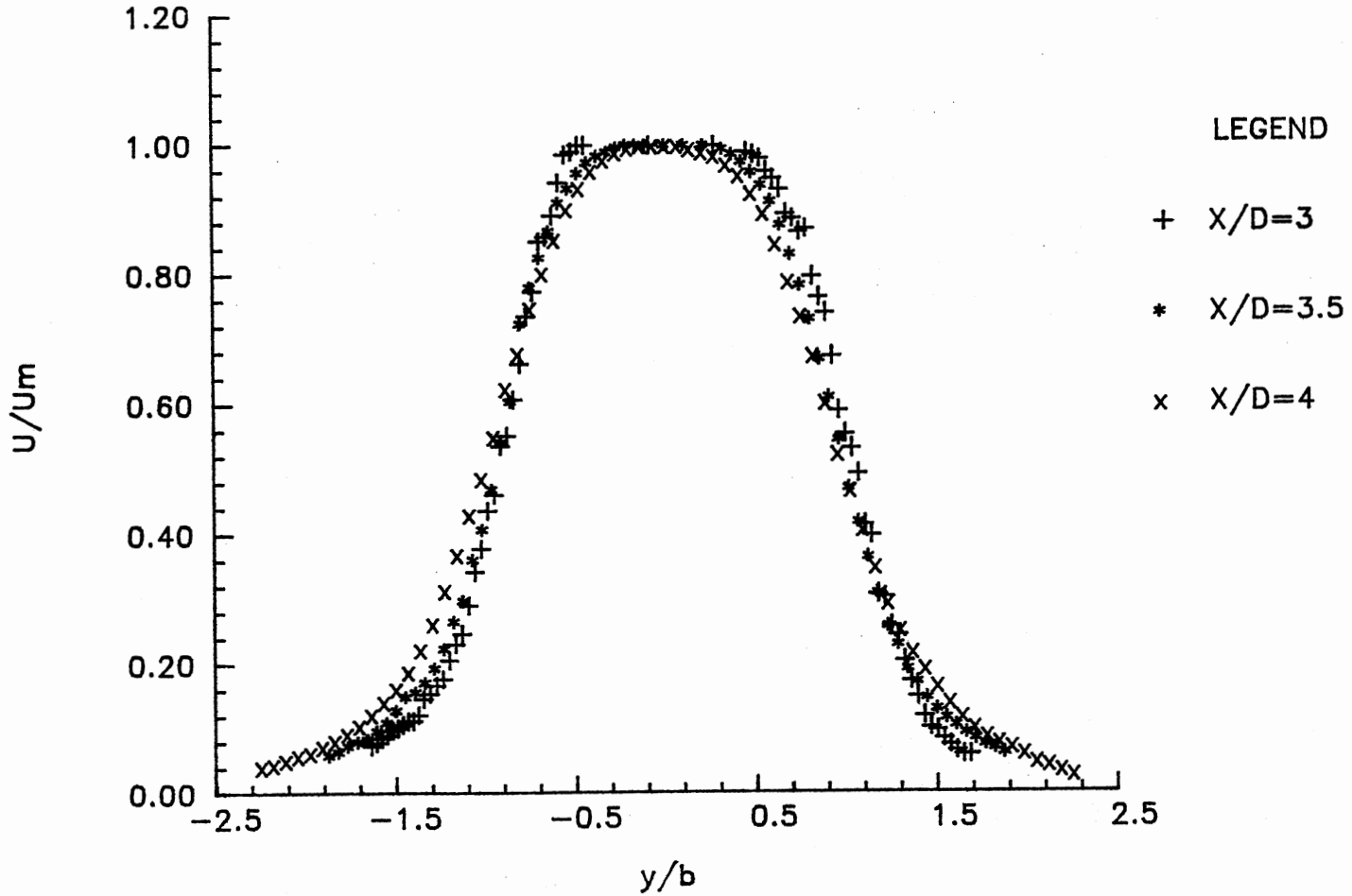

Figure 7. Mean Flow Velocity Profile at x/D = 3.0, 3.5 and 4.0

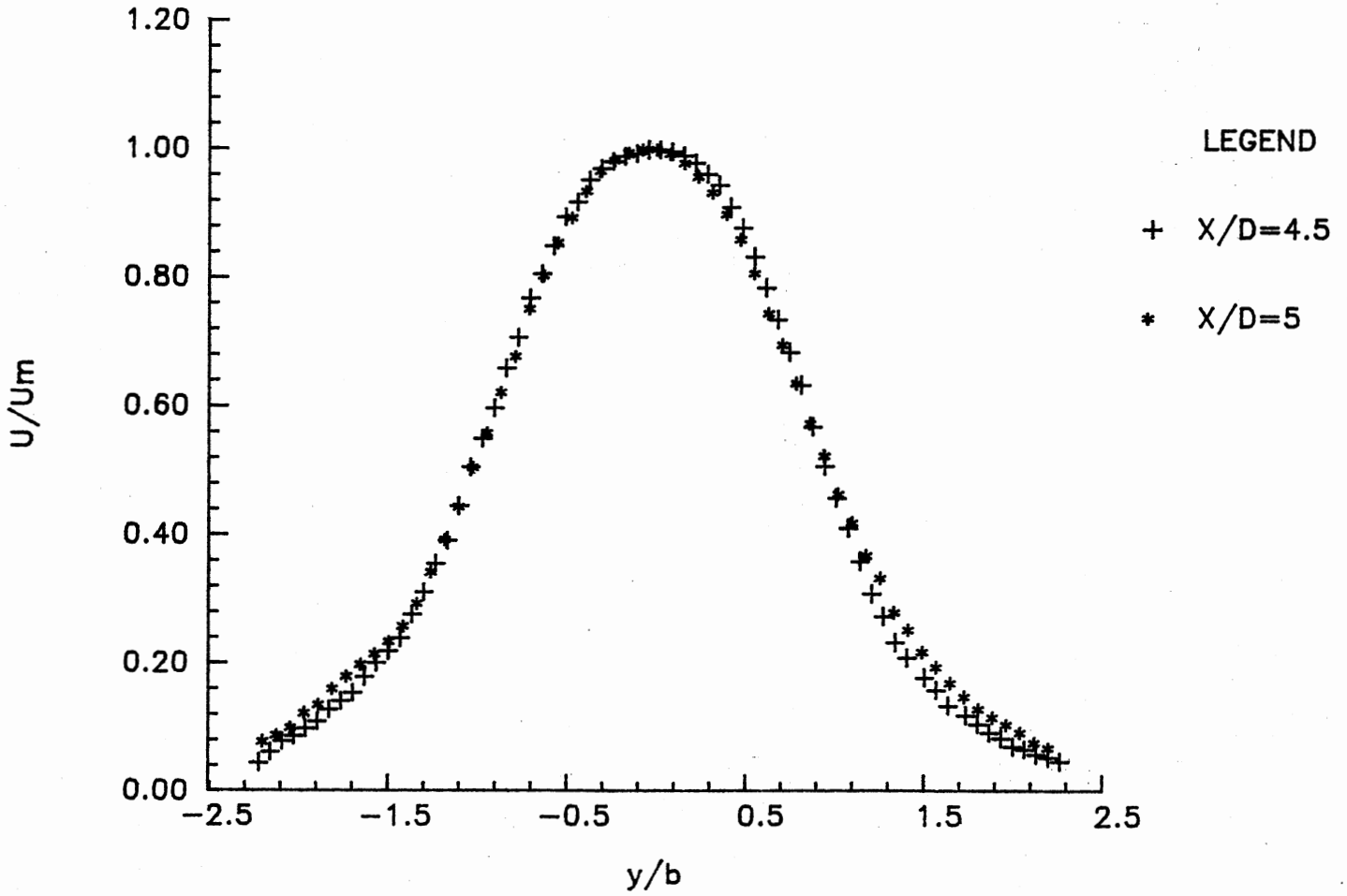

Figure 8. Mean Flow Velocity Profile at x/D = 4.5 and 5.0

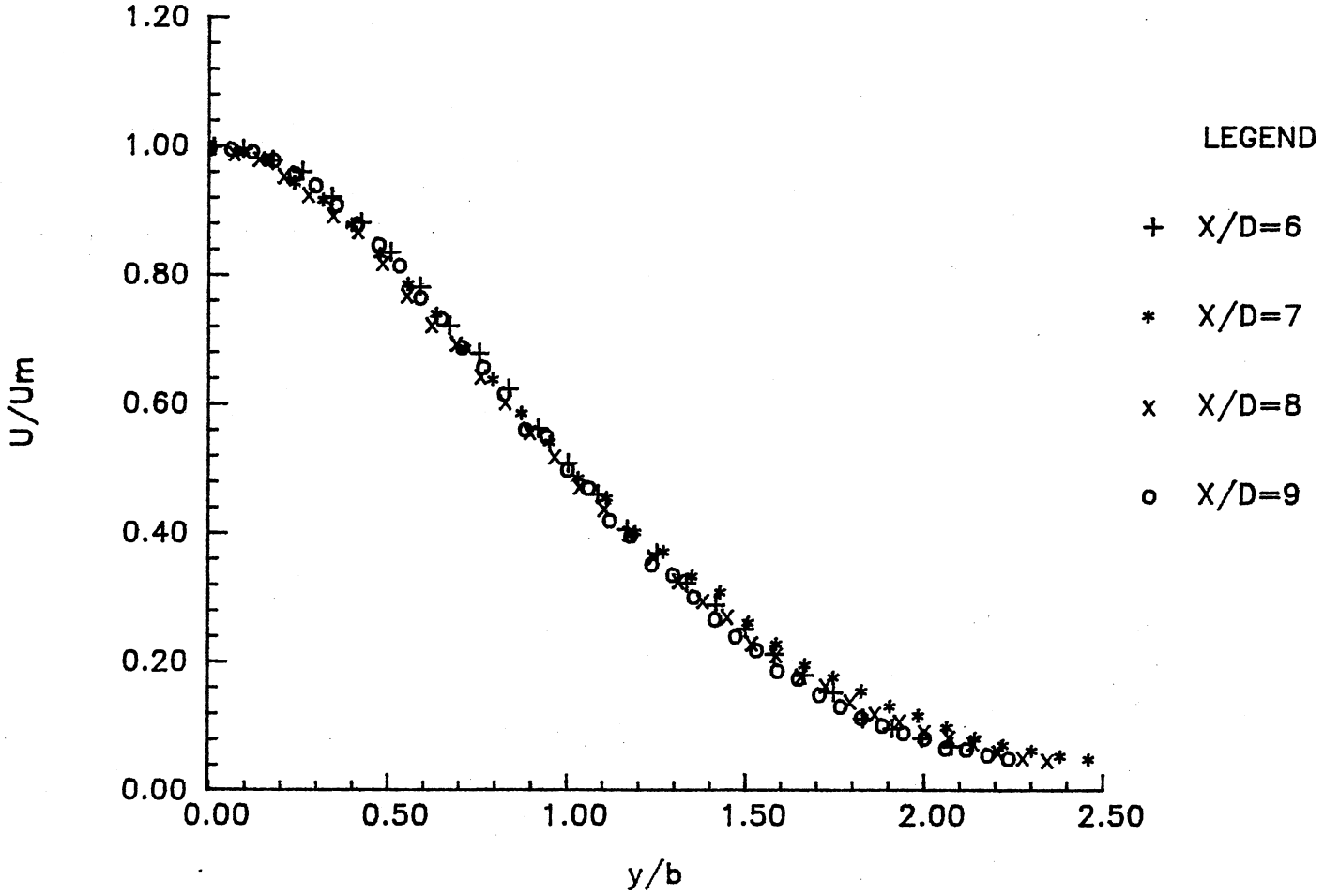

Figure 9. Mean Flow Velocity Profile at x/D = 6, 7, 8 and 9

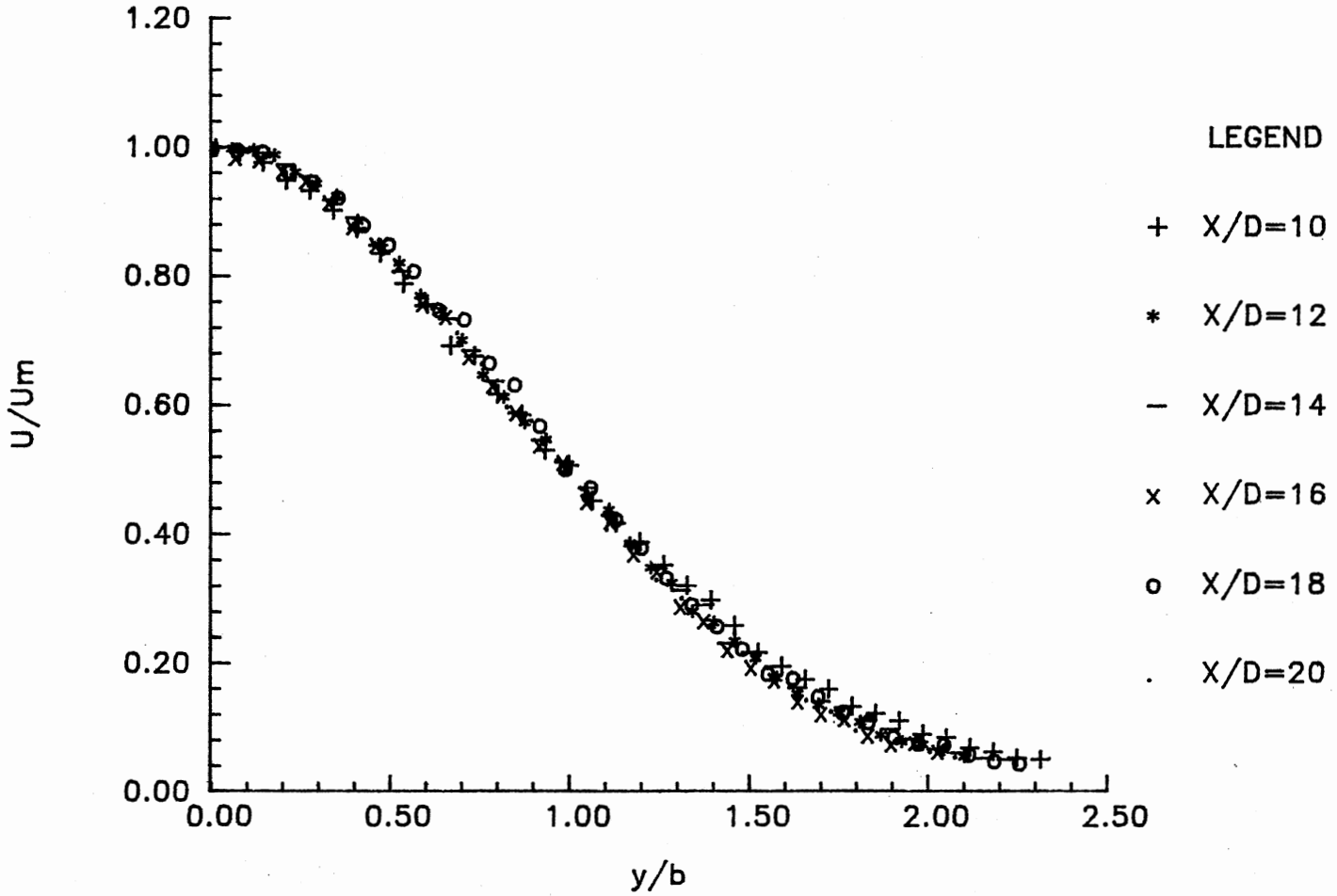

Figure 10. Mean Flow Velocity Profile at x/D = 10, 12, 14, 16, 18 and 20

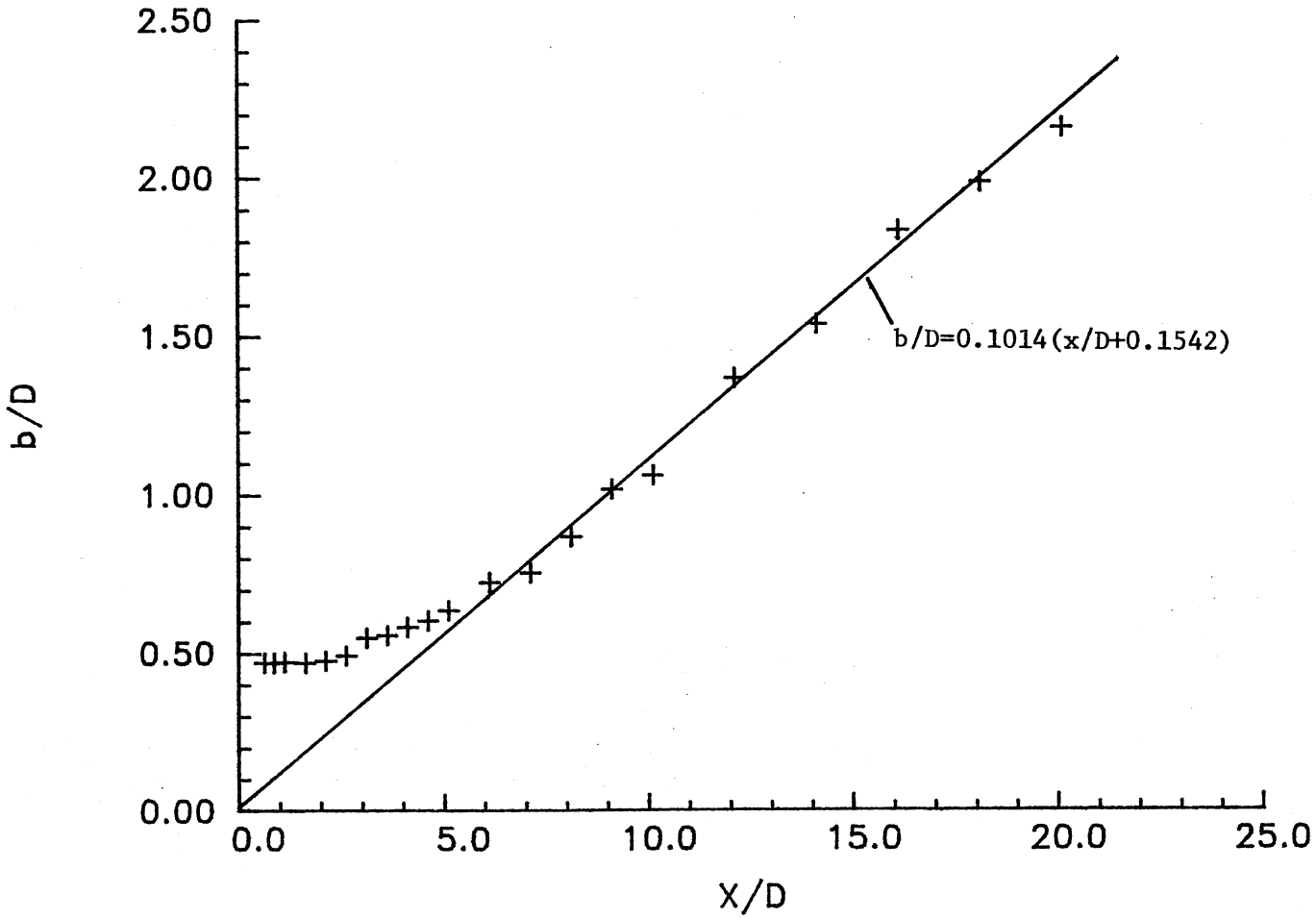

Figure 11. Jet Widening with Downstream Distance

rate K_1 = 0.1014 and the geometric virtual origin C_1 = -1.542. Figure 12 presents data which document the jet centerline mean velocity decay. For x/D > 11 a decay rate characteristic of the self-preserving planar jet is reached with $d((U_m/U_o)^{-2})/d(x/D)$ = 0.220 and the kinematic virtual origin C_2 = -0.597. These results are compared with previously published values in Table I. The widening rate and the mean velocity decay rate are in general agreement with previously measured values, but the virtual origins show some scatter which may possibly be attributed to differences in upstream plenum turbulence levels in the different experimental facilities (see Flora and Goldschmidt (1969)) or experimental uncertainty inherent to the measurement.

Longitudinal fluctuation intensity profiles were obtained at the same x/D locations as the previously presented mean velocity profiles. The longitudinal fluctuation intensities are normalized by the local mean centerline velocity and the lateral coordinate is scaled with the local jet half-width, b. Figures 13-16 show the rapid growth of symmetric peaks originating in the developing shear layers at y/b = 1.0 which corresponds to the location of maximum mean shear dU/dy. Turbulence intensity levels near the jet centerline initially remain quite low. With increasing distance downstream the high levels of the turbulence intensity in the jet shear layers "diffuse" toward the centerline and the profiles take on a characteristic "saddle" shape. The intensity profiles demonstrate a lack of complete similarity for x/D < 20 as shown in Figures 17-18, while similiarity for mean flow quantities has been shown to exist after x/D > 11. It is a general characteristic of the jet flows that mean flow quantities exhibit self-similar behavior before the turbulence quantities do. However, the

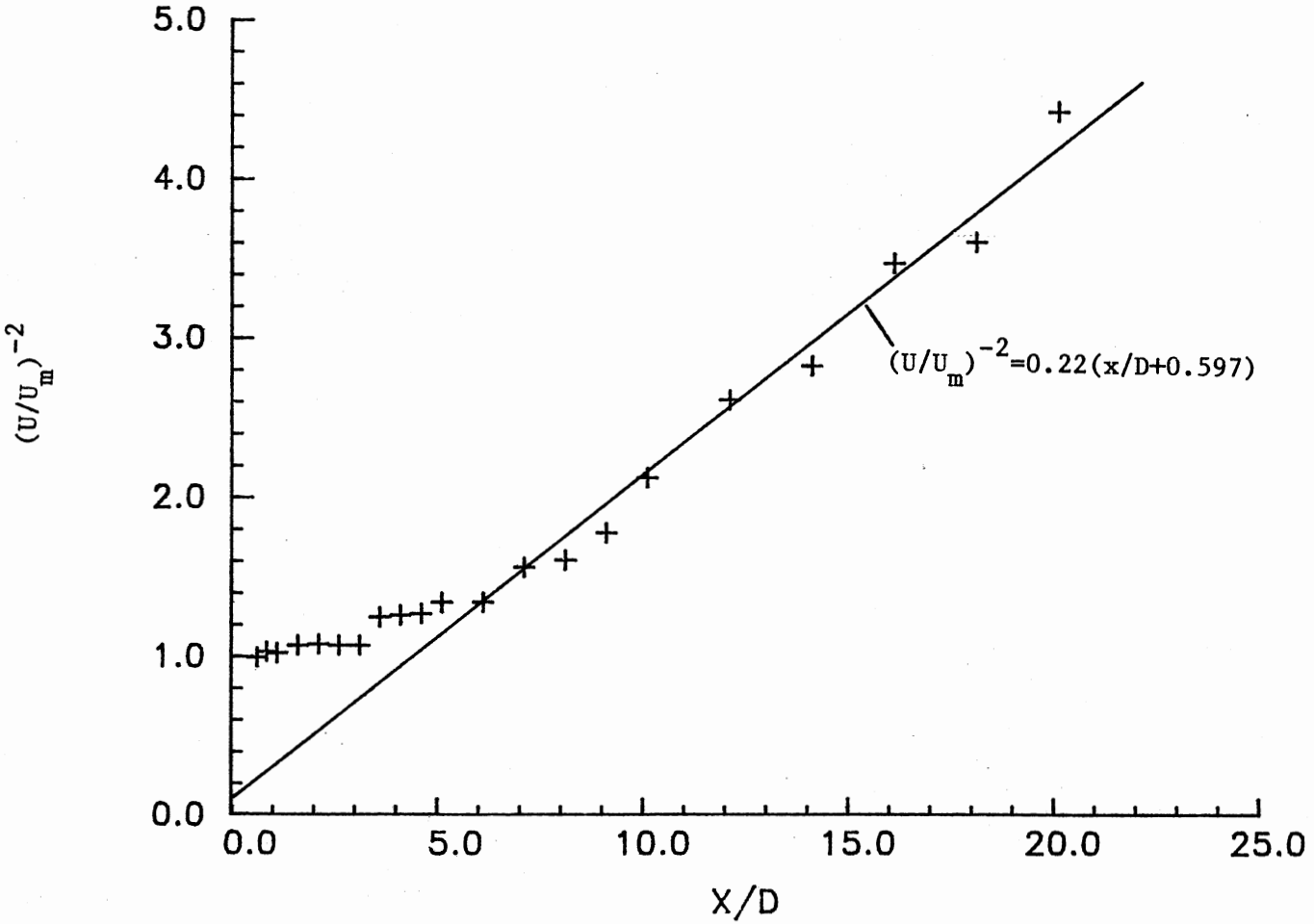

Figure 12. Mean Velocity Decay with Downstream Distance

TABLE I

COMPARISON OF MEAN FLOW PROPERTIES FOR PLANAR JETS

Reference	Re_D	K_1	K_2	C_1	C_2
Flora (1969)	2.00×10^4 to 3.00×10^4 to	0.109 to 0.130	0.158 to 0.227	-15.000	2.000
van der Hegge Zijnen (1958)	1.33×10^4	0.100	0.205	0.000	-1.700
Foss (1965)	5.50×10^4	0.085	0.257	-2.000	6.500
Kaiser (1971)	6.00×10^3	0.101	0.208	-2.600	0.000
Ott (1972)	1.00×10^4	0.097	0.228	-3.000	7.000
Jenkins (1974)	1.45×10^4	0.085	0.160	-6.100	4.000
Mulej (1975)	1.60×10^4	0.095	0.185	-0.789	13.200
Gutmark and Wygnanski (1976)	3.00×10^4	0.100	0.170	-2.000	4.700
Cervantes (1978)	1.00×10^4	0.083	0.240	-6.600	4.500
Chambers (1977)	6.00×10^3	0.100	0.190	-3.500	-3.200
Thomas (1980)	6.00×10^3	0.106	0.214	-3.500	-0.913
Thomas (1983)	6.00×10^3	0.100	0.220	-3.200	-1.600
Thomas and Brehob (1986)	1.50×10^4	0.086	0.253	-4.711	10.371
Prakash (1986)	7.70×10^3	0.104	0.180	-1.800	-0.354
Current (1987)	8.20×10^3	0.104	0.220	-1.542	-0.597

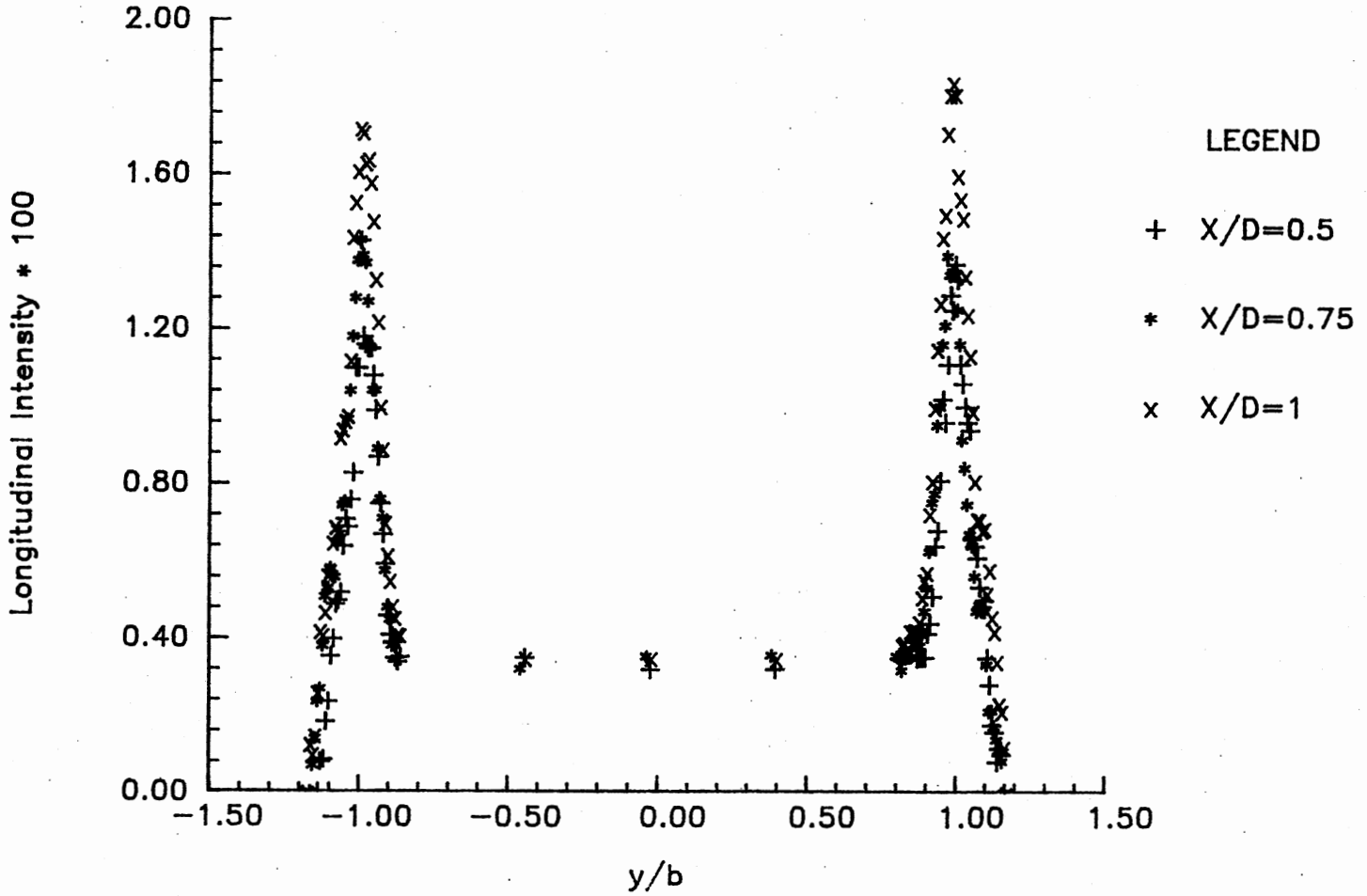

Figure 13. Longitudinal Fluctuation Intensity Profile at x/D = 0.5, 0.75 and 1.0

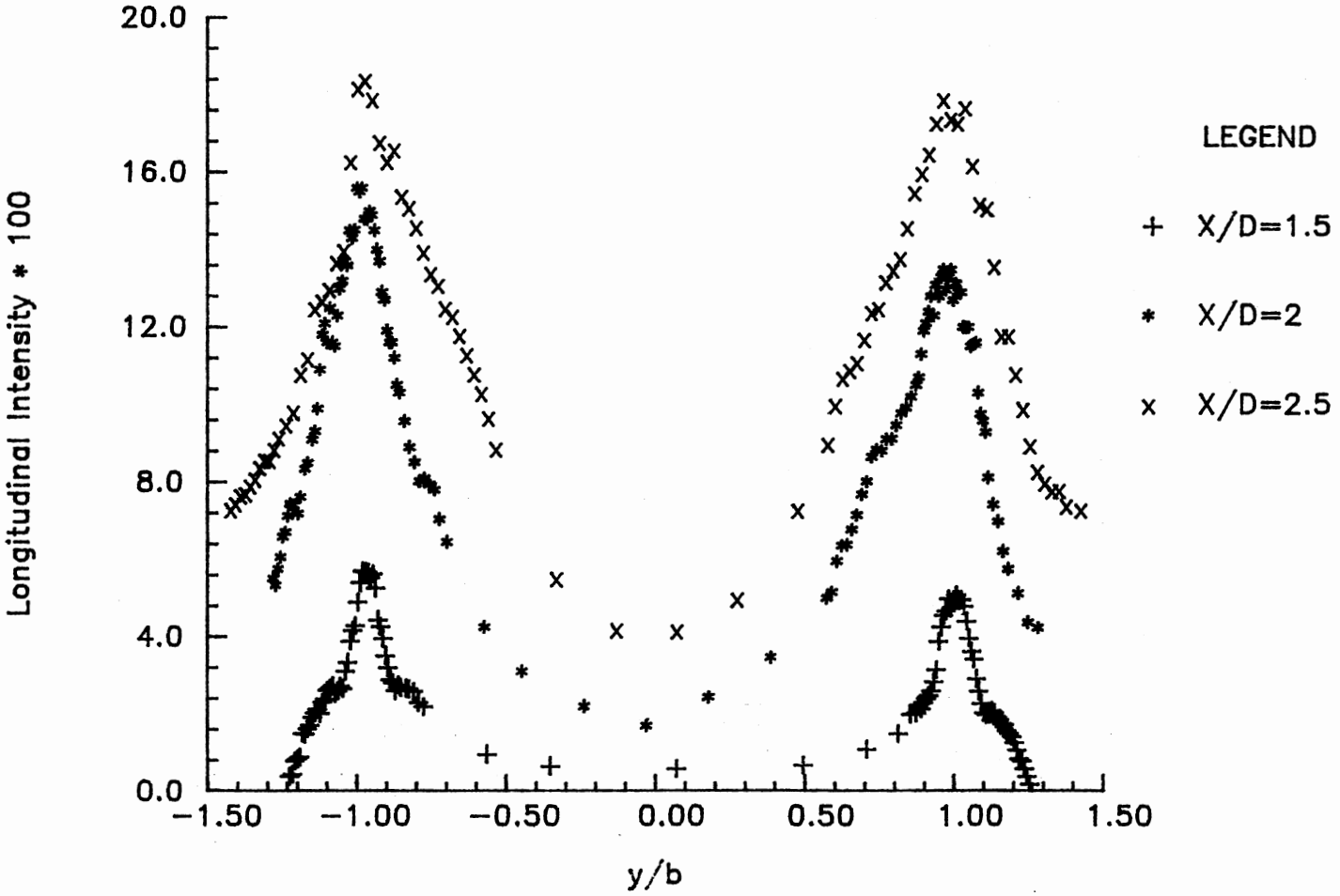

Figure 14. Longitudinal Fluctuation Intensity Profile at x/D = 1.5, 2.0 and 2.5

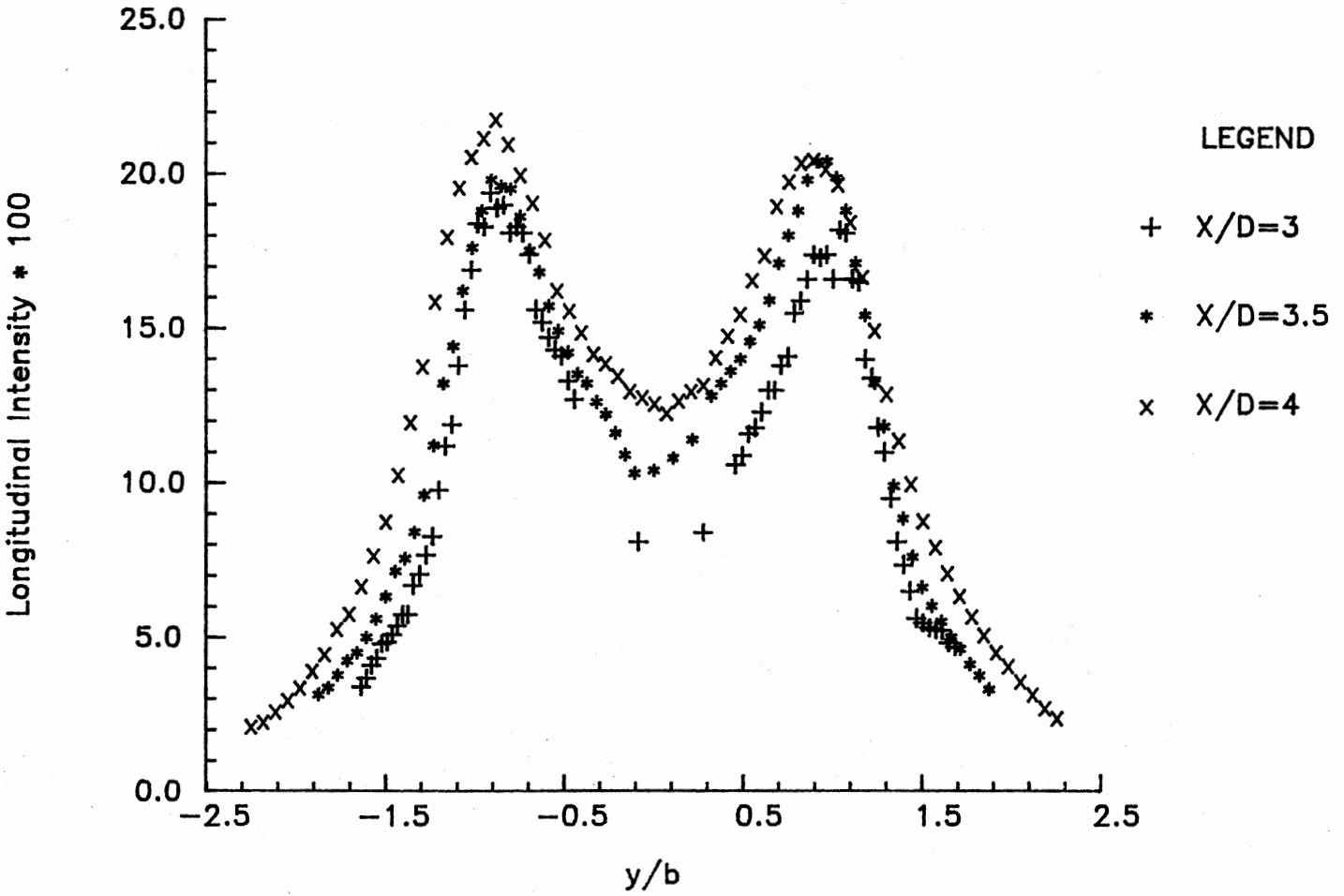

Figure 15. Longitudinal Fluctuation Intensity Profile at x/D = 3.0, 3.5 and 4.0

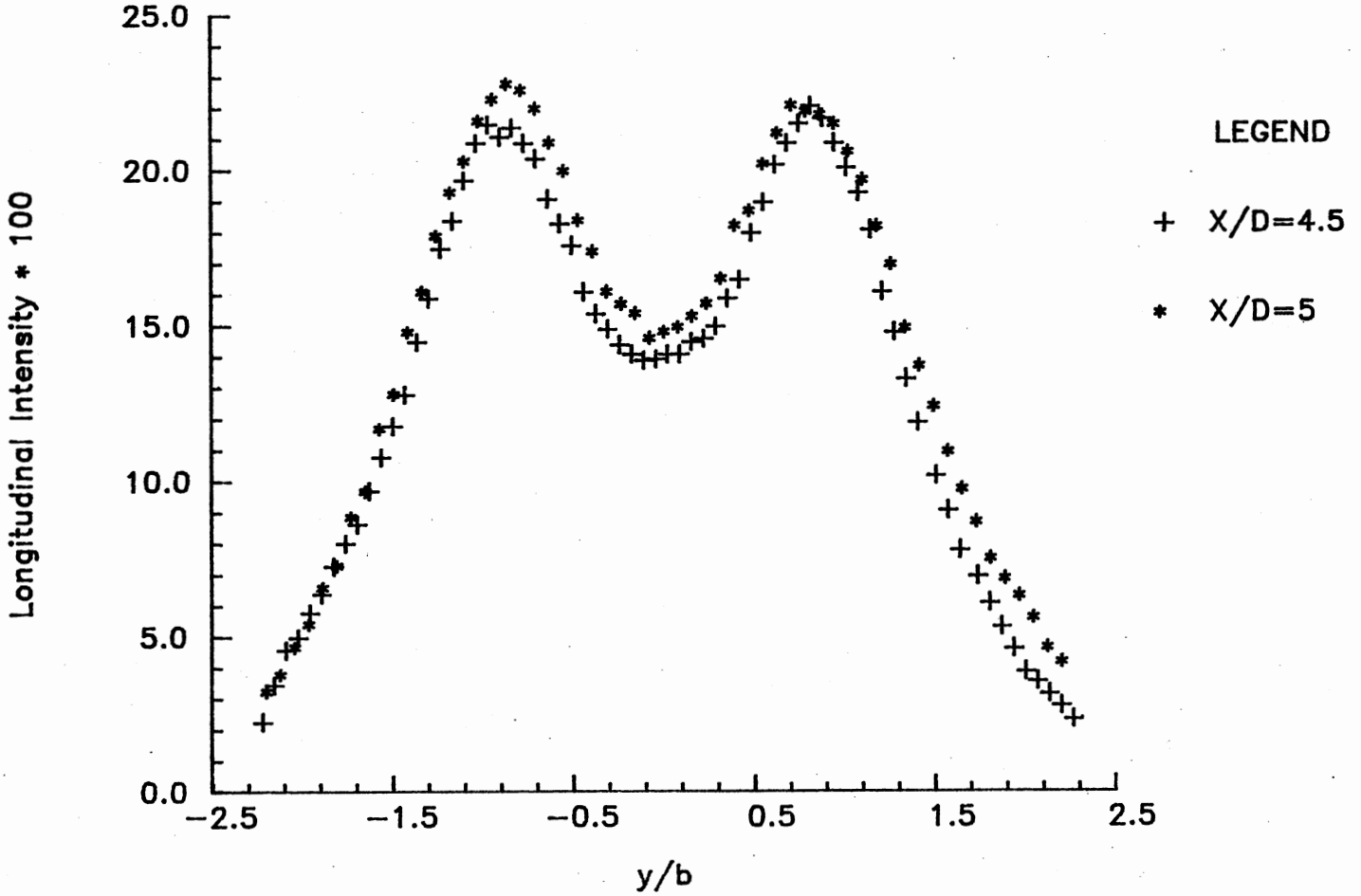

Figure 16. Longitudinal Fluctuation Intensity Profile at x/D = 4.5 and 5.0

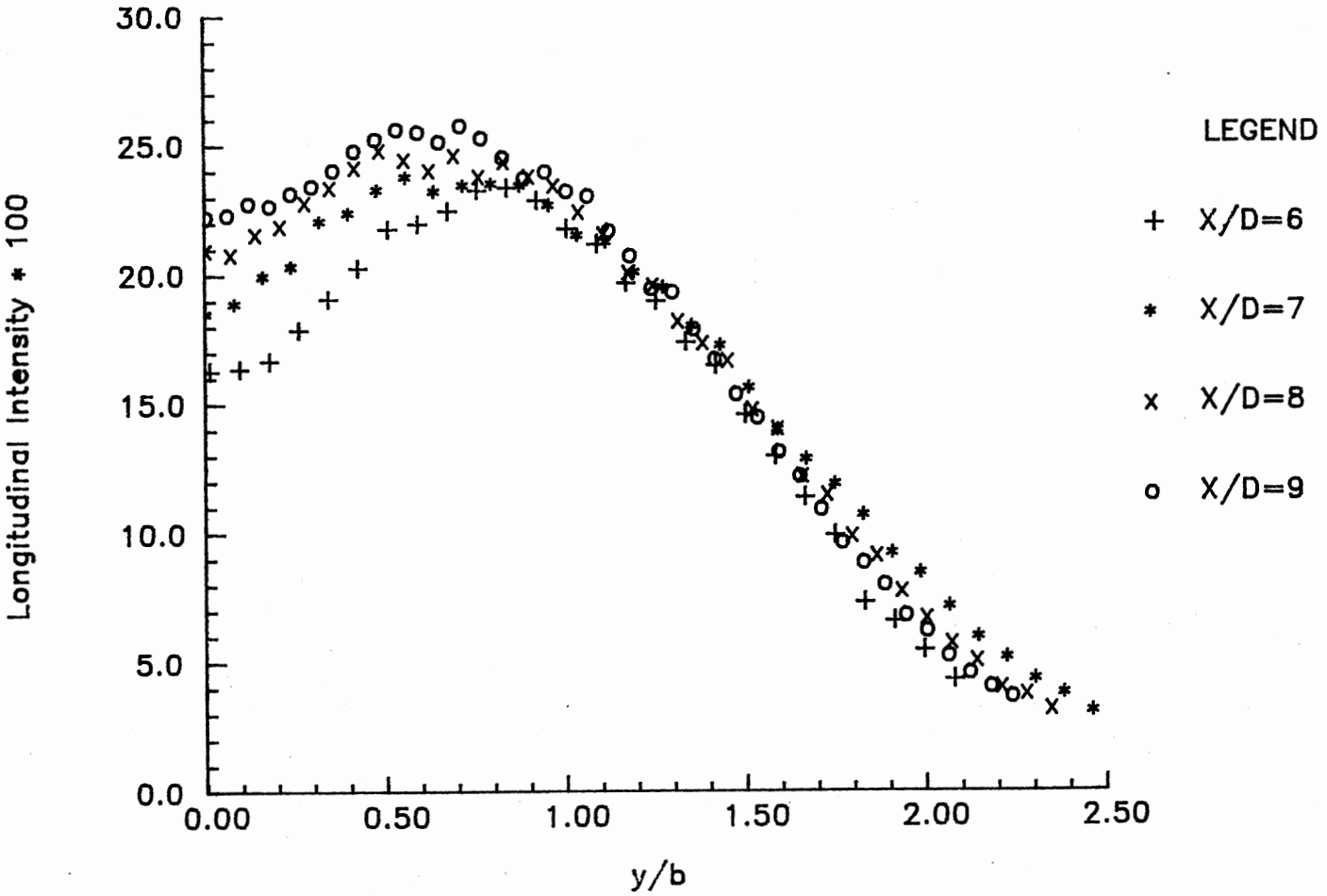

Figure 17. Longitudinal Fluctuation Intensity Profile at x/D = 6, 7, 8, and 9

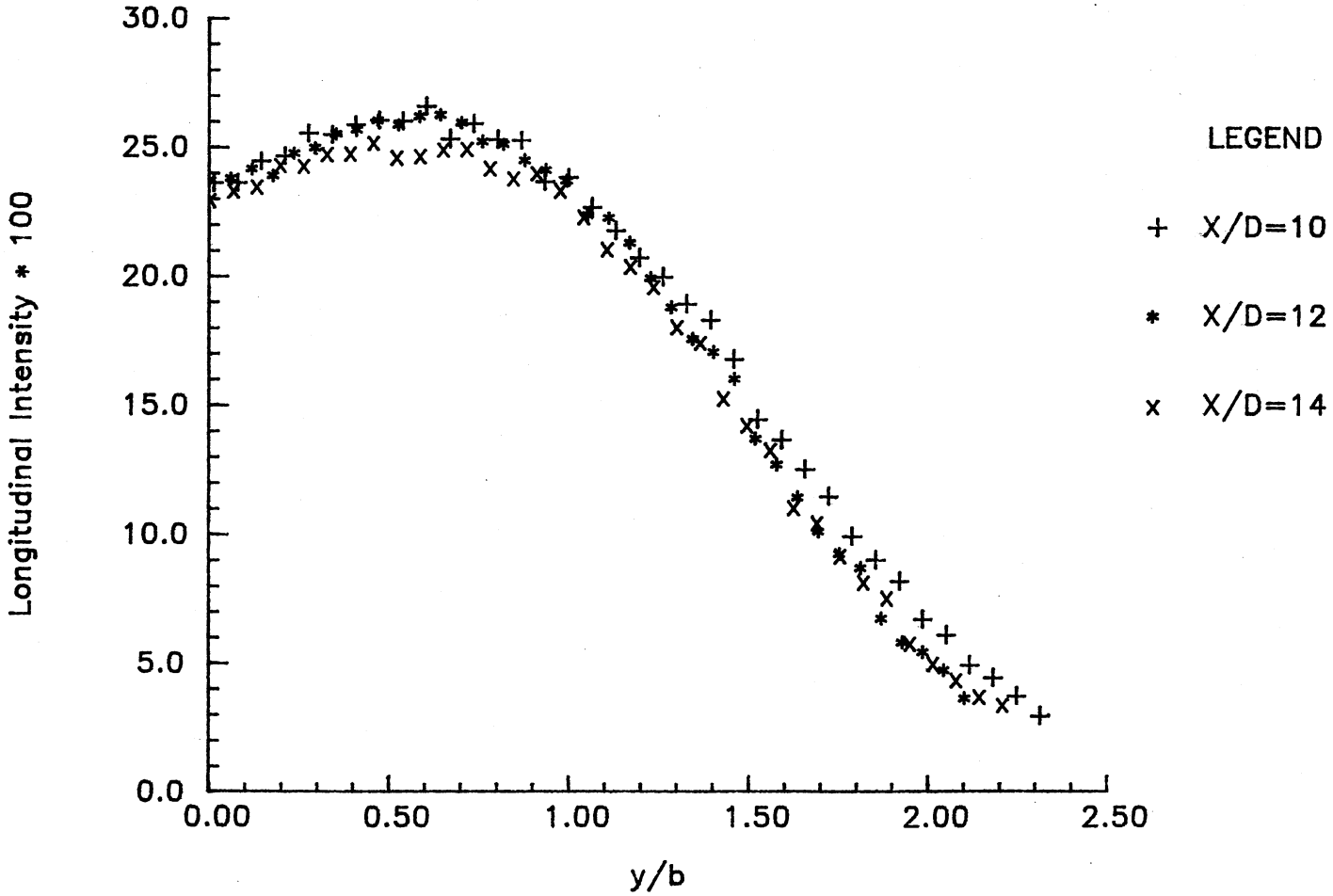

Figure 18. Longitudinal Fluctuation Intensity Profile at x/D = 10, 12 and 14

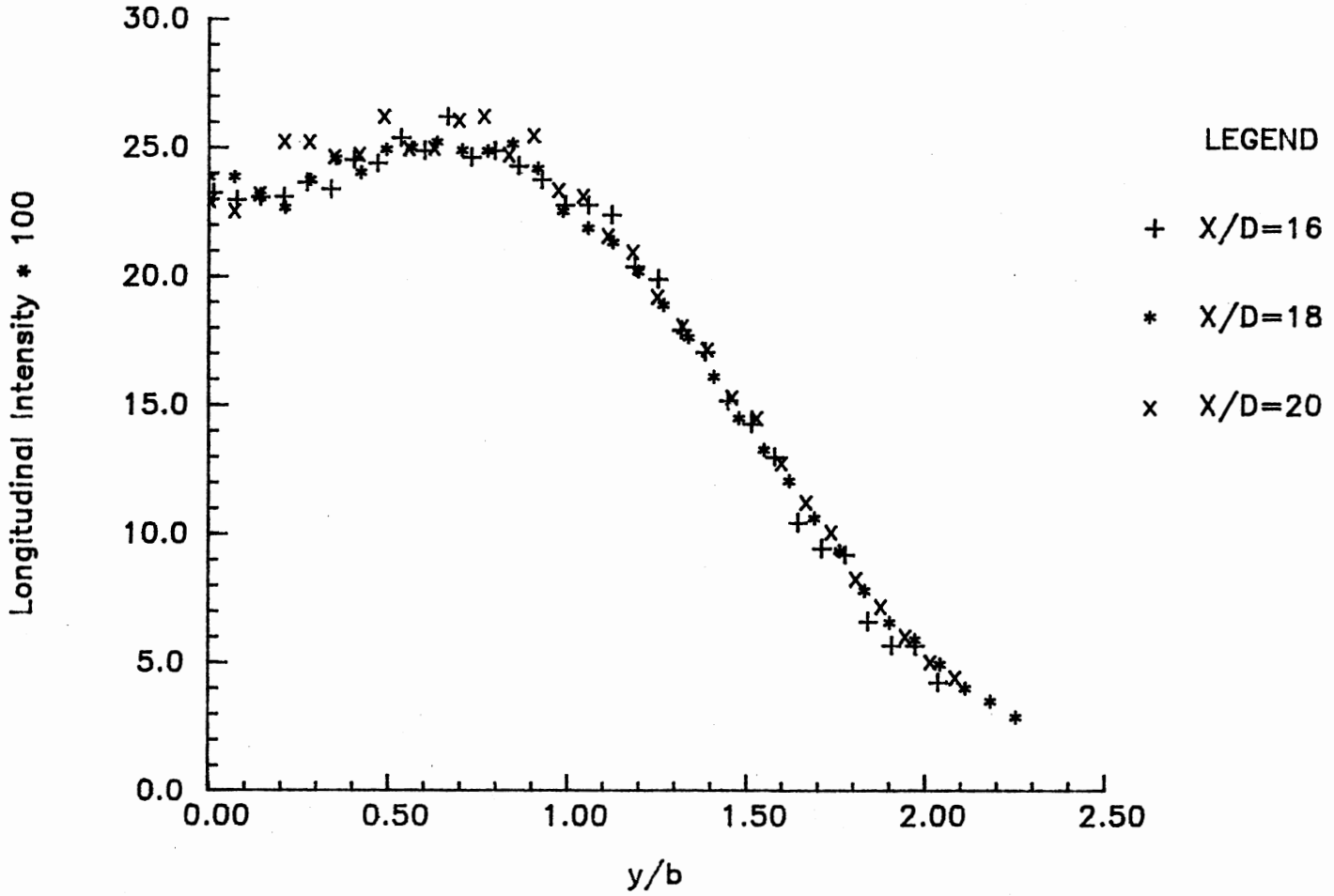

Figure 19. Longitudinal Fluctuation Intensity Profile at x/D = 16, 18 and 20

profiles of Figure 19 clearly show the tendency of the longitudinal turbulence intensity profiles to approach a self-similar shape similar to that reported by Bradbury (1965) and Gutmark and Wygnanski (1976). Figure 20 shows the downstream development of longitudinal turbulence intensity as measured on the jet centerline. The intensity rapidly increases for $x/D > 2$ and is seen to approach an equilibrium condition for $x/D > 12$.

Based on these data presented, it is concluded that the planar jet exhibits behavior which is in general agreement with that observed by other researchers. No unreasonable or unexpected results are indicated. Therefore, the experimental data to be presented in the next chapter is expected to be common to all planar jet flow field facilities.

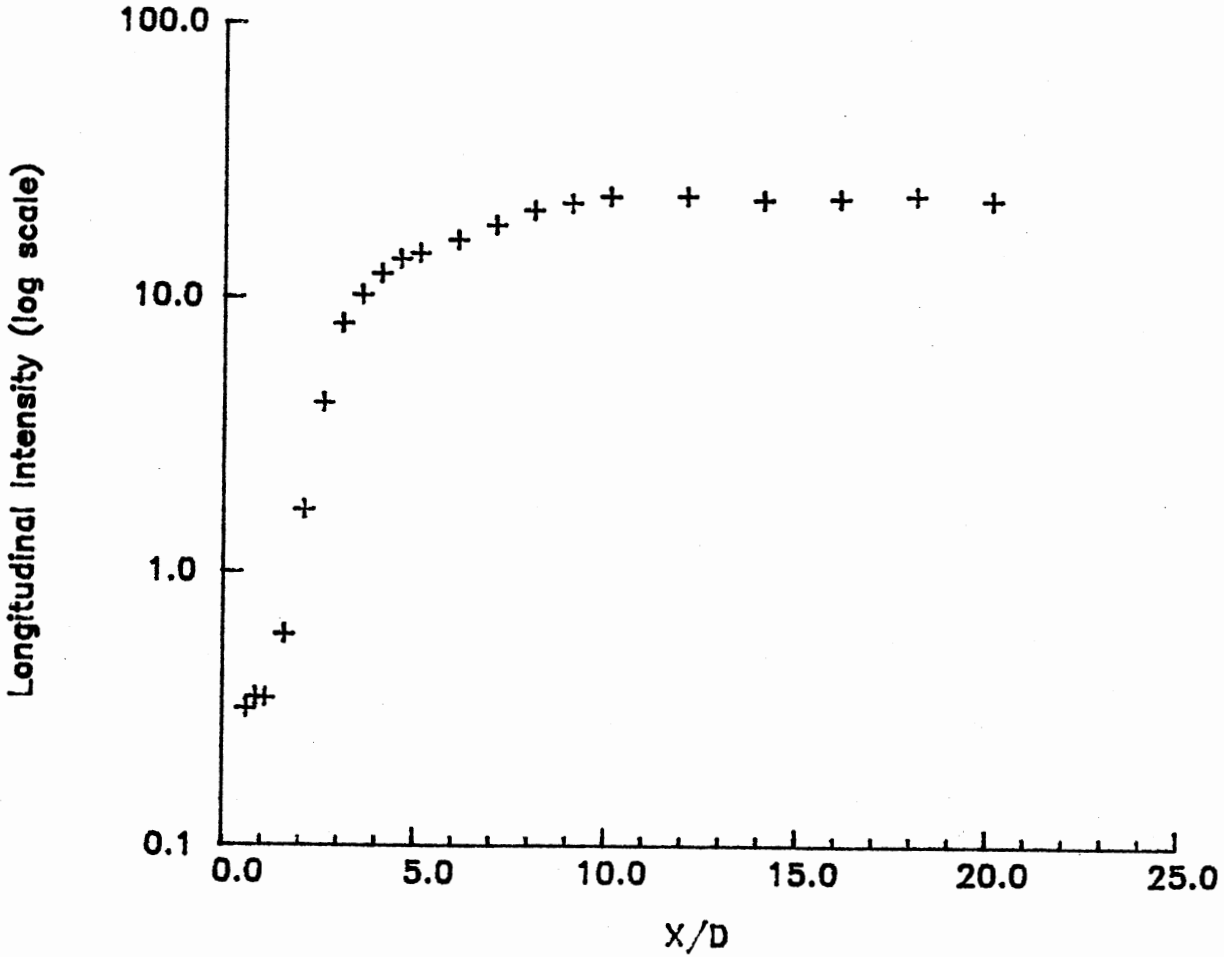

Figure 20. Variation of Centerline Longitudinal Fluctuation Intensity with Downstream Distance

CHAPTER III

MEASUREMENTS CHARACTERIZING JET TRANSITION

This chapter presents the results of detailed measurements which characterize the transition of the two-dimensional turbulent jet. In order to facilitate study of the nonlinear wave development which occurs during transition, low level acoustic excitation was used in order to introduce a controlled instability into the flow. The primary objectives of the research and the role which the acoustic excitation played in the study are next described.

3.1 Objectives of the Research

A detailed investigation regarding the influence of a global resonance mechanism in the natural transition of the planar turbulent jet was performed by Prakash (1986). There it was noted that the initial development of the flow depended upon both the local inviscid jet shear layer instability and global flow dynamics as determined from the requirements of a resonance mechanism. Of particular significance in the dynamics of global resonance was the interaction between the jet shear layers which occurs beyond the potential core. This interaction involves large-scale vorticity of opposite sign and exerts a particularly strong upstream influence on the developing jet shear layers. A simple analytical model of global resonance was found capable of predicting the frequencies and streamwise locations associated with

each large-scale vortex interaction event which characterizes the jet shear layer development. The previous experimental results of Prakash (1986) clearly demonstrated the influence of a global resonance mechanism on planar jet transition but failed to provide insight regarding the detailed dynamics involved. A fundamental goal of this research effort is to understand on a quantitative basis the detailed dynamics of the global resonance mechanism which operates in planar jet transition.

It is well known that the properties of jet flows may be controlled by the application of periodic forcing such as acoustic excitation. Recently, some studies have used acoustic forcing as a tool by which coherent structures may be enhanced for study. In other studies, low level acoustic excitation has been utilized in order to introduce a controlled perturbation into the flow in order to facilitate study of transition to turbulence. In the work to be reported low level acoustic excitation near the most unstable jet shear layer frequency was applied in order to study the nonlinear evolution of an artificially introduced instability wave. Of particular interest is the quantitative measurement of the nonlinear interactions between fluctuations which characterize the transition of the planar jet. Since the excitation is at the most unstable shear layer frequency and is very low in amplitude, it is expected that results inferred from the excited jet study will be applicable to the "natural" planar jet flow. The insight gained regarding the transition of the excited jet should hence facilitate better understanding of the natural jet transition. Measurements made in the excited jet should also provide insight regarding the detailed dynamics of the global resonance mechanism.

3.2 The Effect of Acoustic Excitation

Sinusoidal acoustic excitation from a loudspeaker mounted in the duct upstream of the nozzle exit was used to excite a small amplitude instability at the initially most unstable jet shear layer frequency of 750 Hz (as determined from the linear stability theory of Michalke (1965)). The amplitude of the acoustic excitation was chosen such that at the nozzle exit the rms amplitude $u(f_e)$ of the excited mode did not exceed the level of natural background fluctuations. The longitudinal fluctuation intensity at the excitation frequency f_e was measured to be 0.000079 while the exit longitudinal fluctuation intensity at the same frequency under no acoustic excitation was 0.000043. The total longitudinal turbulence intensity at the nozzle exit was 0.002923 for the excited jet compared to 0.002841 for the natural flow.

Measurements were performed to determine what effect the excitation had upon the basic development of the flow. Figure 21 compares downstream variation in centerline longitudinal turbulent intensity for the natural and excited cases. The figure indicates that the acoustic forcing only significantly influences the near exit region of the planar jet for $x/D < 3$; after which the excited case fluctuation intensity approaches the no sound level. Figures 22-23 present the comparisions of measured mean velocity profiles corresponding to the natural and 750 Hz excitation conditions, at $x/D = 2$ and 5 respectively. Little difference in mean velocity is noted to occur. At $x/D = 2$ the excited jet profile is somewhat wider due to increased shear layer fluctuation intensities and the enhanced diffusivity of the flow which occurs. The mean velocity profiles near the end of the potential core exhibit no significant difference however. Corresponding turbulence intensity

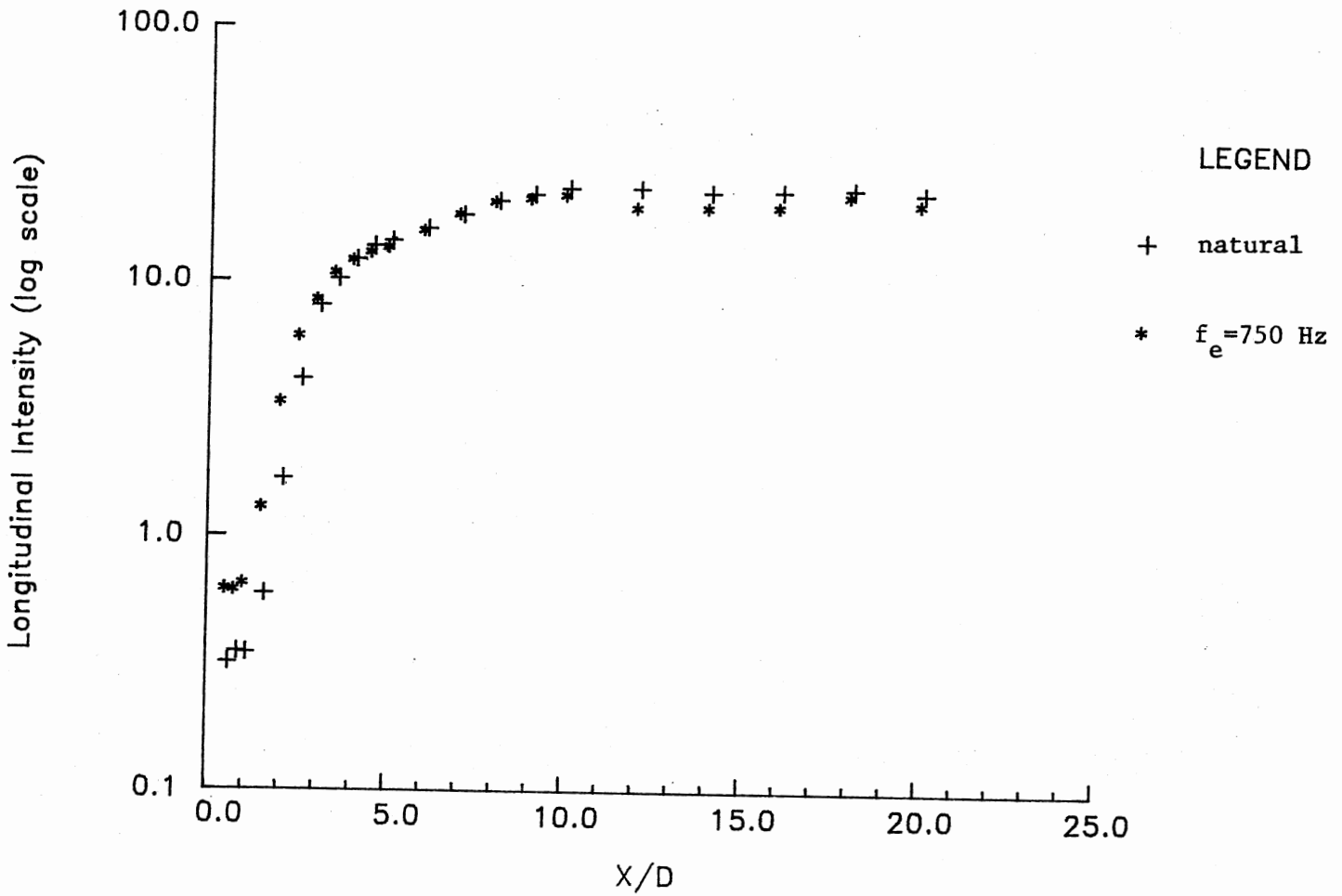

Figure 21. Comparison of Centerline Longitudinal Fluctuation Intensity with Downstream Distance

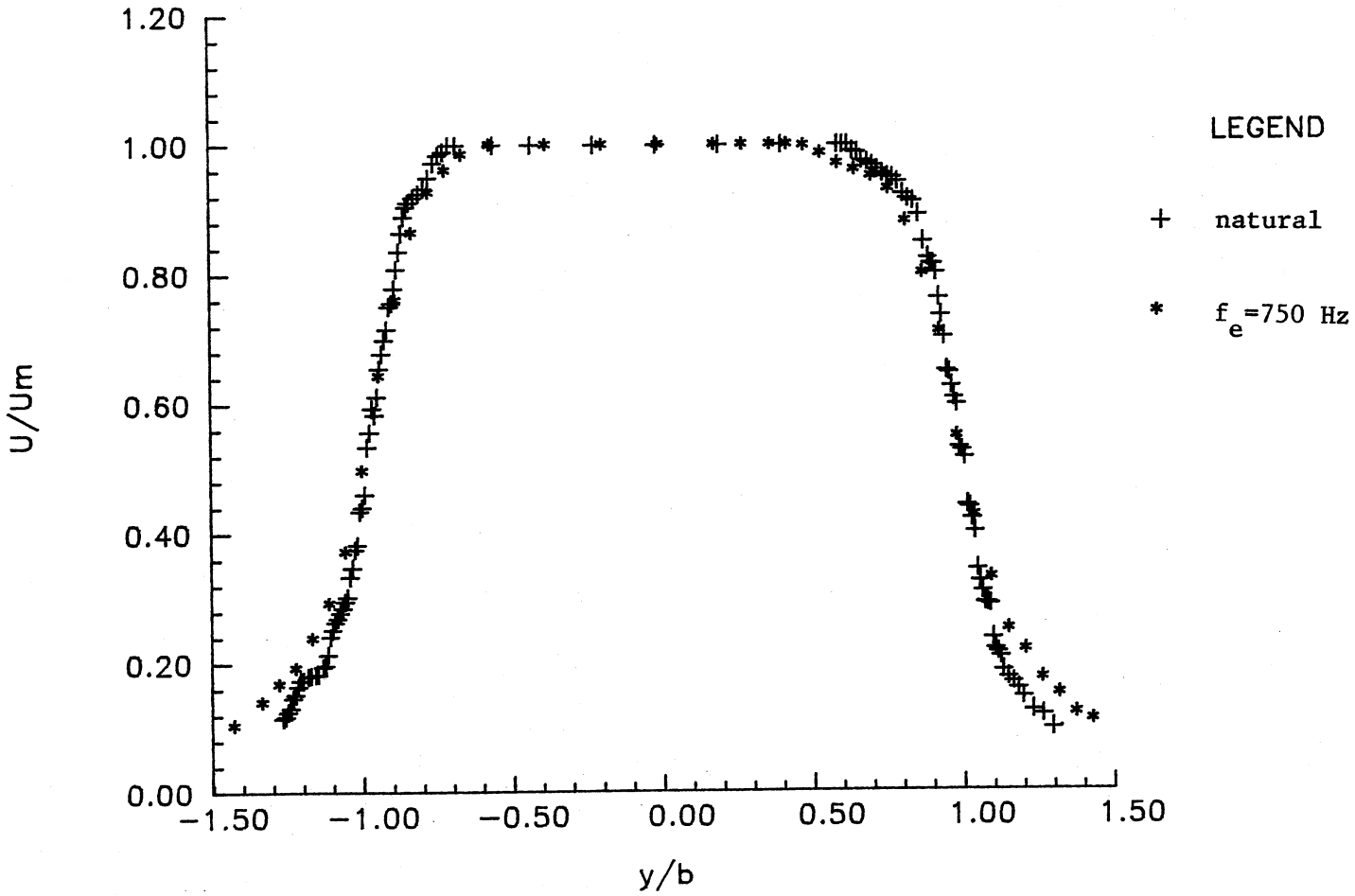

Figure 22. Comparison of Mean Flow Velocity Profile at x/D = 2

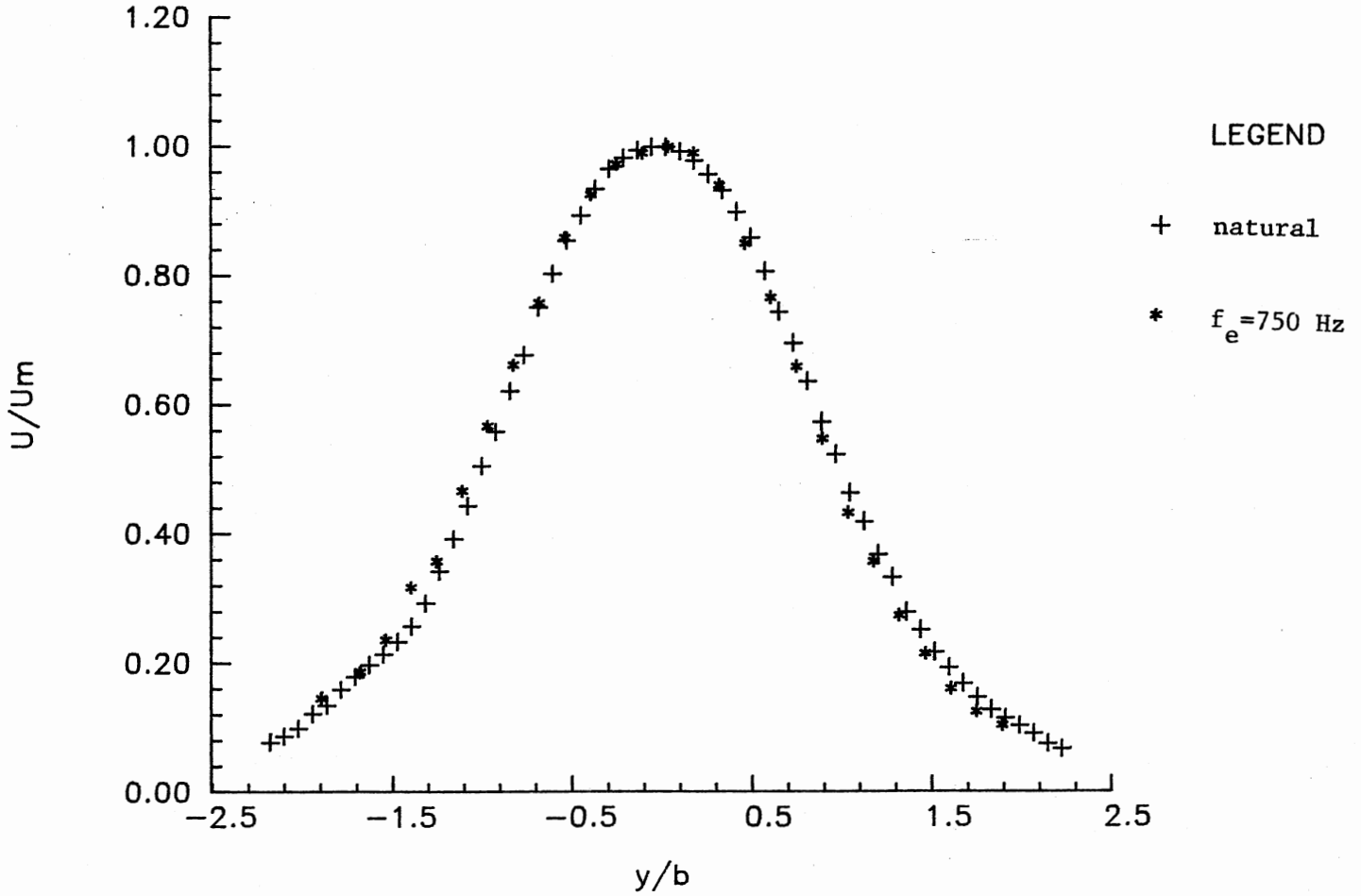

Figure 23. Comparison of Mean Flow Velocity Profile at x/D = 5

profiles for natural and excited conditions are shown in Figures 24 and 25 respectively. Figure 24 shows that the excitation increases the turbulence intensity across the entire span of the jet, though the basic profile shape remains the same. By x/D = 5 the excited case intensity has decayed to values that are generally lower than the natural jet case, though again the profile shapes are very similar.

In the following sections, the measurement of nonlinear wave interactions characterizing the transition of the excited jet by power spectra, bispectra, and coherence techniques are presented.

3.3. Power Spectral Measurements

This section presents detailed power spectral measurements which document the downstream spectral evolution of the jet under natural and excited conditions for x/D = 0.25 to 10. Power spectra are obtained in the developing jet shear layers and on the centerline of the jet.

3.3.1 Spectral Measurement Techniques

For the spectral measurements a standard "straight wire" probe was used in the constant-temperature mode. The hot-wire signals were passed through anti-alias filters and then digitized by an HP-98640A analog/digital conversion board with 1024 samples recorded for each ensemble. Typically each measurement represents an average over 150 ensembles in order to obtain a smooth and repeatable power spectrum. The sampling interval was 250μs yielding a Nyquist frequency of 2000 Hz. A Fast Fourier Transformation algorithm was used to compute the spectral density function from the digitized hot-wire signal.

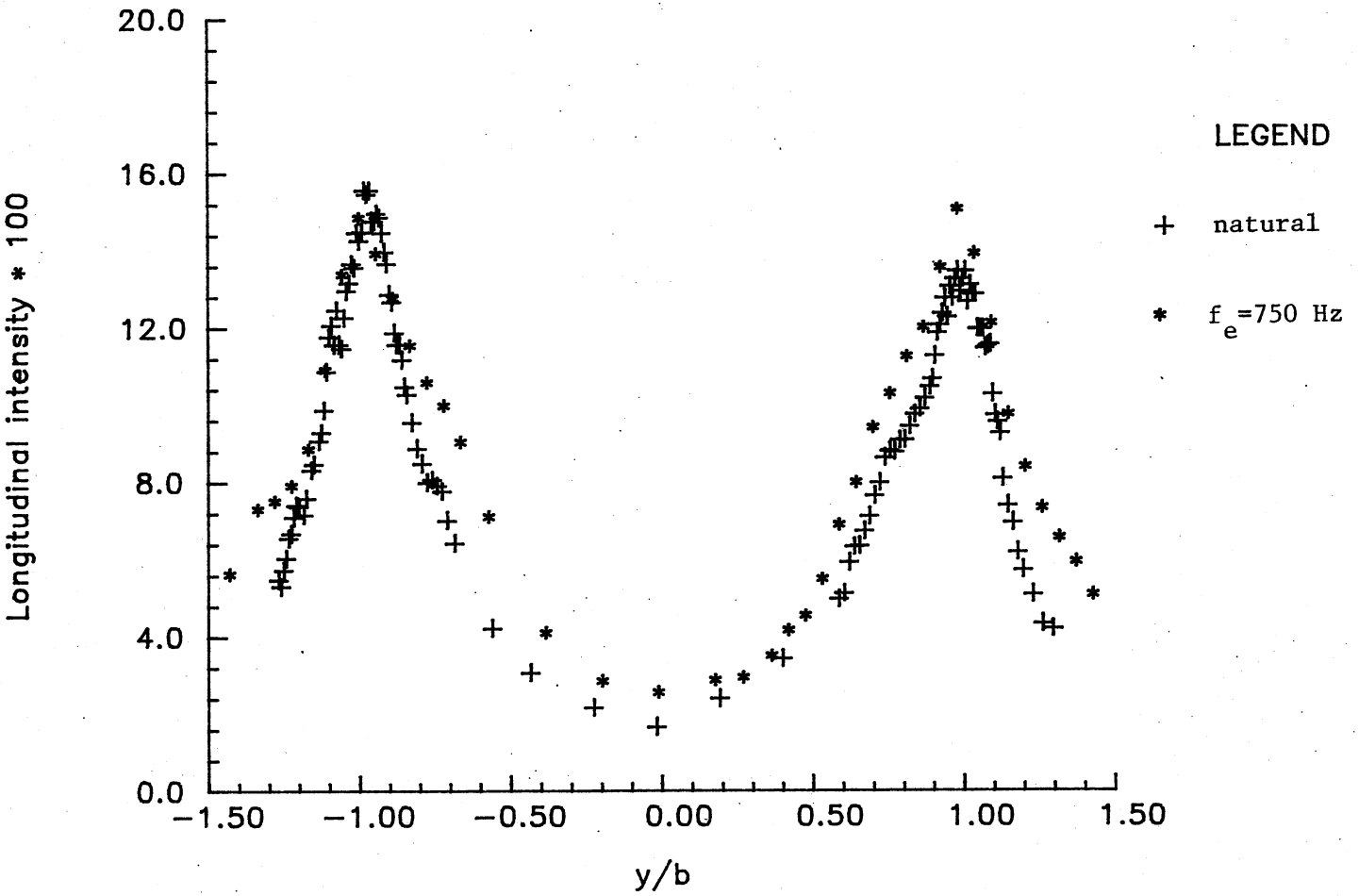

Figure 24. Comparison of Longitudinal Fluctuation Intensity Profile at x/D = 2

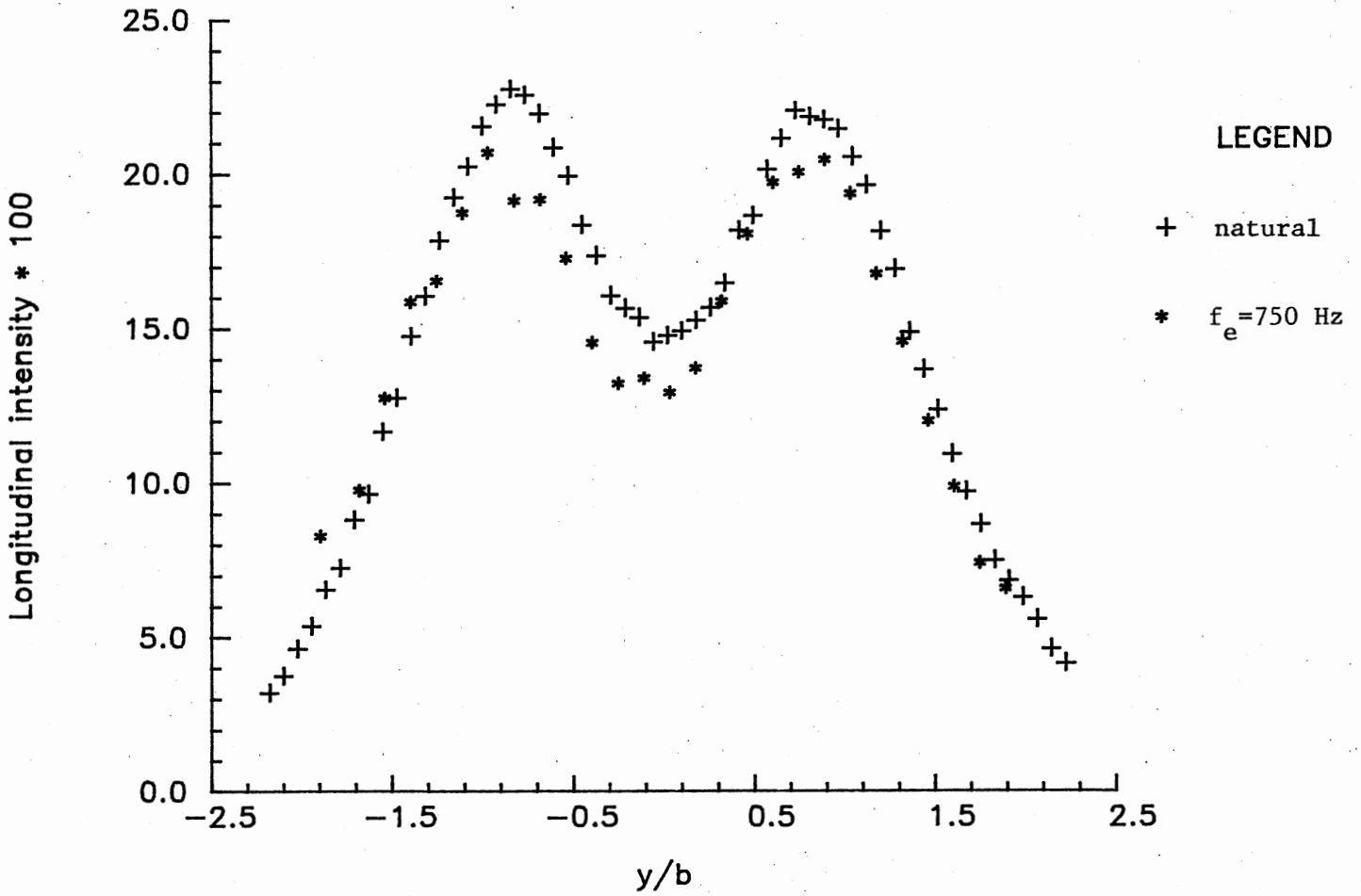

Figure 25. Comparison of Longitudinal Fluctuation Intensity Profile at x/D = 5

3.3.2. Spectral Development

Figure 26 documents the development of the excited jet shear layer power spectra at x/D = 0.25, 0.75, and 1.25. In the work to be reported "shear layer" refers to the lateral location where y/b = 1.0. The spectrum at x/D = 0.25 exhibits a dominant but low level peak near the most unstable jet shear layer frequency of 750 Hz which is due to the upstream acoustic excitation. By x/D = 0.75 the spectrum suggests the onset of nonlinear interactions between instabilities. For example, a harmonic mode forms at 1500 Hz, and spectral growth near the the subharmonic of 375 Hz may be noted. By x/D = 1.25, there is a significant increase in energy to both the 1500 Hz harmonic and nearby modes with frequency greater than 1000 Hz. Also, modulation effects appear to play an important role in the energy transfer phenomenon as evidenced by the formation of multiple sidebands. Figure 27 summarizes the downstream evolution of the fundamental, harmonic, and subharmonic excited jet shear layer modes (centered on a 7.8 Hz bandwidth) as determined from the shear layer power spectra. It may be noted from this figure that the growth of the fundamental mode is linear for x/D < 0.75 which indicates exponential amplification. The fundamental saturates at approximately x/D = 1.0. The saturation of the fundamental appears to be associated with rapid growth of the harmonic which saturates near x/D = 1.25. Beyond x/D = 0.75 the growth rate of the harmonic greatly exceeds the subharmonic, and the deviation from linear growth indicates onset of nonlinear interactions between instabilities. As is seen in Figure 27, the subharmonic exhibits reduced growth near x/D = 0.75 but recovers and becomes saturated at x/D = 2.0. Beyond x/D > 4, it seems that all three modes are in slow decay.

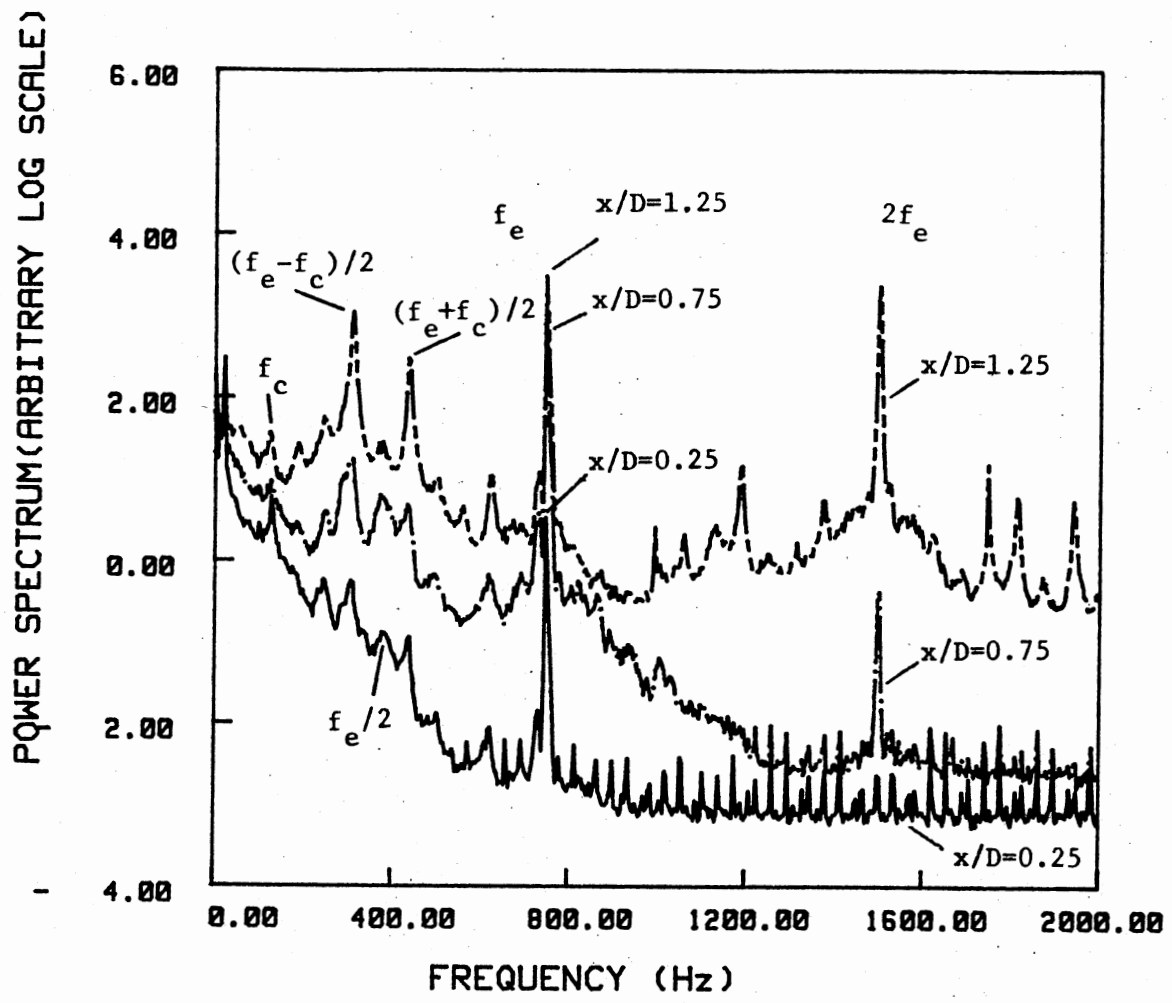

Figure 26. Initial Excited Jet Shear Layer Spectral Development at x/D = 0.25, 0.75 and 1.25

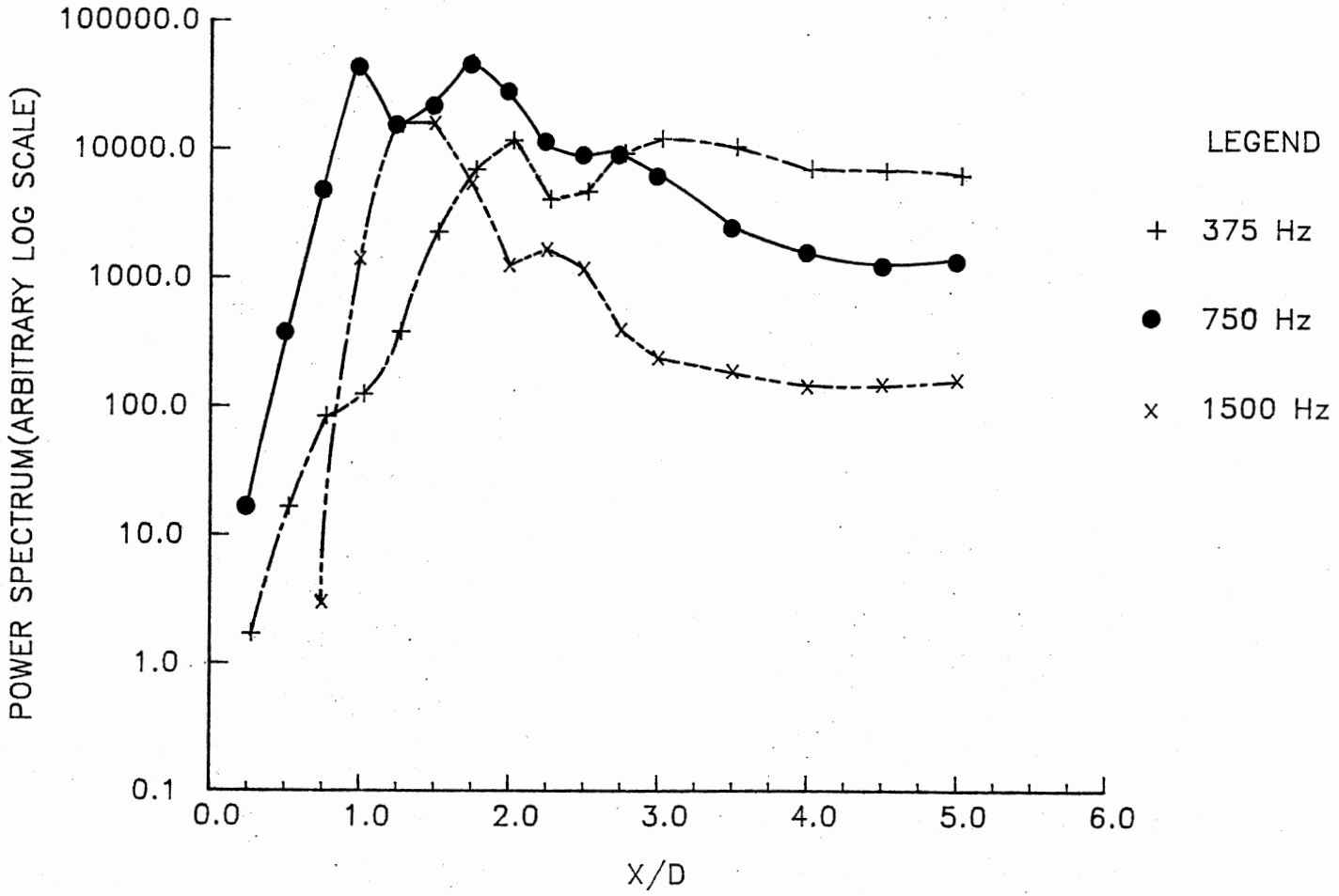

Figure 27. Comparison of Spectral Density Variation with Downstream Distance at Frequencies 375 Hz, 750 Hz and 1500 Hz

Figure 28 presents the excited jet shear layer power spectrum obtained at x/D = 1.5. This shear layer power spectrum displays multiple modes involving combinations of the primary modes $f_e/2$, f_e, $2f_e$ and the "jet column mode" f_c, which is defined as the passage frequency of the large-scale vortical structures near the end of the potential core. For this study f_c = 126 Hz. These modes suggest nonlinear interactions between the primary shear layer instability modes and the jet column mode. Figures 29-31 illustate the development of the excited jet shear layer spectra from x/D = 1.25 to 2.0. With particular emphasis on the subharmonic, Figure 29 compares the jet shear layer spectra at x/D = 1.25 and 1.5. This figure clearly shows that the development of the subharmonic is retarded while two symmetric sidebands at 312 Hz and 438 Hz grow significantly. The separation between the subharmonic and its two symmetric sidebands is approximately 63 Hz which is just half of the jet column mode, $f_c/2$. Figure 30 compares spectra at x/D = 1.5 and 1.75 and demonstrates the beginning of saturation of the modes near 312 Hz and 438 Hz. In addition this figure shows growth of the modes at f_c and the mode at $(f_e-3f_c)/2$. As shown in Figure 31, comparison of shear layer spectra at x/D = 1.75 and 2.0 indicates the continued growth of modes at f_c and $(f_e-3f_c)/2$ while the modes at 312 Hz and 438 Hz are in rapid decay. Thus, there is a fairly sudden shift in energy to the lower frequency modes. Of particular interest in the spectra which have been presented is the small growth of the subharmonic mode and the large growth of symmetric modes at $(f_e-f_c)/2$ and $(f_e+f_c)/2$. Figure 32 presents the variation of the development of the subharmonic and its two sidebands in the excited jet shear flow. The modes at 312 Hz and 438 Hz are seen to grow in a similar fashion

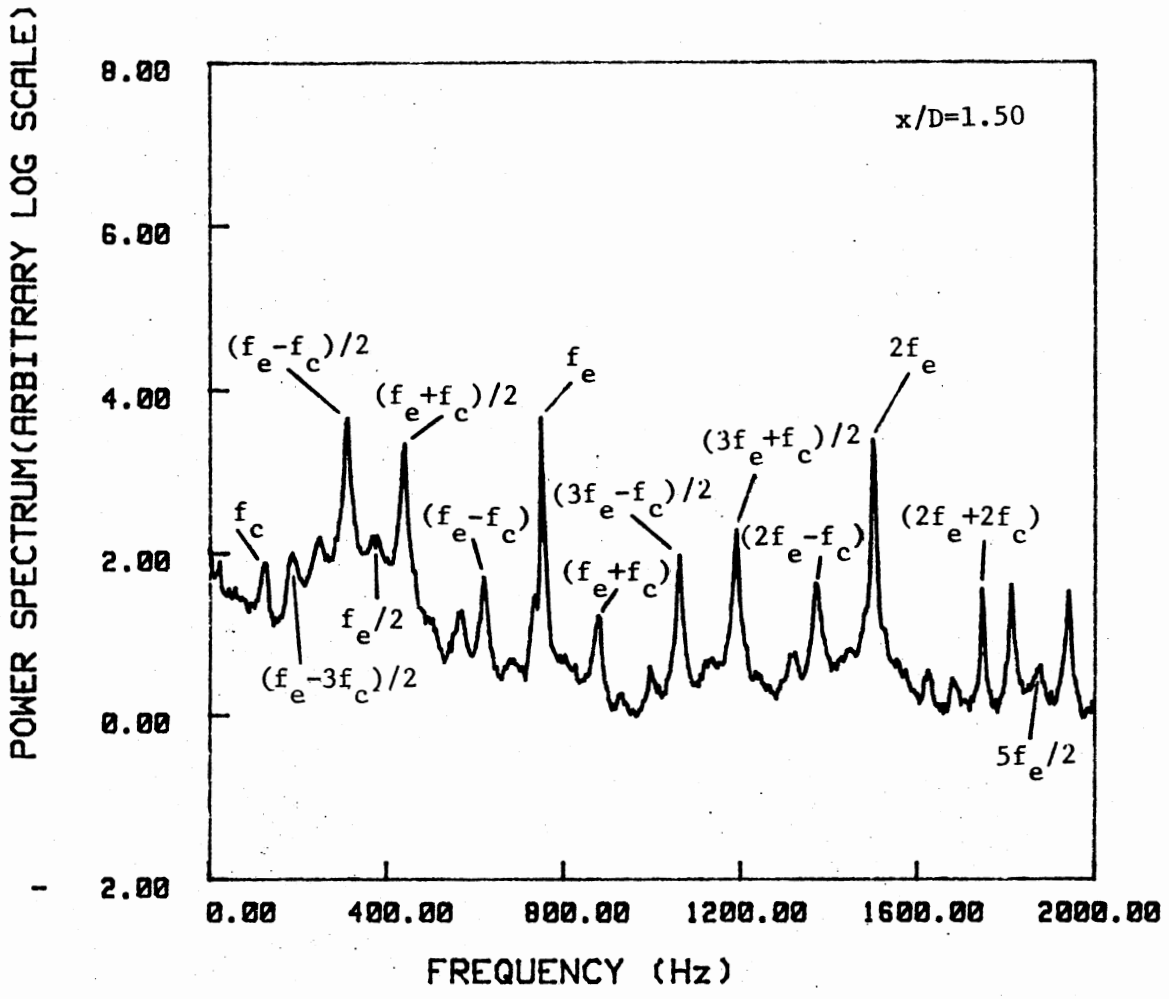

Figure 28. Excited Jet Shear Layer Power Spectrum at x/D = 1.5

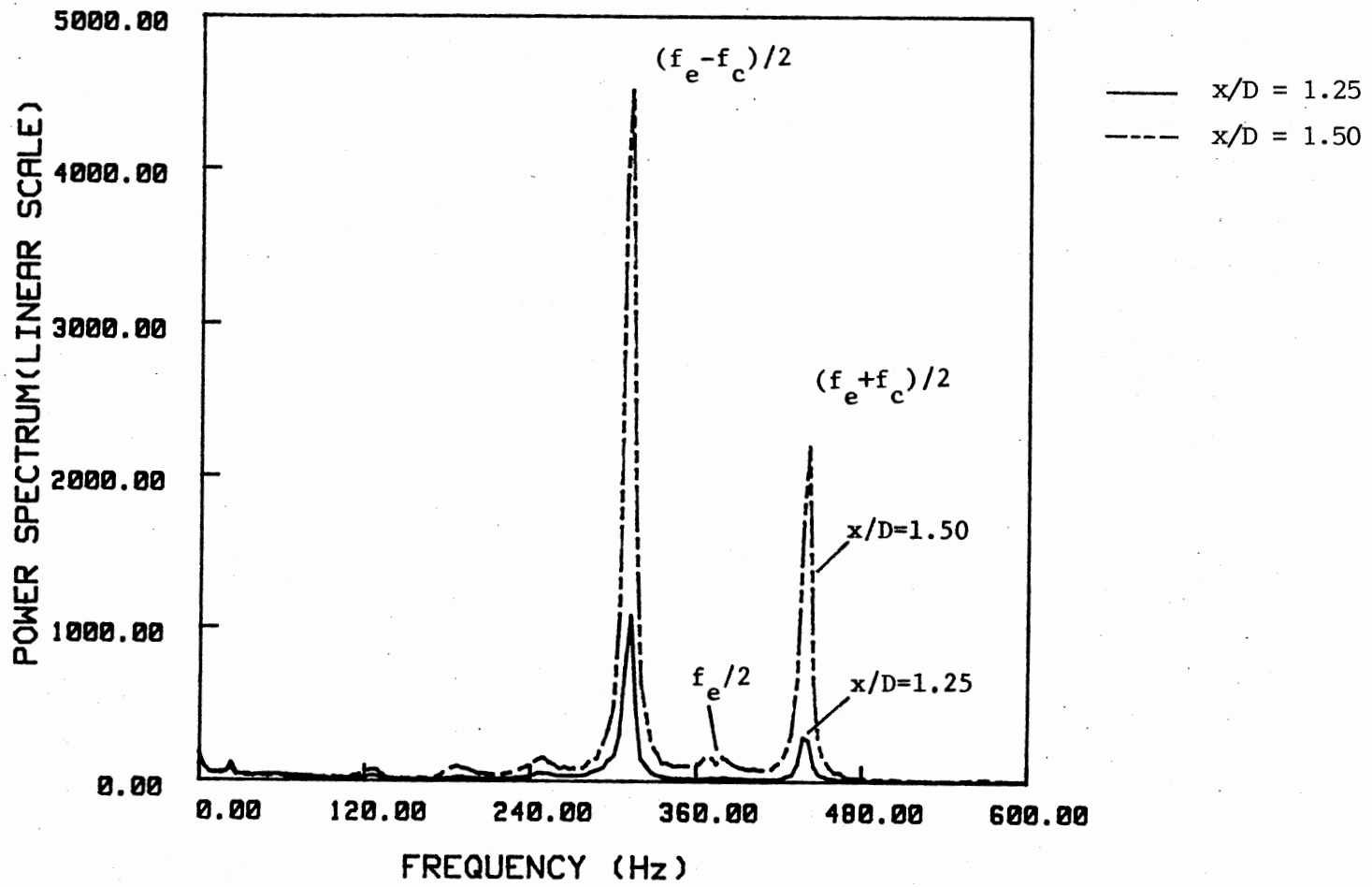

Figure 29. Comparison of the Growth of $(f_e-f_c)/2$ and $(f_e+f_c)/2$ spectral Modes at x/D = 1.25 and 1.5

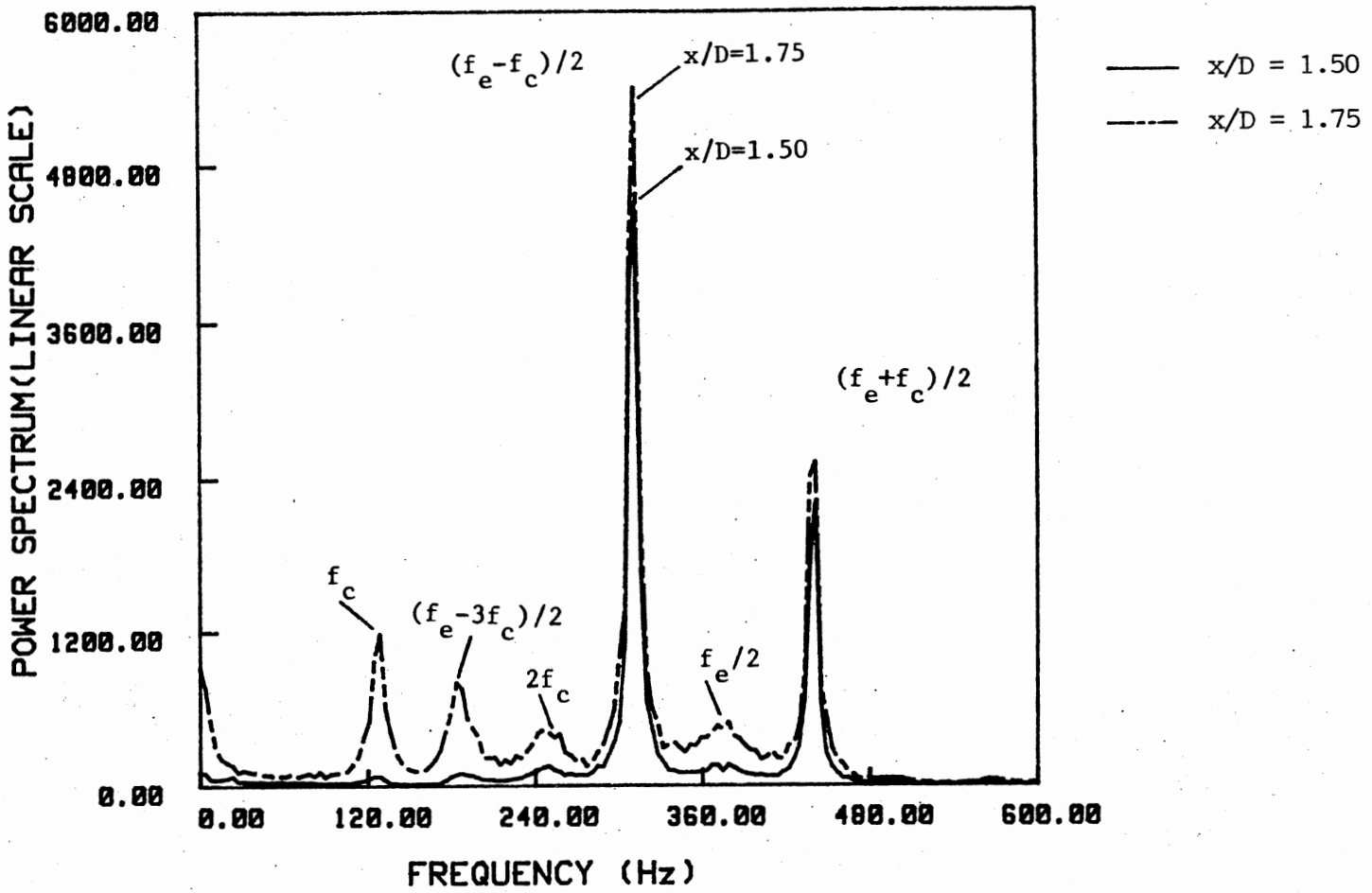

Figure 30. Comparison of the Excited Power Spectra at x/D = 1.5 and 1.75

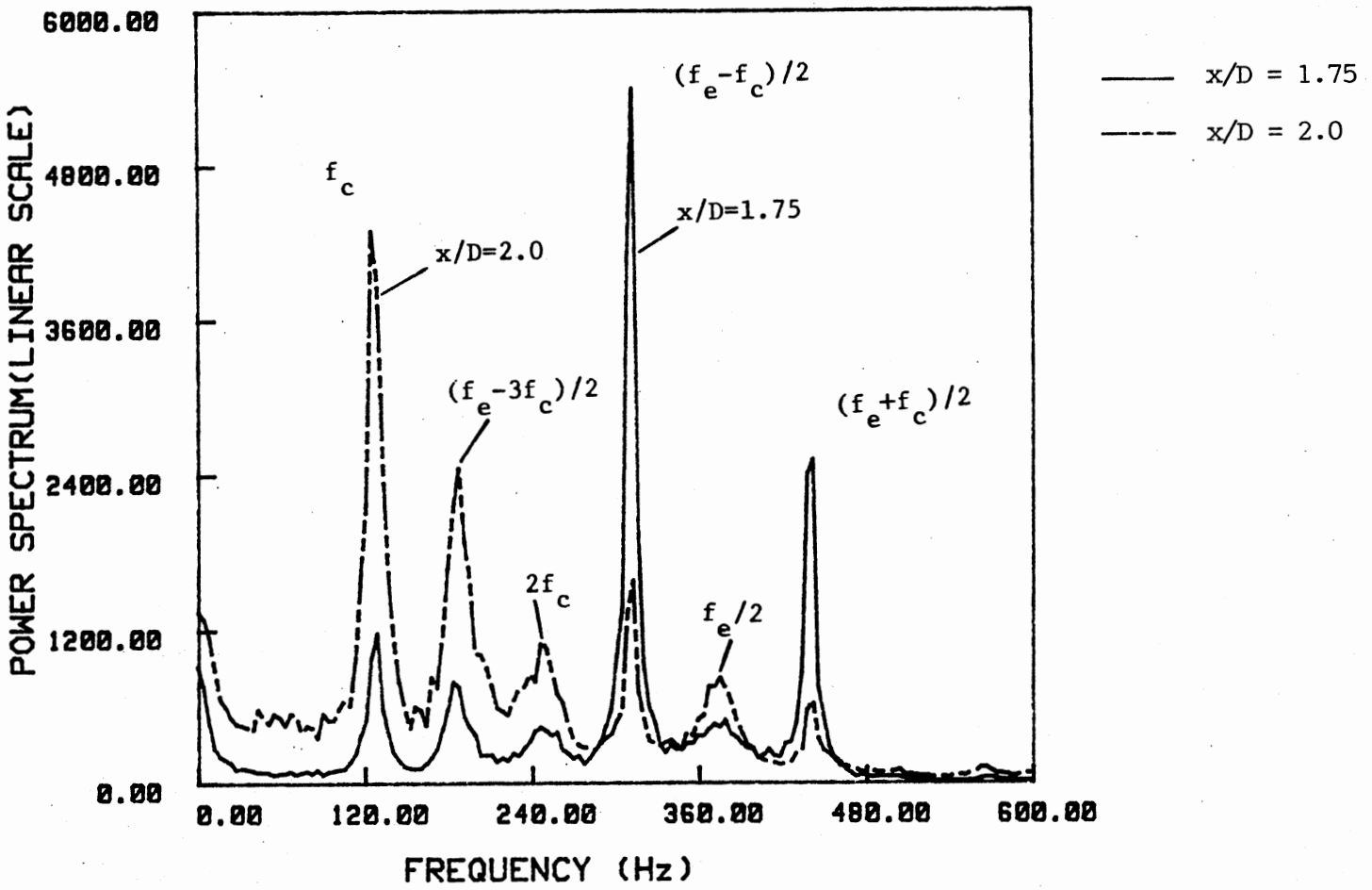

Figure 31. Comparison of the Excited Power Spectra at x/D = 1.75 and 2.0

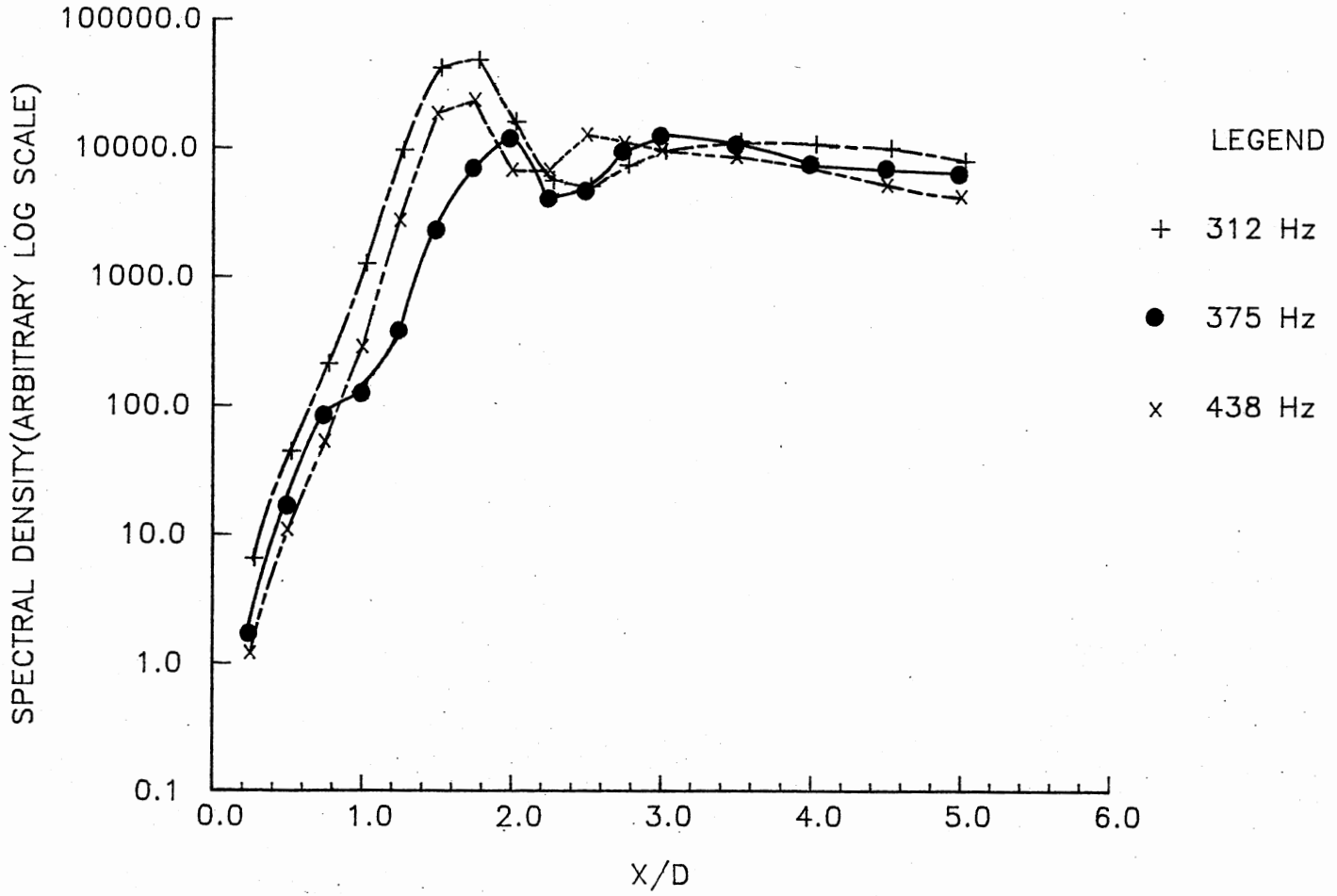

Figure 32. Variation of Spectral Density at Frequencies $(f_e-f_c)/2$, $f_e/2$ and $(f_e+f_c)/2$ with Downstream Distance

suggesting that they are related to the same phenomenon while the subharmonic exhibits a different growth pattern. As noted in the previous spectra the two modes at 312 Hz and 438 Hz will become saturated simultaneously near x/D = 1.75. The relationship between subharmonic and these two sidebands will be quantified in the next section.

Figures 33-36 present the development of the excited shear layer power spectra at x/D = 2, 2.5, 3, 4, and 5. Figure 33 compares the excited shear layer spectra at x/D = 2 and 2.5. It clearly shows the decay of the fundamental f_e, the subharmonic $f_e/2$, the lower sideband $(f_e-f_c)/2$ and the jet column mode f_c. The mode $(f_e+f_c)/2$ exhibits some growth while the saturation of the mode at $(f_e-3f_c)/2$ is apparent. It may also be noted at x/D = 2.5 that the valleys between discrete spectral modes begin to be filled due to the growth of random instabilities which characterize the transition to turbulence. The low frequency spectral content is enhanced due to the formation of a peak near $f_c/2$. Figure 34 compares the excited jet shear layer spectra obtained at x/D = 2.5 and 3. The saturation of the modes at f_c and $(f_e-3f_c)/2$ is apparent and appears to be associated with the growth of a low frequency mode at $f_c/2$. Also, the decay of the fundamental f_e, the lower sideband of the fundamental (f_e-f_c), and the upper sideband of the subharmonic $(f_e+f_c)/2$ appear to be associated with the growth of the subharmonic $f_e/2$ and its lower sideband $(f_e-f_c)/2$. The growth of the subharmonic $f_e/2$ and its lower sideband $(f_e-f_c)/2$ plays a role in filling the spectral valleys between the subharmonic and its two sidebands. In order to clearly interpret these phenomena, the detailed relationships between these primary modes will be discussed in the next

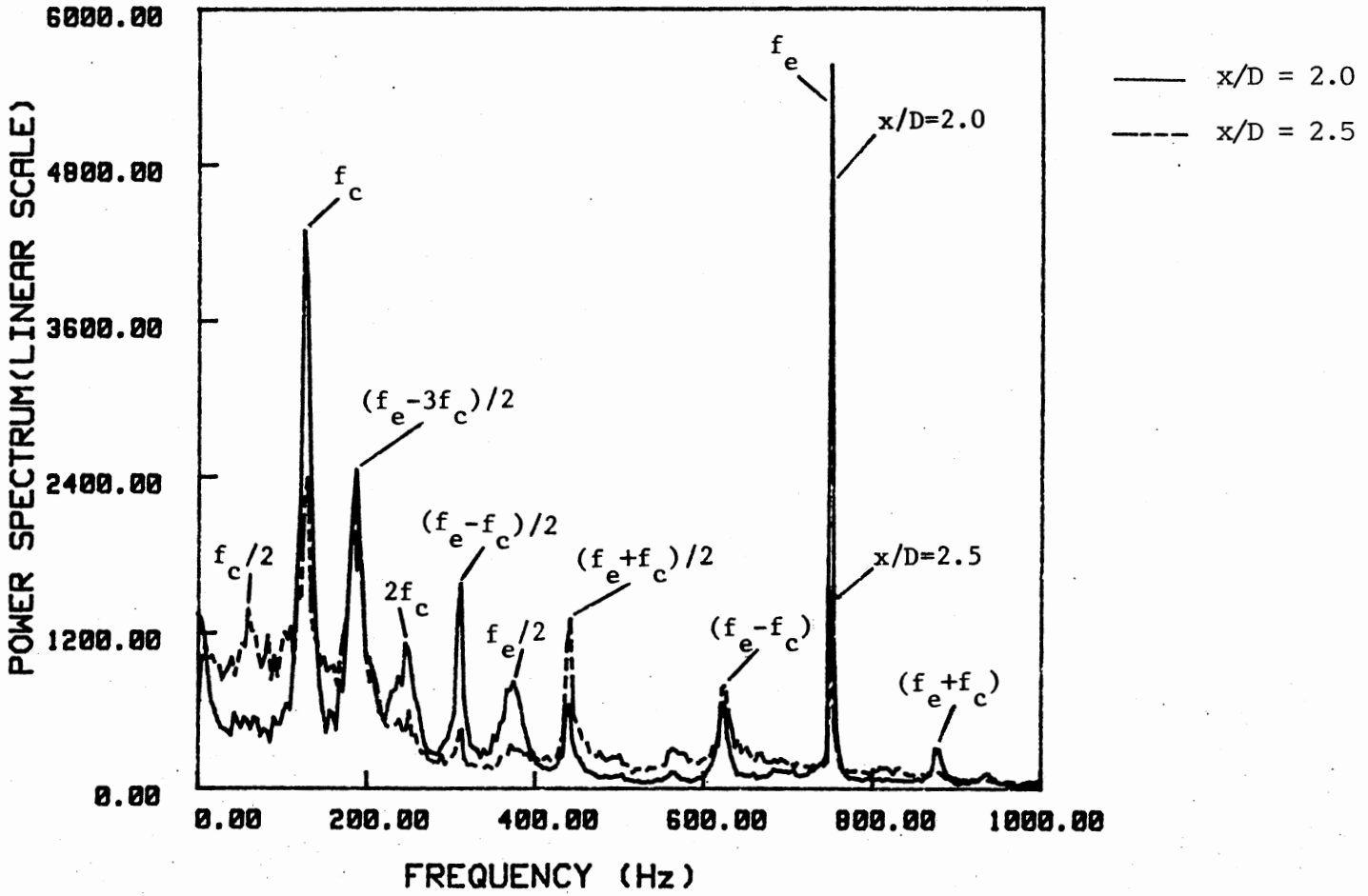

Figure 33. Comparison of the Excited Power Spectra at x/D = 2.0 and 2.5

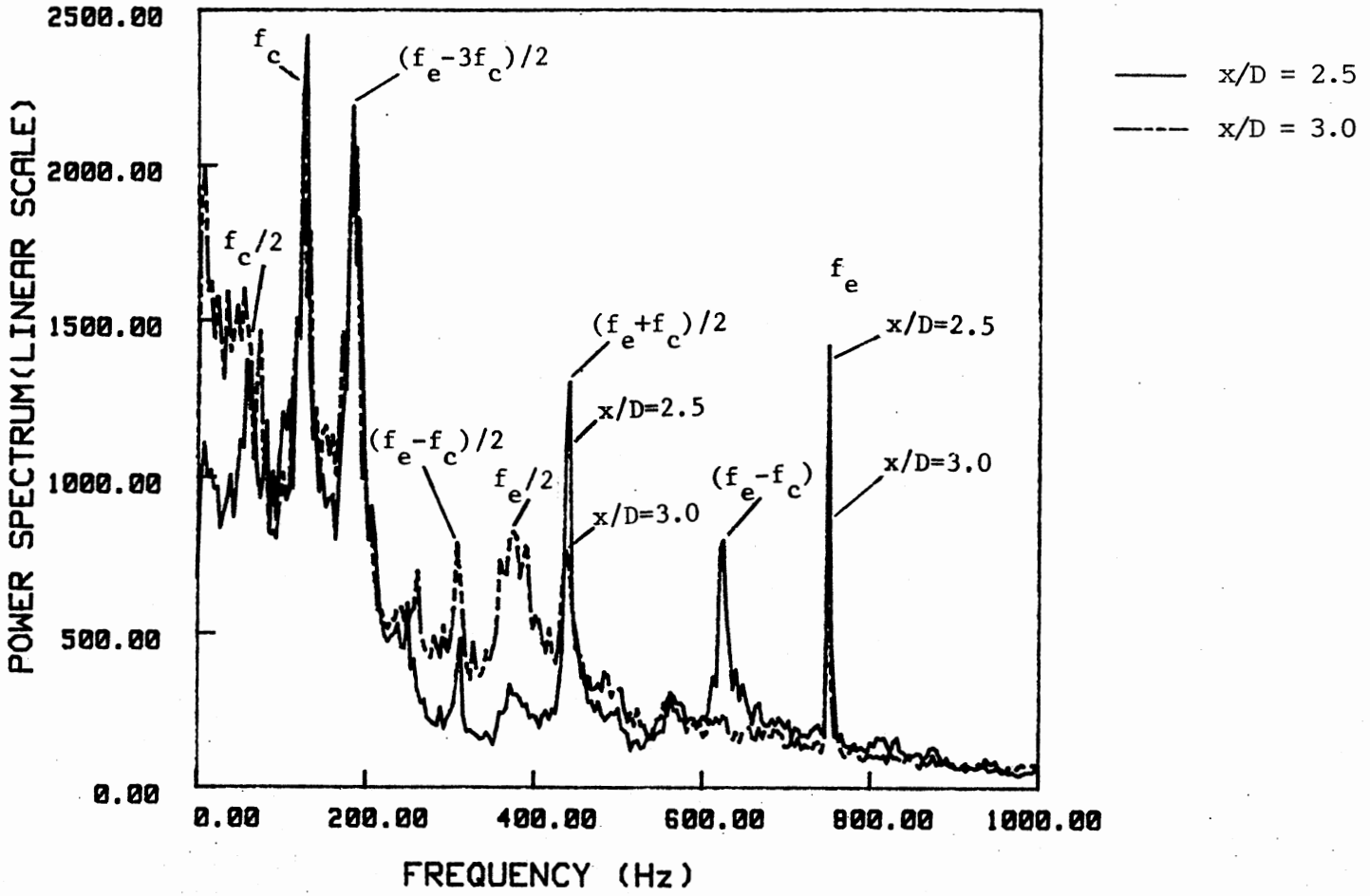

Figure 34. Comparison of the Excited Power Spectra at x/D = 2.5 and 3.0

section. Figure 35 at x/D = 3 and 4 clearly demonstrates renewed growth of the jet column mode and low frequency modes while other modes are in slow decay. Considerable "smoothing" of the spectrum has occurred and the spectrum at x/D = 4 becomes more broadband in nature. Figure 36 shows the excited jet shear layer spectrum obtained at x/D = 5. It is a broadband power spectrum with no dominant peaks observed. Excited jet shear layer power spectra obtained farther downstream are not shown but are also basically broadband in nature which is indicative of the flow being fully turbulent at these locations.

The power spectra which have been presented above were obtained with low level acoustic excitation at the initially most unstable jet shear layer frequency. It is expected that results inferred from the excited jet spectra will be applicable to the case of "natural" jet transition as well since the excitation amplitude was very low with the jet shear layer inflectional instability mechanism providing the amplification. The following data presents a comparison of jet shear layer spectra under excited and natural conditions for selected downstream locations. In particular, Figures 37-39 compare shear layer power spectra under natural and excited conditions at x/D = 0.5, 1.5, and 2.0, respectively. It is clearly seen from these figures that the excited power spectra basically follow the shapes of the unexcited power spectra except for discrete modes that are introduced by the acoustic excitation. In effect, the natural jet spectra resemble "smoothed" or randomized versions of the corresponding excited cases. This is to be expected since the primary function of excitation at the most unstable frequency is to organize the initial instabilities. Therefore, the comparison of natural and excited shear layer power spectra shown above

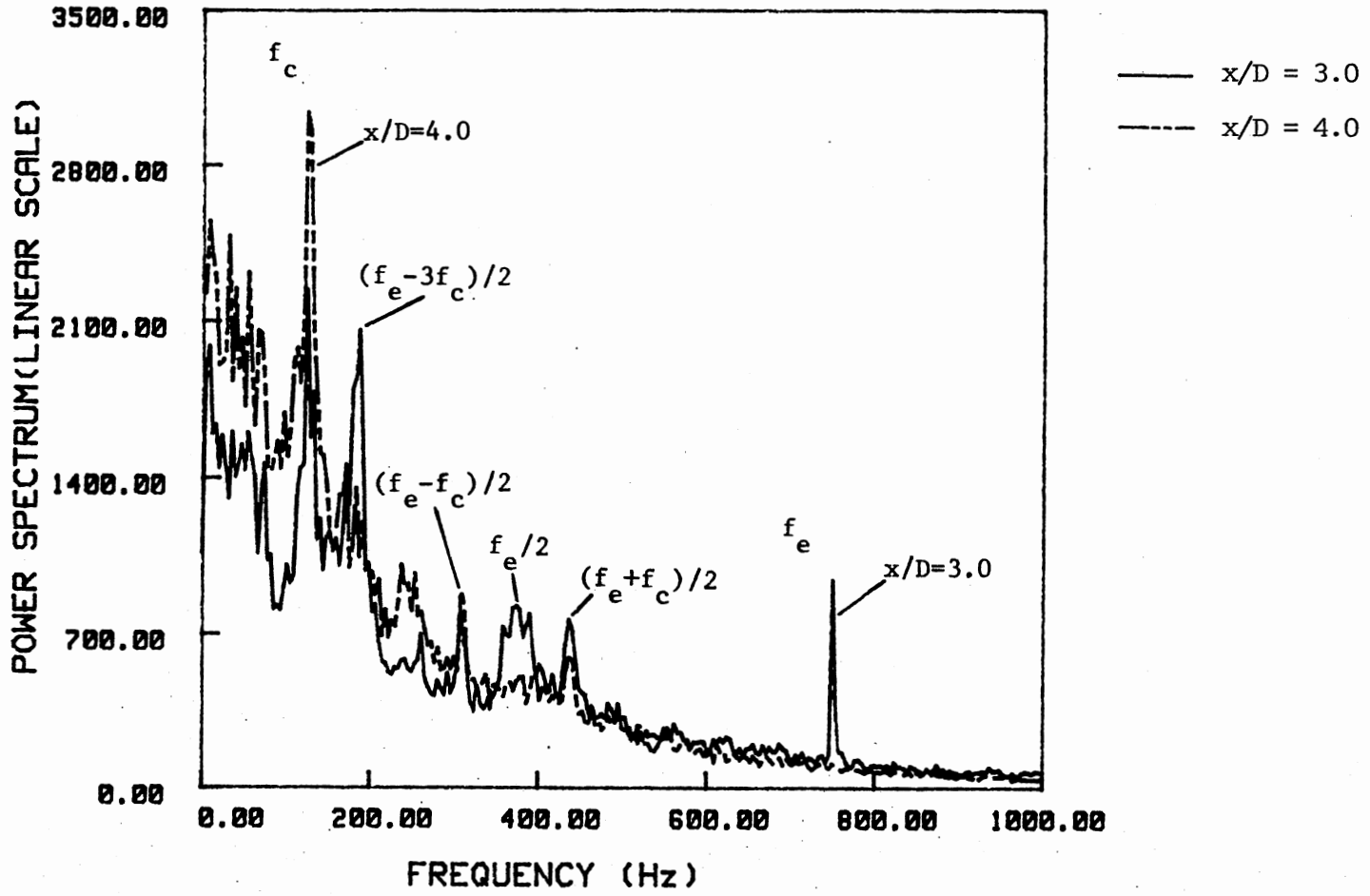

Figure 35. Comparison of the Excited Power Spectra at x/D = 3.0 and 4.0

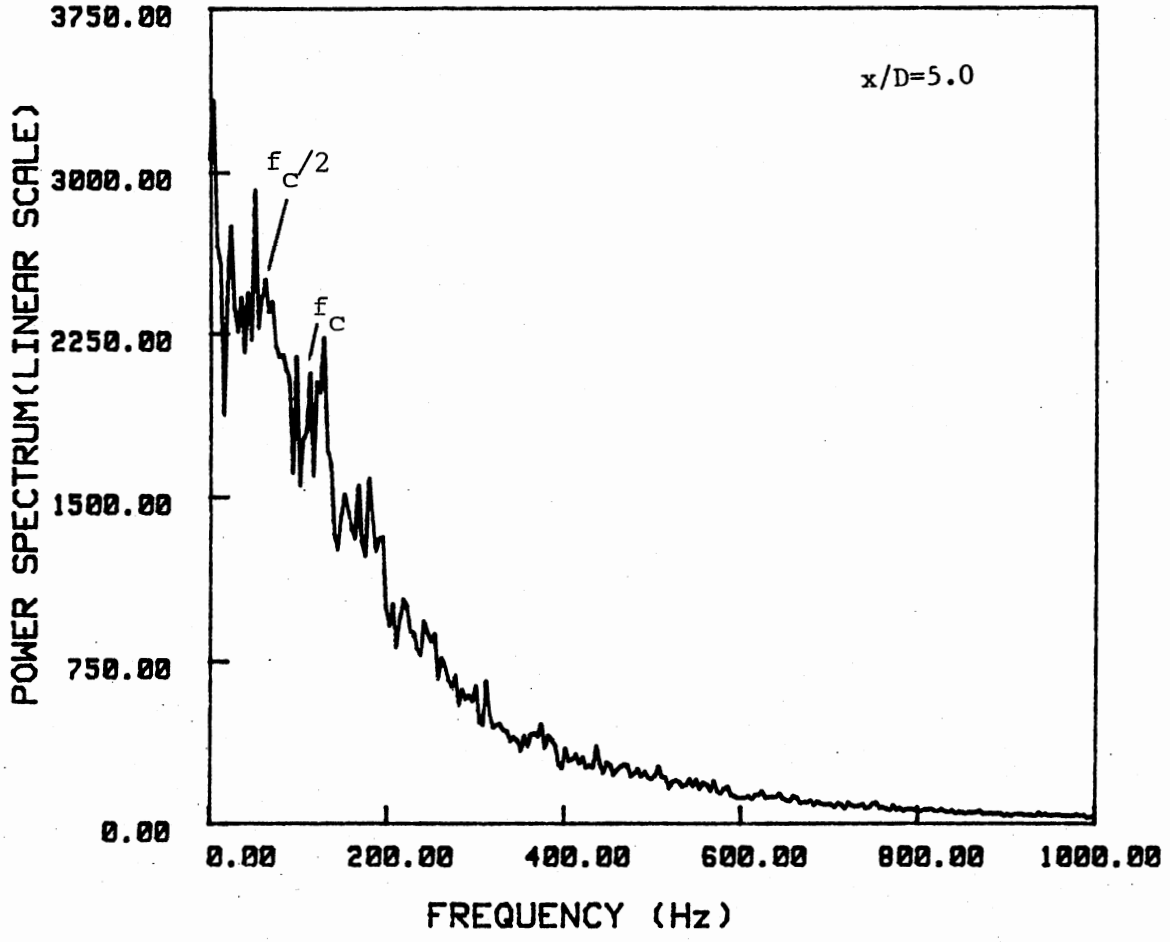

Figure 36. Excited Jet Shear Layer Power Spectrum at x/D = 5.0

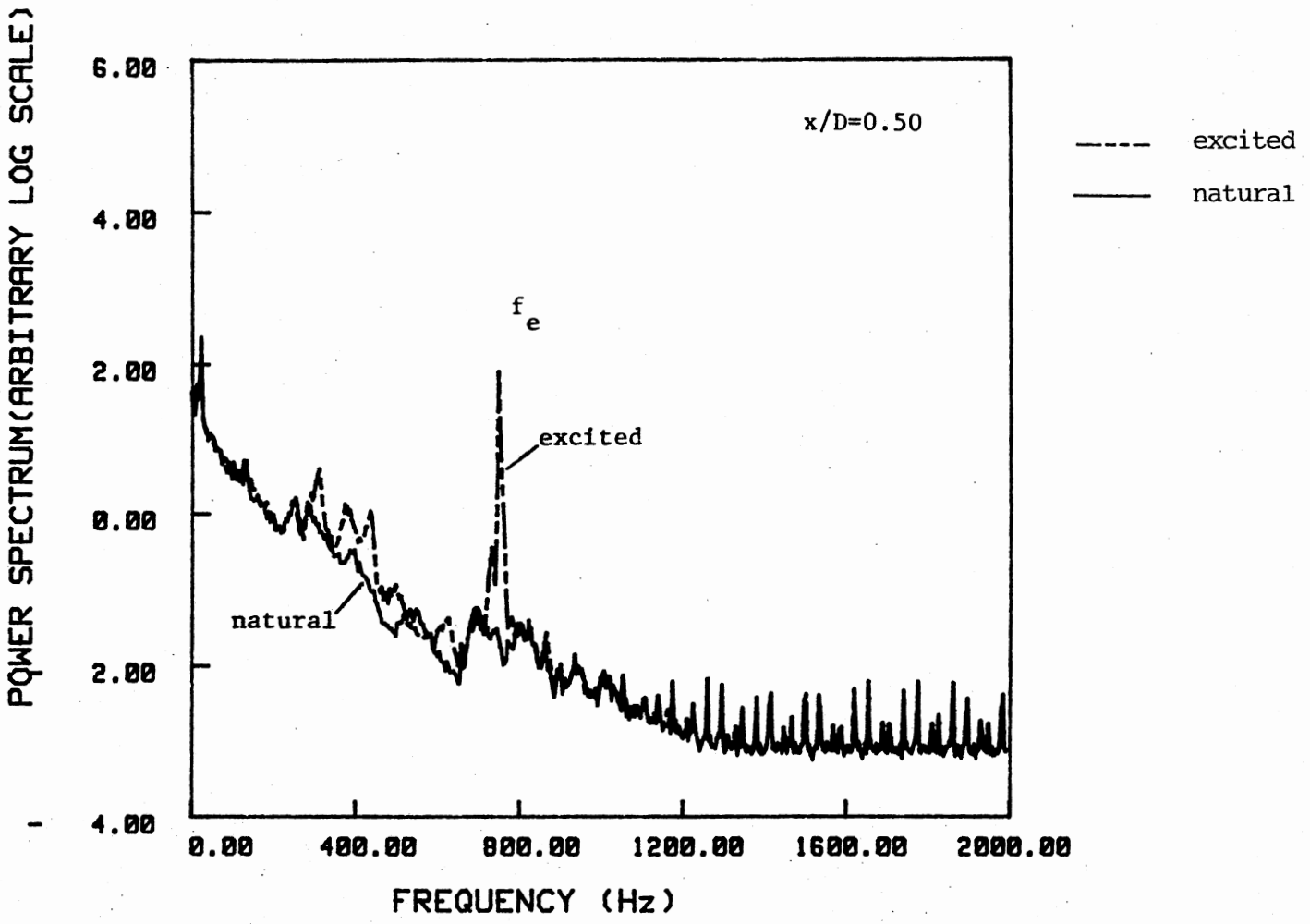

Figure 37. Comparison of the Jet Shear Layer Power Spectra at x/D = 0.5

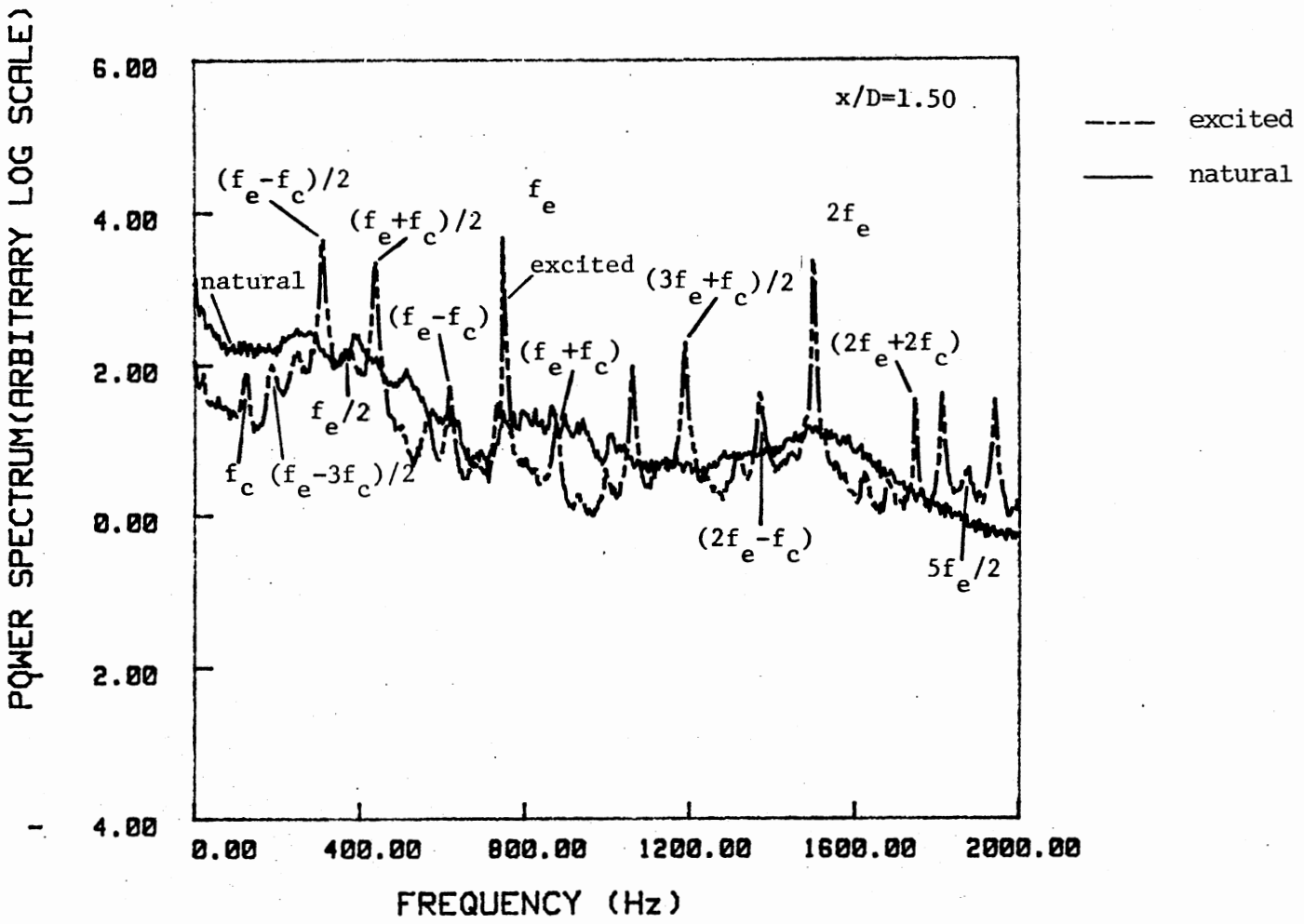

Figure 38. Comparison of the Jet Shear Layer Power Spectra at x/D = 1.5

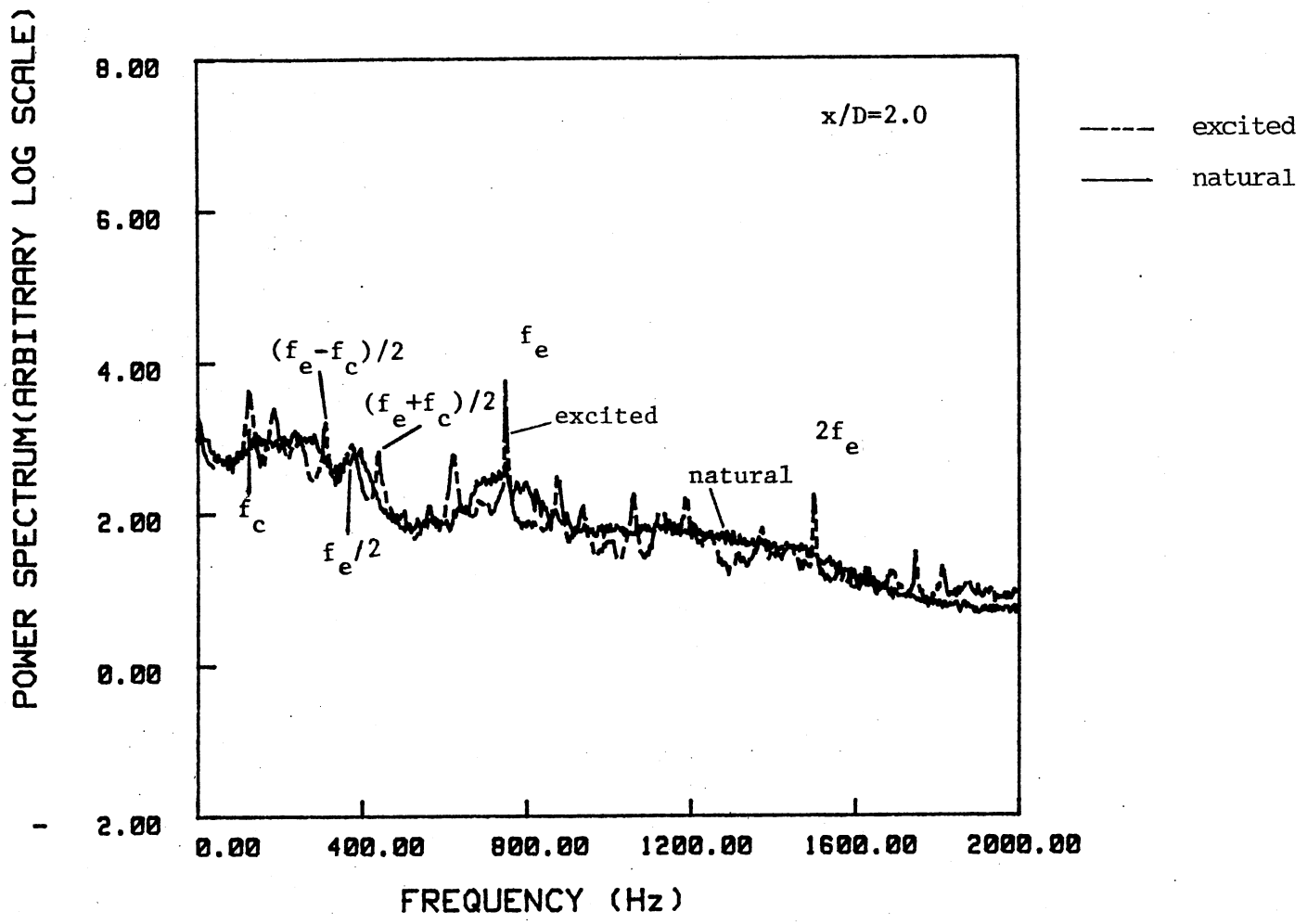

Figure 39. Comparison of the Jet Shear Layer Power Spectra at x/D = 2.0

support the previous assumption that the excited jet study is applicable to the "natural" jet transition. The presented results regarding the transition of the excited jet should facilitate a better understanding of the natural jet transition.

Since the excited jet shear layer spectra are broadband beyond x/D = 5 due to the large turbulence intensity that characterizes the shear layer, it is difficult to discern details regarding the further development of structural patterns in the flow. It is expected, however, that the power spectra measured on the jet centerline may show more distinct peaks as compared to those obtained in the shear layer spectra due to reduced turbulence levels. Therefore, in order to obtain more information about the transition of the jet, the spectra of longitudinal velocity fluctuations were measured on the jet centerline for both natural and excited conditions for x/D = 4 to 10 and are sequentially presented in Figures 40-46. The natural and excited centerline spectra obtained at x/D = 4 are compared in Figure 40. The excited case exhibits four peaks at 312 Hz = $(f_e-f_c)/2$, 253 Hz = $(2f_c)$, 186 Hz = $(f_e-3f_c)/2$, and 126 Hz = (f_c). The separation between consecutive peaks is approximately 63 Hz which corresponds to the half of the jet column mode. Each of these modes were present at higher amplitude in the shear layer spectra which suggests that the peaks observed reflect the presence of shear layer modes on the jet centerline. The peaks are "cleaner" due to the lower centerline turbulence levels. Notice also the similarity between the excited and natural jet centerline spectra at x/D = 4. The natural case resembles a smoothed version of the excited spectrum.

It may be noted from Figures 41 and 42 that by x/D = 5 and 6 only

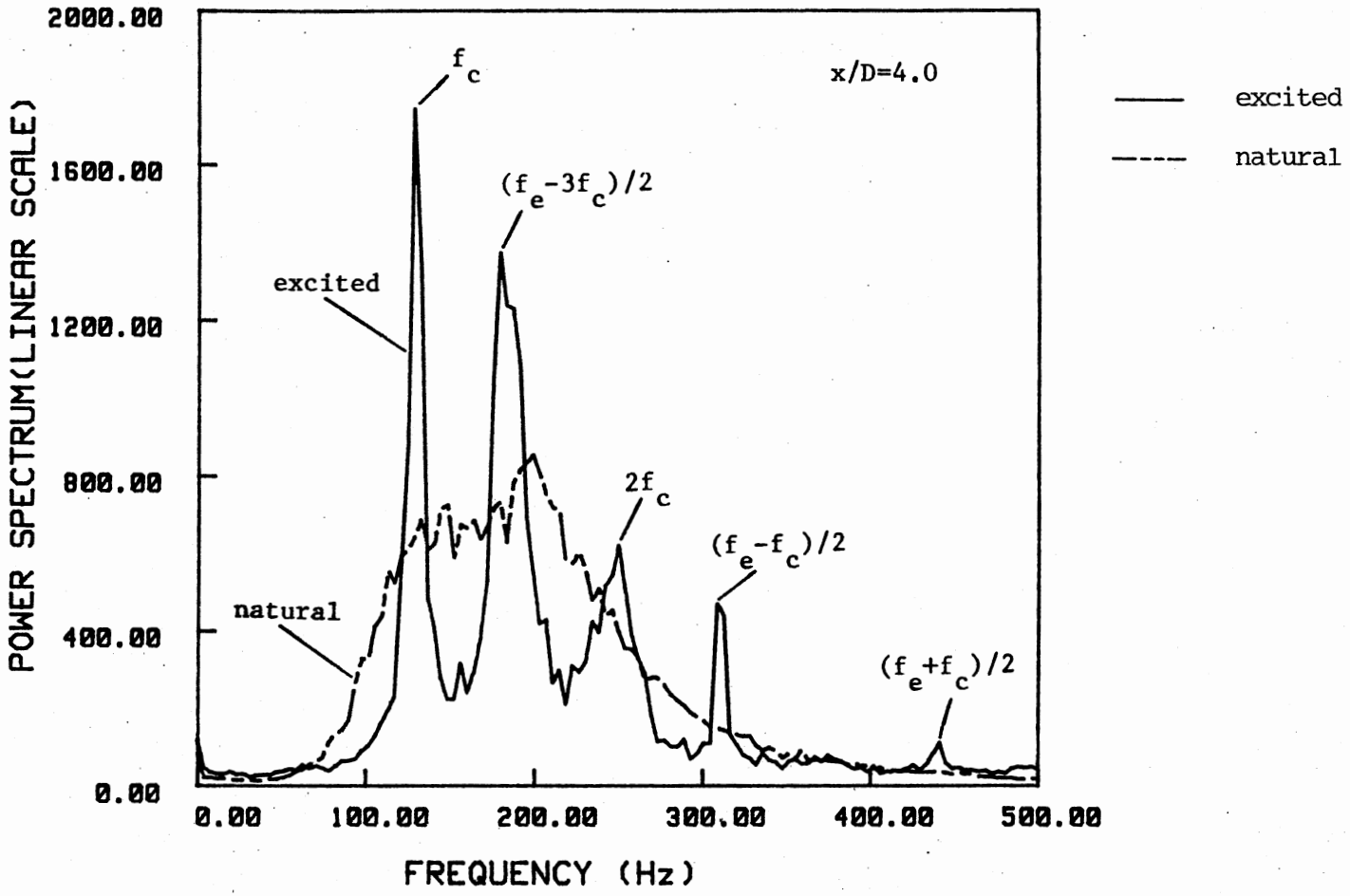

Figure 40. Comparison of the Natural and Excited Centerline Power Spectra at x/D = 4.0

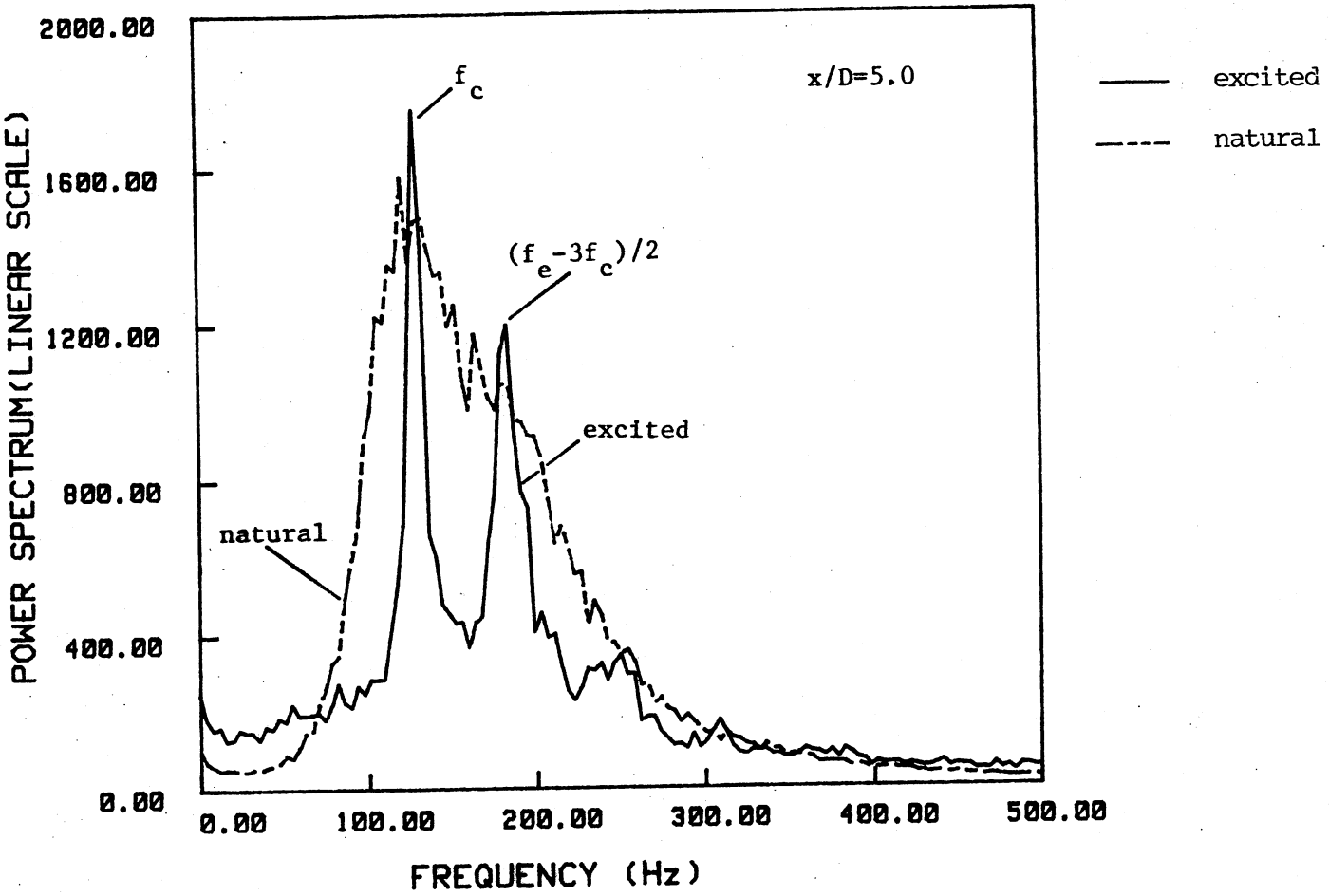

Figure 41. Comparison of the Natural and Excited Centerline Power Spectra at x/D = 5.0

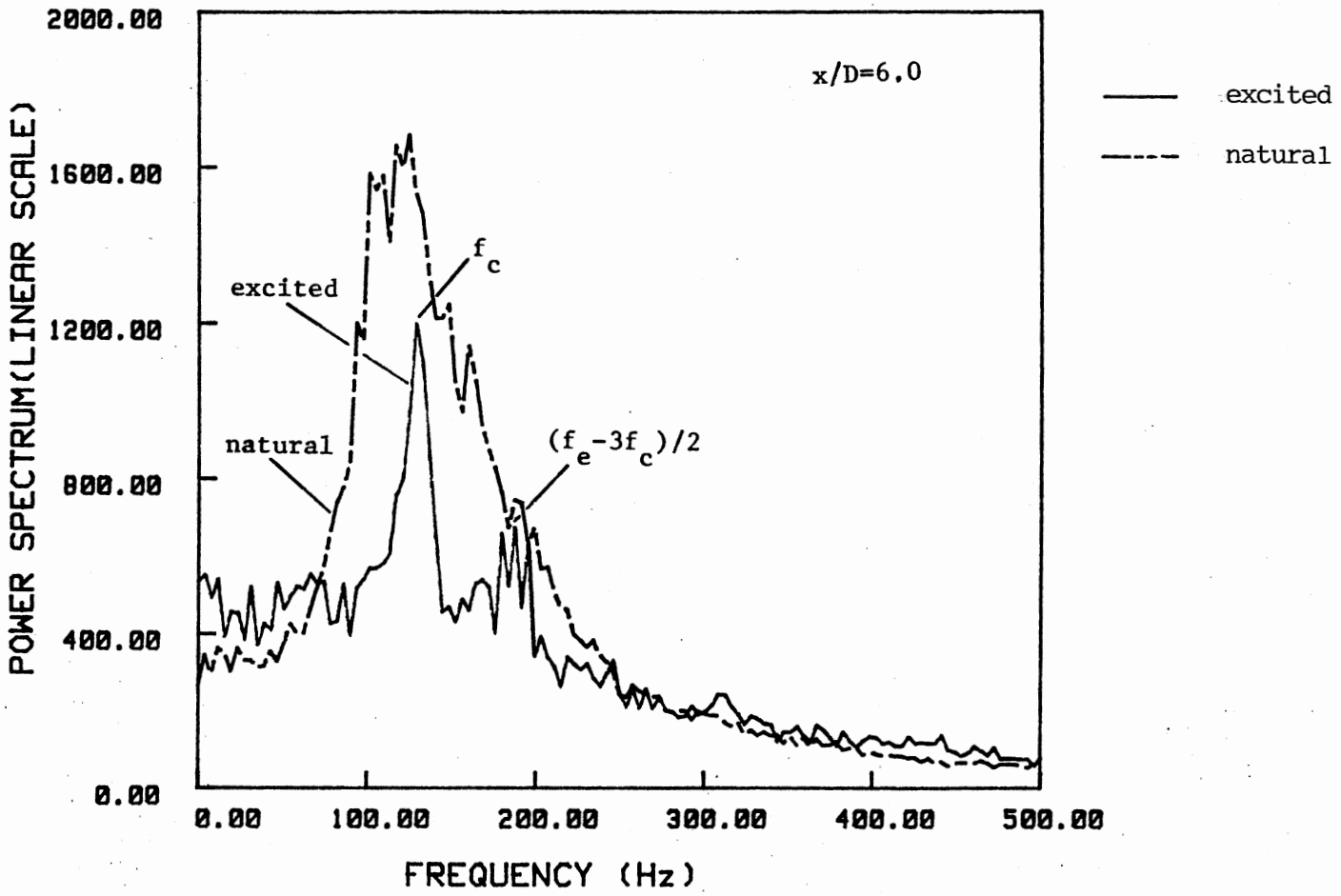

Figure 42. Comparison of the Natural and Excited Centerline Power Spectra at x/D = 6.0

two dominant peaks may be found from the excited cases. These occur at the jet column mode f_c, and at $(f_e-3f_c)/2$. The other higher frequency discrete modes present at x/D = 4 have decayed. The frequency of the highest peak is 126 Hz which corresponds to the structural passage frequency near the end of potential core. The natural jet spectra also shows a strong peak at this frequency indicating that the application of excitation has not changed the jet column mode frequency. However, the total energy in this mode is greater in the natural case as is evident from a comparison of the spectra. With increasing downstream distance there is a gradual shift in energy to half of the jet column mode as seen in Figure 43 at x/D = 7. The lower frequency mode may correspond to the merging of structures beyond the jet potential core as was suggested by Prakash (1986) for natural jet transition. Such an event is obscure in the downstream shear layer spectra due to the presence of the high turbulence levels for x/D > 5. The natural jet centerline spectrum obtained at x/D = 8 in Figure 44 shows two broad bands near the jet column mode and its subharmonic $f_c/2$ while the excited shear layer spectrum just exhibits one dominant band near $f_c/2$ mode. These spectra suggest that beyond the potential core the developing planar turbulent jet still contains organized components as evidenced by the interactions of the jet column mode f_c and its subharmonic mode $f_c/2$. Figures 45 and 46 at x/D = 9 and 10 show a comparison of the excited and natural centerline spectra. Though these spectra are broadband in nature they exhibit a broad peak at half of the jet column mode which suggests that this mode will play an important role with increasing downstream distance. Also, the higher frequency modes are in decay at these downstream locations which is due to the formation of the random

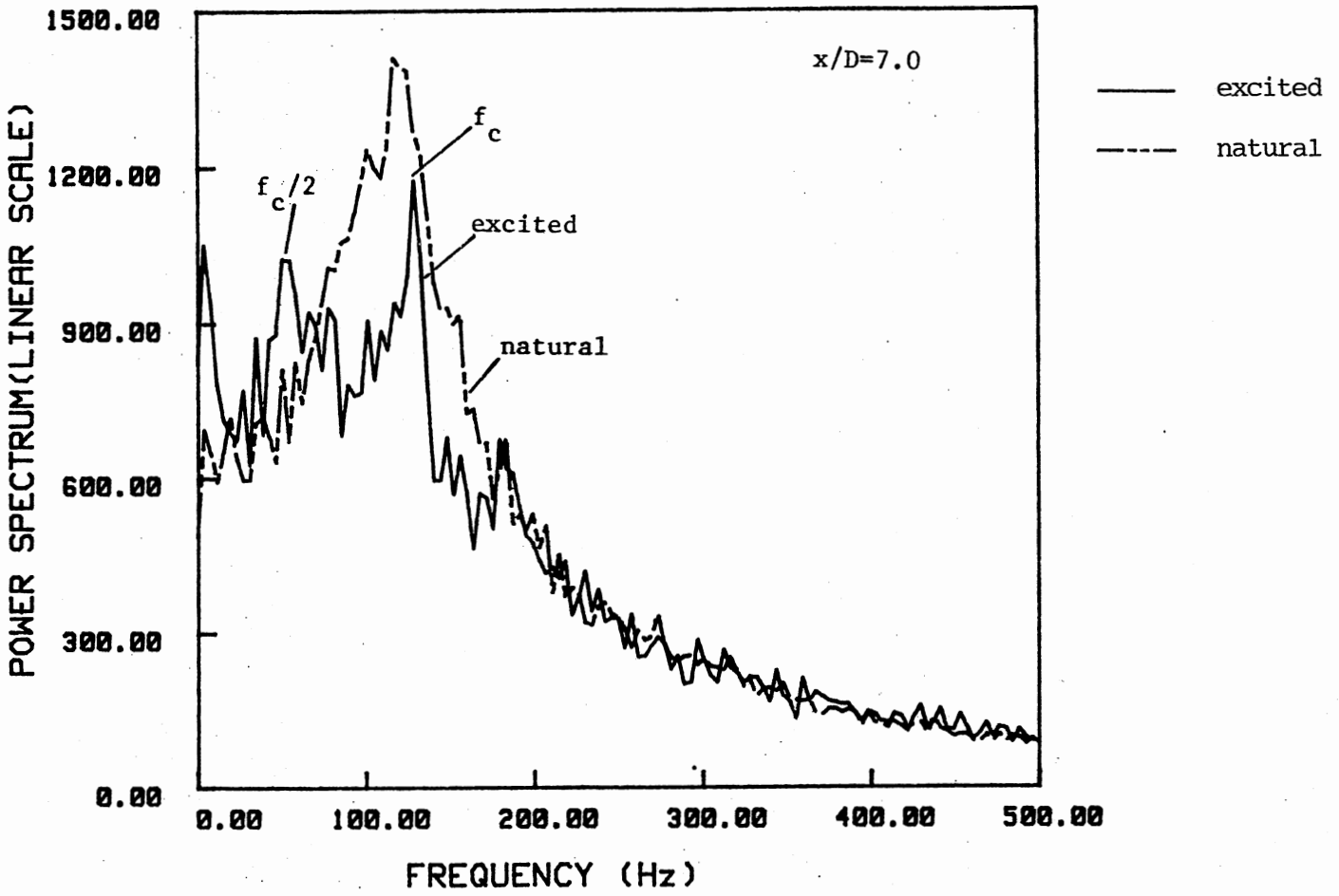

Figure 43. Comparison of the Natural and Excited Centerline Power Spectra at x/D = 7.0

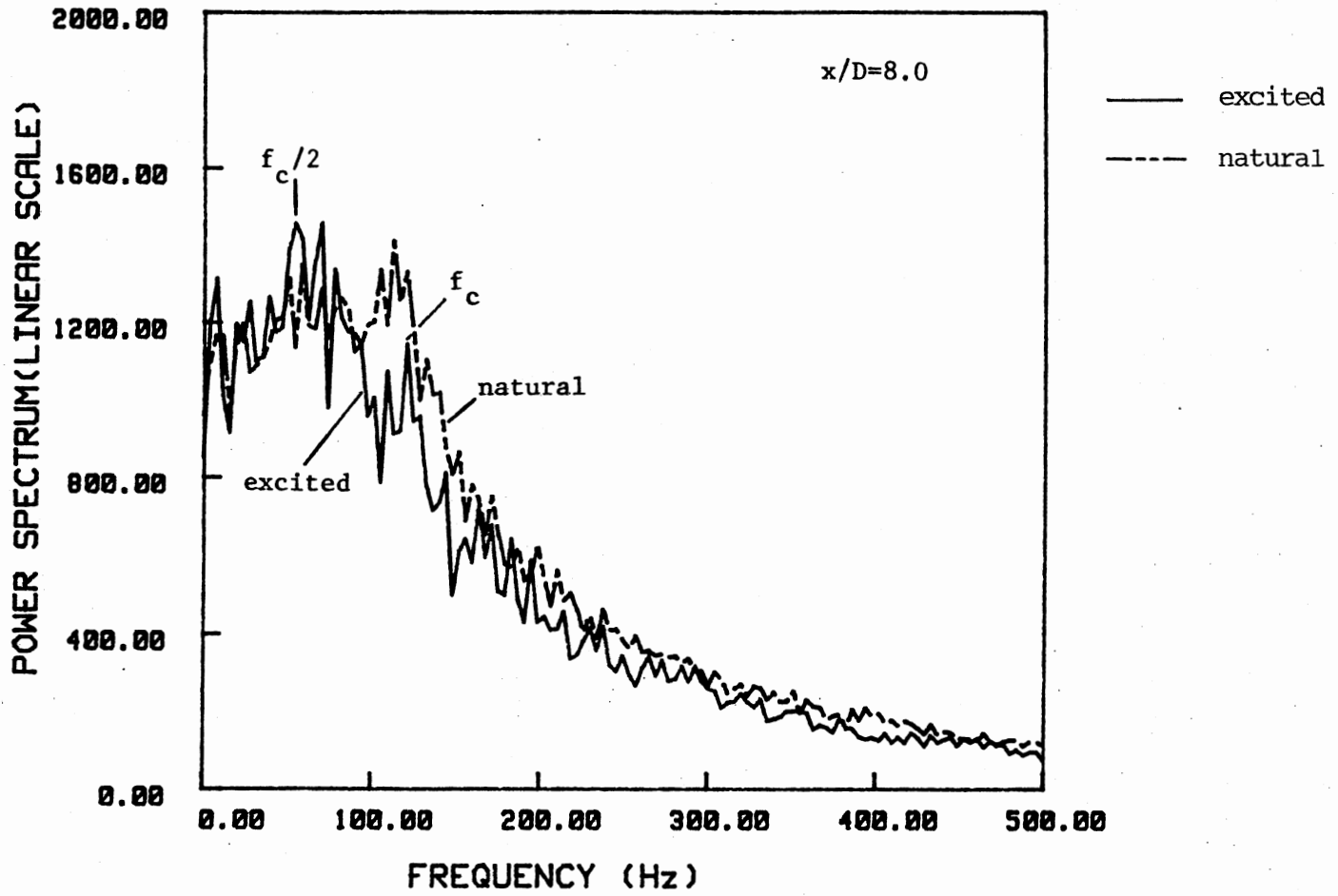

Figure 44. Comparison of the Natural and Excited Centerline Power Spectra at x/D = 8.0

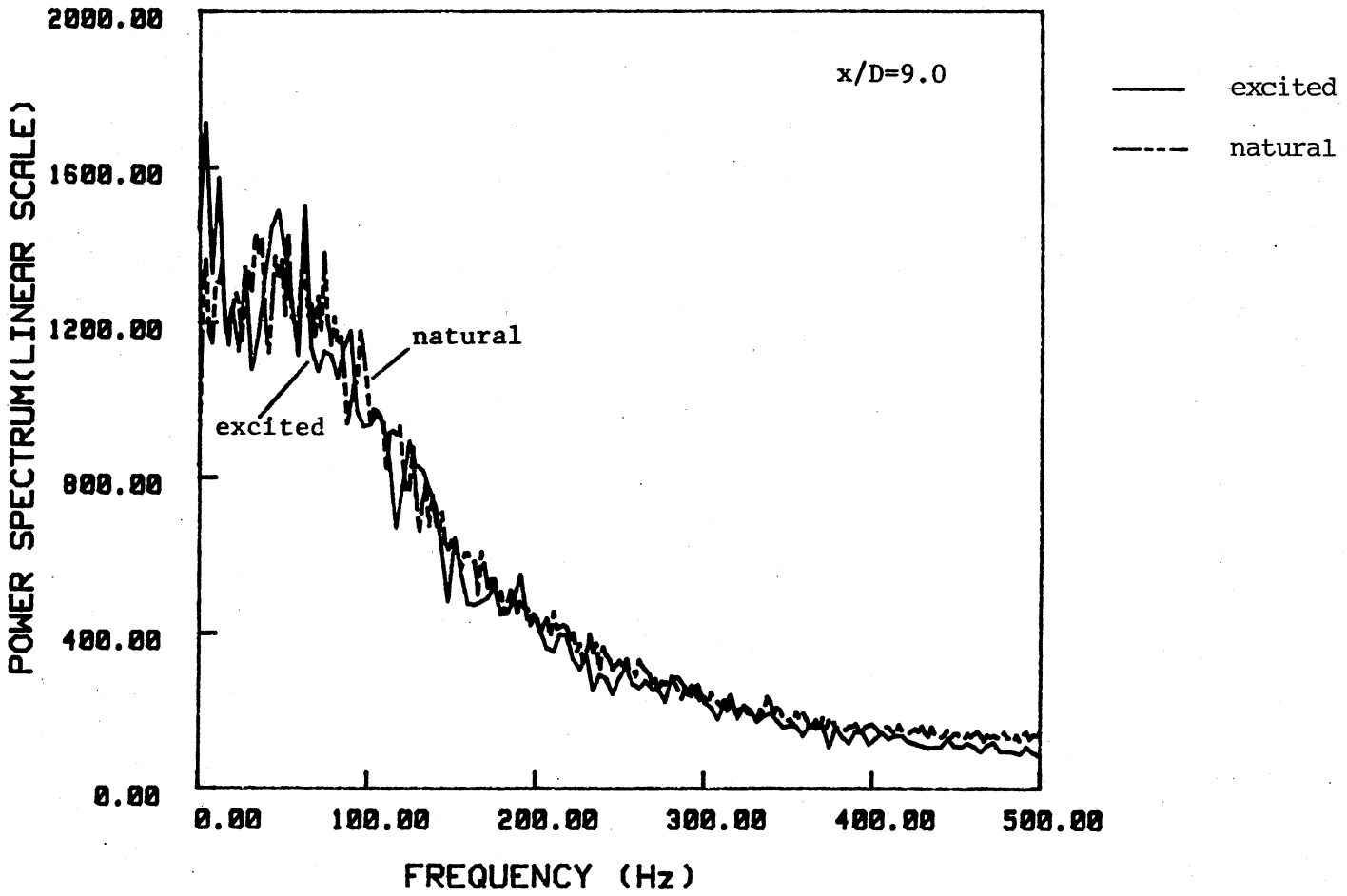

Figure 45. Comparison of the Natural and Excited Centerline Power Spectra at x/D = 9.0

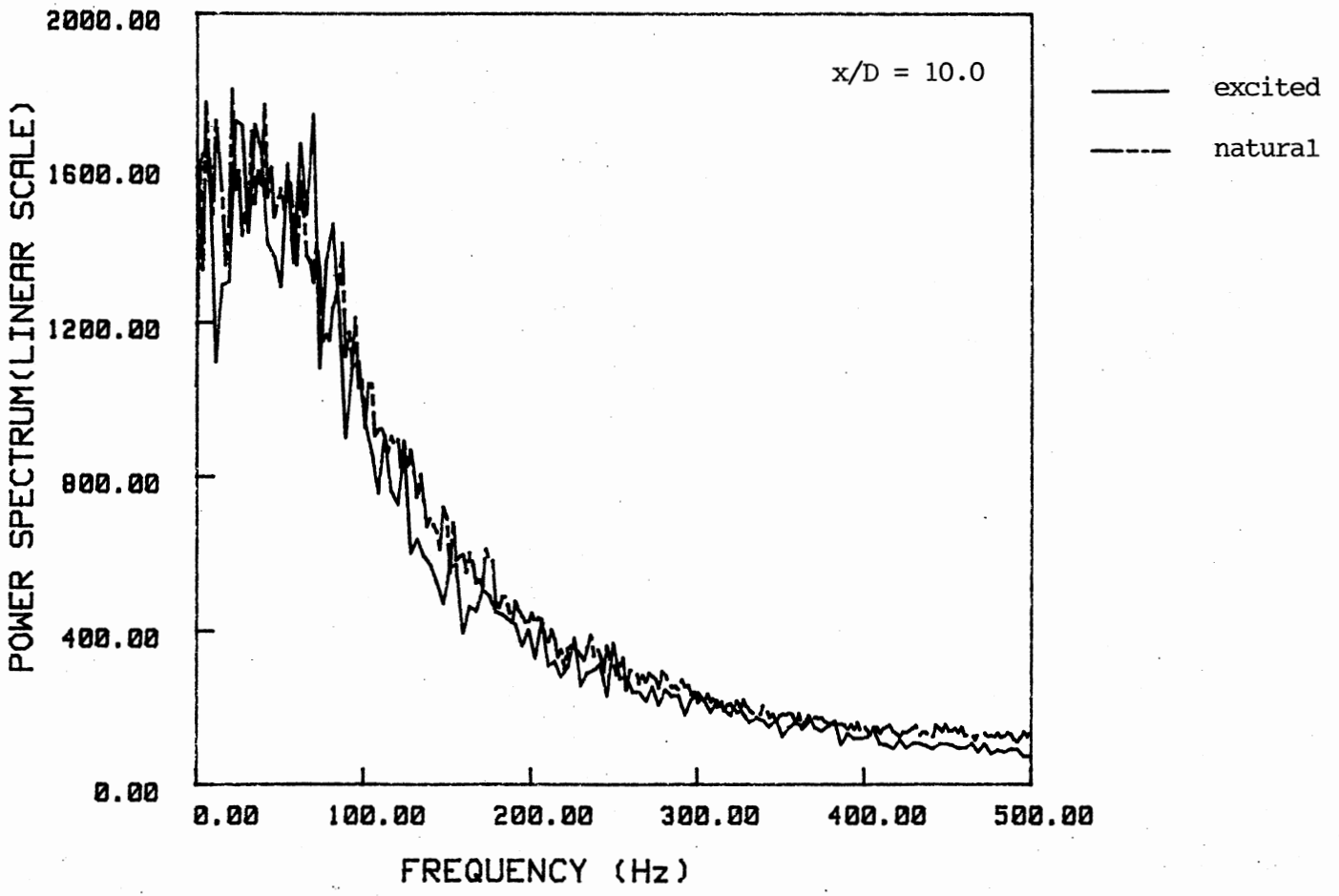

Figure 46. Comparison of the Natural and Excited Centerline Power Spectra at x/D = 10.0

instabilities.

The spectra which have been presented document on a qualitative basis the transition of the natural and excited planar turbulent jet. Power spectral techniques alone are not able to provide quantitative measure of the interactions which characterize the transition phenomenon. In order to distinguish between nonlinear coupled waves and linear independent waves and to quantitatively measure the strength of the nonlinear interactions between fluctuations, the bicoherence technique will be applied. In the next section the measured bicoherence spectra will be used to provide more insight regarding the detailed nonlinear interactions in the developing jet flow.

3.4 Bicoherence Spectra

The mathematical and statistical background of the bicoherence spectrum is reviewed in section 1.2.1. In this section, bicoherence spectra are used in conjunction with linear power spectral measurements to study on a quantitative basis the nonlinear interactions which govern the dynamics of the transition of an excited planar turbulent jet. The measurements were taken at selected downstream locations using a standard hot-wire probe placed in the developing jet shear layer (i.e. $y/b = 1.0$) for $x/D = 0.25$ to 4 and on the centerline of the jet ($y/b = 0.0$) for $x/D = 3$ to 5. For the bicoherence measurements the Nyquist frequency, f_N, was 2000 Hz. The bicoherence was computed digitally via FFT techniques from sampled velocity fluctuation data. The PASCAL program used to compute the bicoherence spectra is listed in Appendix A. Each bicoherence spectrum represents an ensmeble average over 150 samples of 512 points each for $x/D \leq 2.0$ and 200 samples of 512 points

each for x/D > 2.

It is well known that for quadratic nonlinear wave-wave interactions, the interacting wave frequencies (f_i,f_j) must satisfy the following resonance condition: $f_k = f_i+f_j$. In real fluctuation data, the f_k mode may be a spontaneously excited independent mode which is unrelated to f_i and f_j or a coupled mode resulting from quadratic nonlinear interaction. Standard power spectra are not able to distinguish between the two cases. In order to determine whether a wave triad which satisfies the resonance condition is the result of nonlinear coupled waves or linear independent waves, a third-order spectral technique is required. As noted in section 1.2.1 the bicoherence spectrum is able to discriminate between spontaneously excited instabilities and coupled modes by measuring the degree of phase coherence among a wave triad. When nonlinear interactions are indicated, the bicoherence provides a spectral map of the interactions and quantifies their relative importance.

It should be noted that due to the symmetry of the Fourier components $X_{-K} = X_K^*$ (* indicates a complex conjugate) it is sufficient to compute and plot the bicoherence spectrum in only the triangular region of the f_i, f_j plane which is defined as follows: $0 \leq f_i \leq f_N/2$, $f_i \leq f_j \leq f_N-f_i$, where f_N is the Nyquist frequency. Also, the bicoherence values are bounded by $0 \leq b^2(f_i,f_j) \leq 1$. When nonlinear coupling between interacting modes is present, the bicoherence spectrum will take on a non-zero value less than or equal to unity due to phase coherence between the interacting modes. A value of the bicoherence spectrum near zero will indicate that the three modes f_i, f_j, and f_k do not exhibit phase coupling and are therefore not the result of nonlinear

interactions but rather are independent or self-excited.

The bicoherence plots which are next presented provide a clear spectral map of the multiple nonlinear interactions that take place during the transition of the excited planar turbulent jet. Shown in each of the bicoherence plots are the lines of constant frequency $f_k = f_i+f_j$ which corresponds to a basic quadratic nonlinear interaction described by the bispectral technique. Values of bicoherence which fall along these lines can be interpreted as representing interactions between different pairs of instabilities with a sum frequency equal to f_k. However, because of the symmetry properties of the bispectrum, the interactions $f_k-f_j = f_i$ and $f_k-f_i = f_j$ will also be mapped into the $b^2(f_i,f_j)$ interaction. Thus a value of $b^2(f_i,f_j)$ can be contributed by any of three possible interactions and reference to corresponding power spectra is required to discern which interaction is involved.

3.4.1. Results of Bicoherence Measurements at Excitation Frequency f_e = 750 Hz

Figures 47-51 corresponding to x/D = 0.25 to 1 document the development of shear layer bicoherence spectra which are measured in the early stage of the excited jet transition. In the following data to be presented the probe was placed in the jet shear layer at y/b = 1. The bicoherence spectrum obtained at x/D = 0.25 is presented in Figure 47. A peak at $b^2(f_e/2,f_e/2) = 0.52$ is shown and is a manifestation of the subharmonic resonance mechanism proposed by Kelly (1967). It represents subharmonic production through an interaction of the form $f_e-f_e/2 \rightarrow f_e/2$. Note that the symbol "-->" is to be read "undergo nonlinear interaction to yield". The value of $b^2(f_e/2,f_e/2) = 0.52$ indicates that

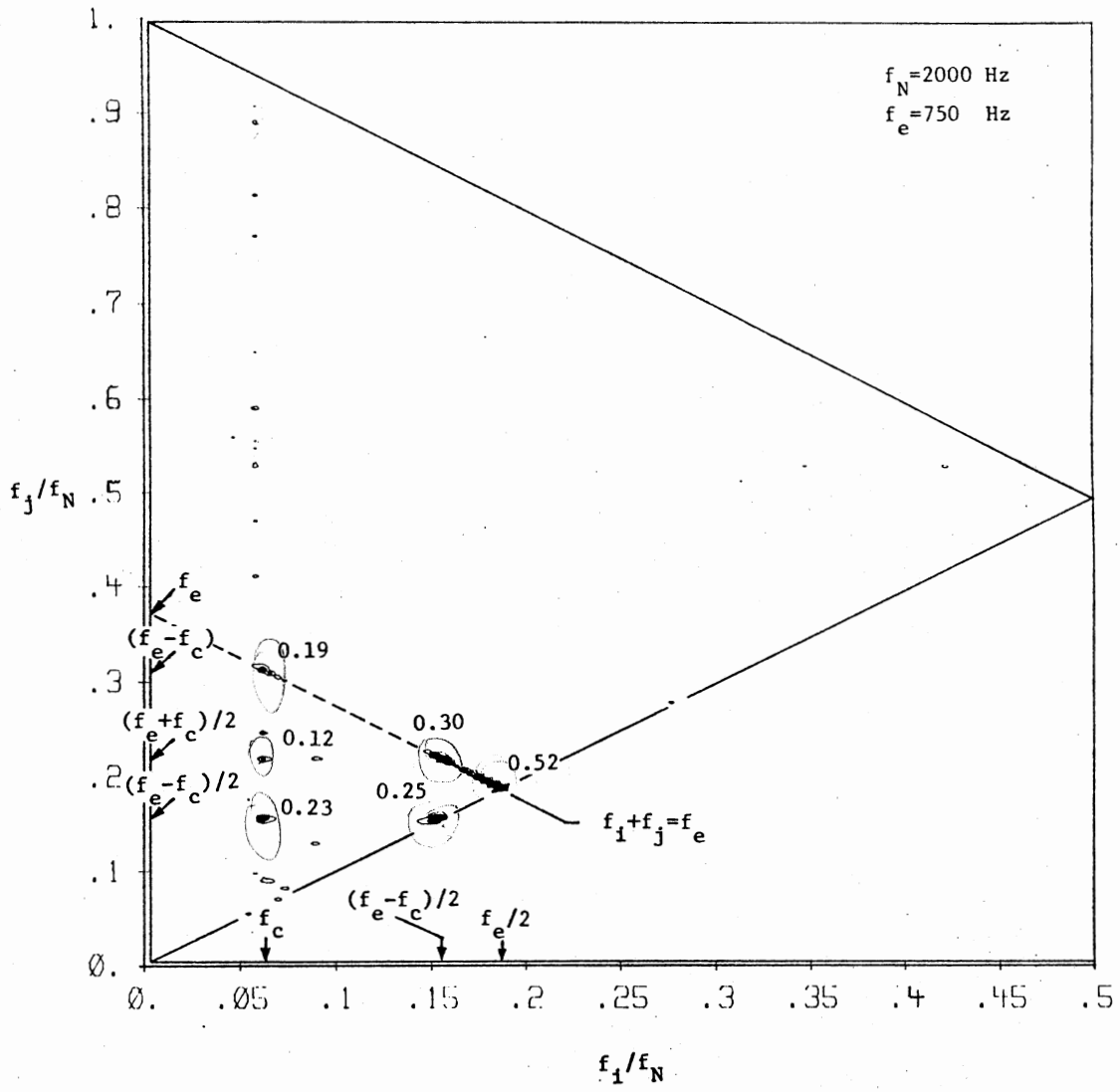

Figure 47. Excited Jet Shear Layer Bicoherence Spectrum at x/D = 0.25. Contours are from 0.05. The Contour Interval is 0.05.

the developing spectral mode at 375 Hz is truly the subharmonic of 750 Hz and is not a spontaneously excited mode. Also, this bicoherence spectrum shows elevated peaks, $b^2((f_e-f_c)/2,(f_e-f_c)/2) = b^2(312,312) = 0.25$ and $b^2((f_e-f_c)/2,(f_e+f_c)/2) = b^2(312,438) = 0.30$, which correspond to the nonlinear interactions of the forms $(f_e-f_c)-(f_e-f_c)/2 \rightarrow (f_e-f_c)/2$ and $f_e-(f_e-f_c)/2 \rightarrow (f_e+f_c)/2$. The first of these two interactions indicates a subharmonic resonance as proposed by Kelly (1967) involving the (f_e-f_c) mode. Thus, the 312 Hz mode is the subharmonic mode of $(f_e-f_c) = 624$ Hz (which is the lower sideband of the fundamental frequency). This mode is created through the nonlinear difference interaction $f_e-f_c \rightarrow (f_e-f_c)$ and is shown in the bicoherence spectrum as $b^2(f_c,(f_e-f_c))$. The interaction $f_e-(f_e-f_c)/2 \rightarrow (f_e+f_c)/2$ corresponding to $b^2((f_e-f_c)/2,(f_e-f_c)/2) = 0.30$ shows that the 438 Hz spectral mode (i.e. the upper sideband of the subharmonic) is produced by the nonlinear interaction between the excitation frequency f_e and the lower sideband $(f_e-f_c)/2 = 312$ Hz. Additional lower sideband production will occur due to the interaction $b^2(f_c,(f_e-f_c)/2) = 0.23$ which may be written $(f_e+f_c)/2 - f_c \rightarrow (f_e-f_c)/2$. Of particular interest in Figure 47 are several low level spectral contours indicating interaction between $f_i = f_c$ and multiple modes f_j. The near exit interactions which have been noted to involve f_c indicate that the jet column mode exerts an upstream influence on the near exit flow field. The strongest of these peaks are $b^2(f_c,(f_e-f_c)/2) = 0.23$, $b^2(f_c,(f_e+f_c)/2) = 0.12$, and $b^2(f_c,(f_e-f_c)) = 0.19$ and therefore suggest the existence of nonlinear interactions between the jet column mode and shear layer instabilities even in the near exit region where the shear layer fluctuations are of very low level.

The bicoherence spectrum at x/D = 0.5 is shown in Figure 48. Contours have formed at $b^2(f_e,f_e)$ = 0.22 which indicates harmonic production through an interaction of the form f_e+f_e --> $2f_e$. This gives rise to the 1500 Hz harmonic seen in the power spectra of the previous section. The subharmonic resonant interaction $f_e-f_e/2$ --> $f_e/2$ is still apparent. In addition nearby contours along the line $f_k = f_e$ indicate that multiple modes between $f_e/2$ and $(f_e-f_c)/2$ are also involved in the subharmonic resonance. The interaction $b^2(f_e/2,f_e/2)$ representing subharmonic production is strengthened while the interaction $b^2((f_e-f_c)/2,(f_e-f_c)/2)$ which produces the lower subharmonic sideband has nearly doubled in strength.

Figure 49 shows the bicoherence obtained at x/D = 0.75. This figure indicates that bicoherence values of $b^2(f_e/2,f_e/2)$, $b^2((f_e-f_c)/2,(f_e-f_c)/2)$ and $b^2((f_e-f_c)/2,(f_e+f_c)/2)$ show only small growth while the harmonic production interaction $b^2(f_e,f_e)$ increases from 0.22 to 0.85. As shown in Figure 50, bicoherency contours extend in the $f_i = f_e$ and $f_j = f_e$ directions from the interaction $b^2(f_e,f_e)$. These elongated contours represent the nonlinear interaction between the excitation frequency and nearby naturally occurring modes to enrich the harmonic content of the spectrum. In particular, the horizontal contours suggest that lower sidebands of f_e are interacting with the excitation frequency f_e to produce the lower skirt of the $2f_e$ band. Similarly, the vertical contours indicate that the upper sidebands of f_e are interacting with the dominant f_e band to broaden the upper skirt of the $2f_e$ band. The reader is referred to Figure 26 which demonstrates the enhanced harmonic spectral content due to these nonlinear interactions.

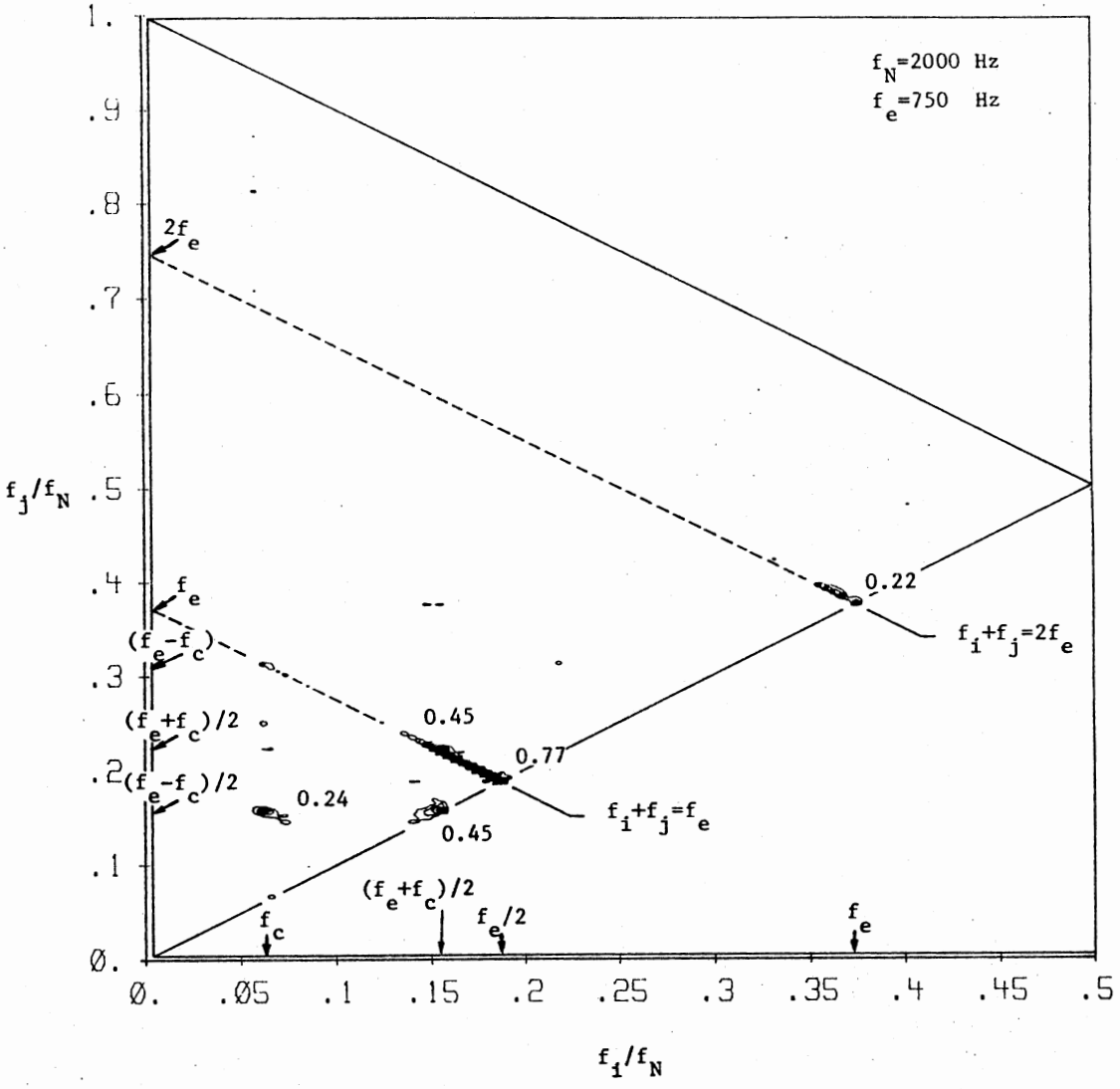

Figure 48. Excited Jet Shear Layer Bicoherence Spectrum at x/D = 0.5. Contours are from 0.05. The Contour Interval is 0.05.

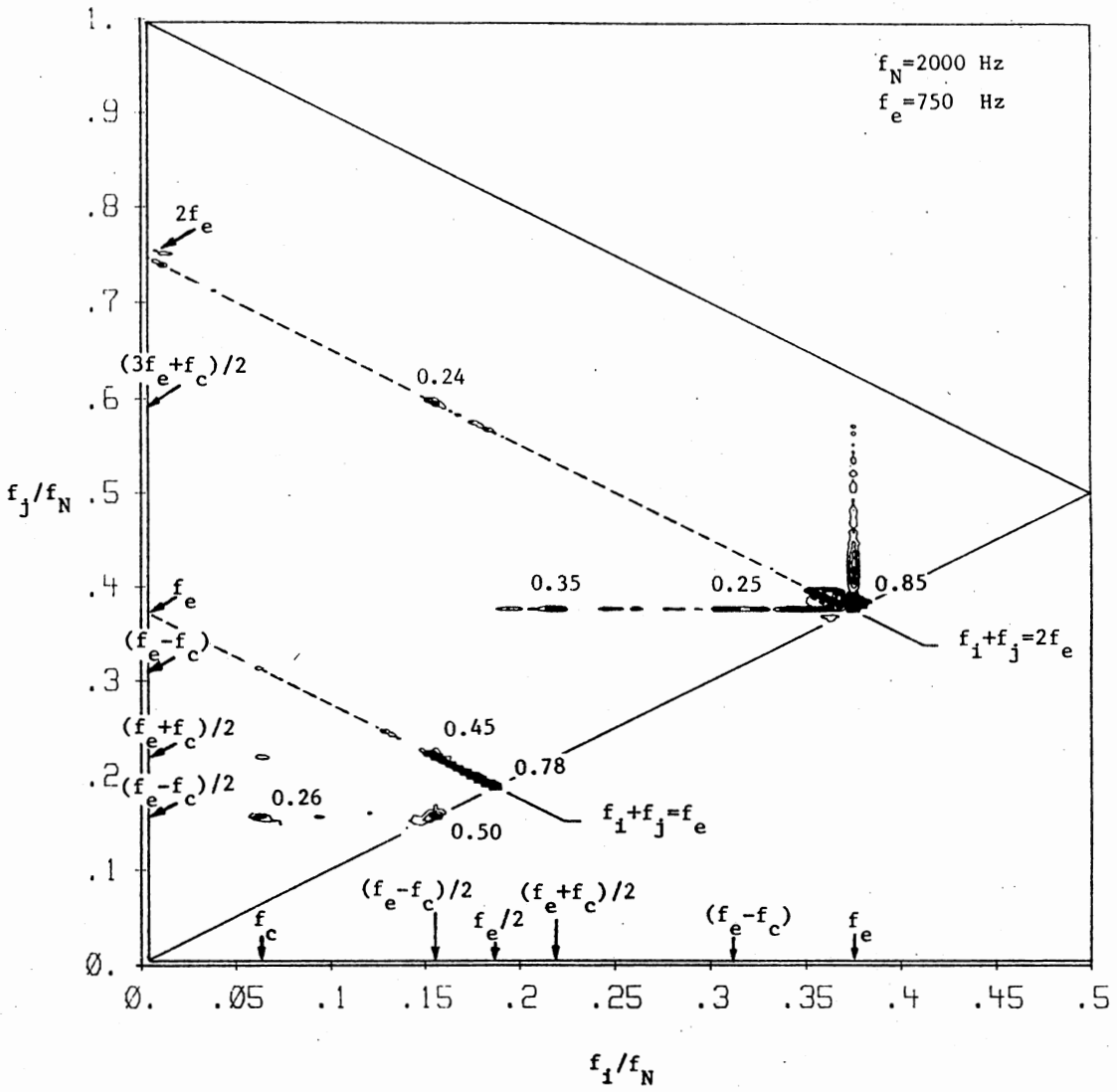

Figure 49. Excited Jet Shear Layer Bicoherence Spectrum at x/D = 0.75. Contours are from 0.075. The Contour Interval is 0.075.

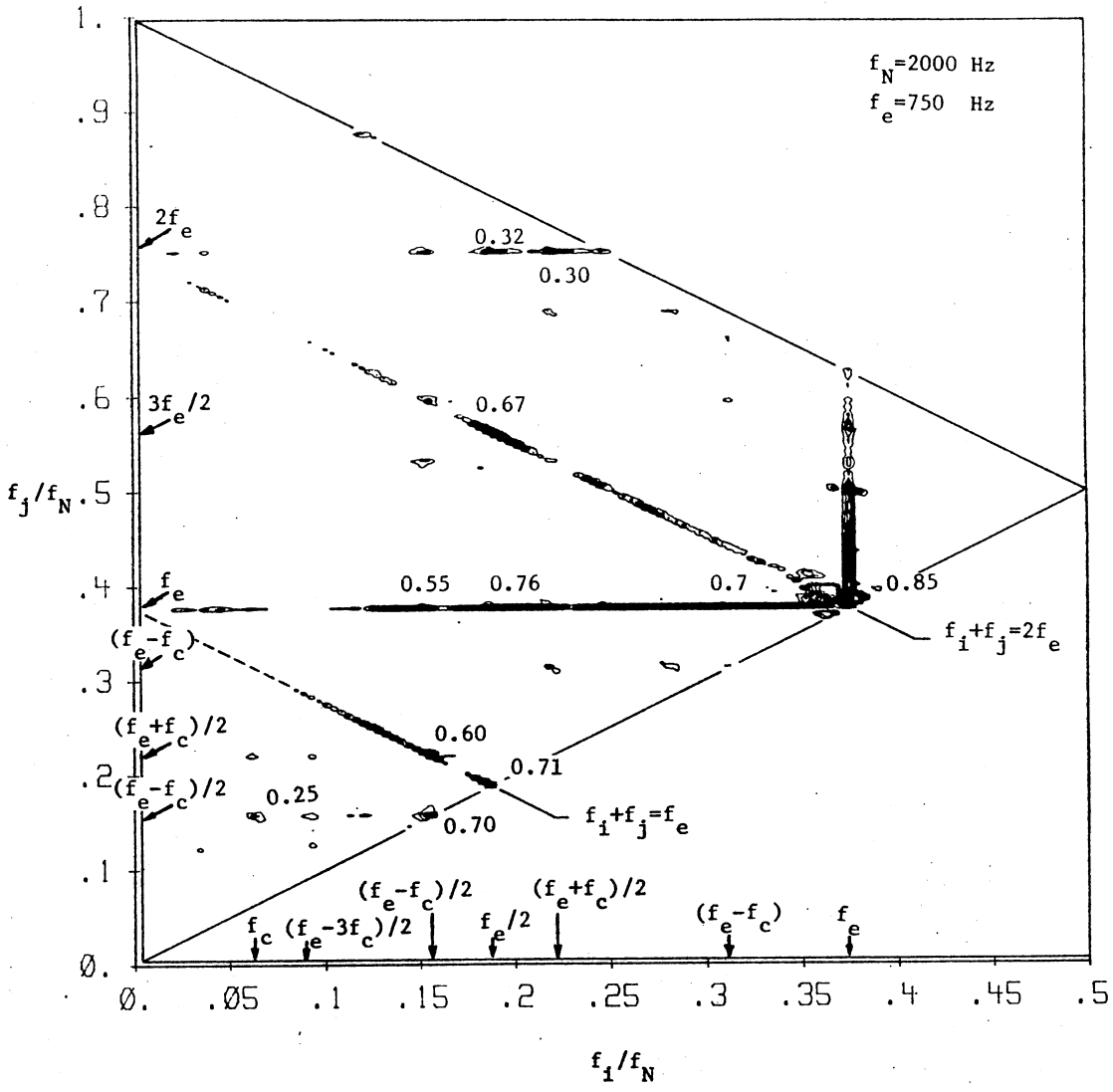

Figure 50. Excited Jet Shear Layer Bicoherence Spectrum at x/D = 1.0. Contours are from 0.1. The Contour Interval is 0.1.

Figure 51 presents the computed bicoherence at x/D = 1.25. The nonlinear interactions previously described are still very apparent. Of particular interest in this bicoherence spectrum is the interaction $b^2((f_e-f_c)/2,(f_e-f_c)/2) = 1.0$ which indicates perfect phase coherence between the 312 Hz and 624 Hz modes via the nonlinear interaction $(f_e-f_c)-(f_e-f_c)/2 \rightarrow (f_e-f_c)/2$. This helps to explain the rapid growth of this mode in the shear layer power spectrum of Figure 29. Other dominant interactions at this location are $b^2((f_e-f_c)/2,(f_e+f_c)/2) = 0.84$, $b^2(f_e/2,f_e/2) = 0.50$ and $b^2(f_e,f_e) = 0.83$. In addition to these, several new multiple nonlinear interactions are apparent in Figure 51 involving combinations of the modes f_e and f_c. The f_i, f_j, f_k frequency triads involved are indicated. As an example, consider the interaction labeled "A" for which $f_i = (f_e-f_c)/2$, $f_j = (3f_e-f_c)/2$ and $f_k = 2f_e-f_c$. The interaction may be written $(2f_e-f_c)-(f_e-f_c)/2 \rightarrow (3f_e-f_c)/2$ thus involving production of a low frequency sideband on the harmonic mode $3/2f_e$. Another example is that labeled "B" in Figure 51. For this case the computed bicoherence $b^2((f_e-3f_c)/2,(f_e+f_c)/2) = 0.8$ for which $f_i = (f_e-3f_c)/2$, $f_j = (f_e+f_c)/2$ and $f_k = f_e-f_c$. The interaction may be interpreted as $(f_e-f_c)-(f_e+f_c)/2 \rightarrow (f_e-3f_c)/2$ which indicates the mode at $(f_e-3f_c)/2$ is produced by the interaction between the (f_e-f_c) and $(f_e+f_c)/2$ modes. It is clear then that interactions such as these have an important effect on the energy transfer over a wide frequency range.

Figure 52 presents the bicoherence obtained at x/D = 1.5. It may be noted from this figure that the multiple nonlinear interactions are strengthened and contours spread to nearby modes which are not multiples of f_e and f_c indicating that there is energy transfer involving neighboring modes. The bicoherence spectrum shows two of the strongest

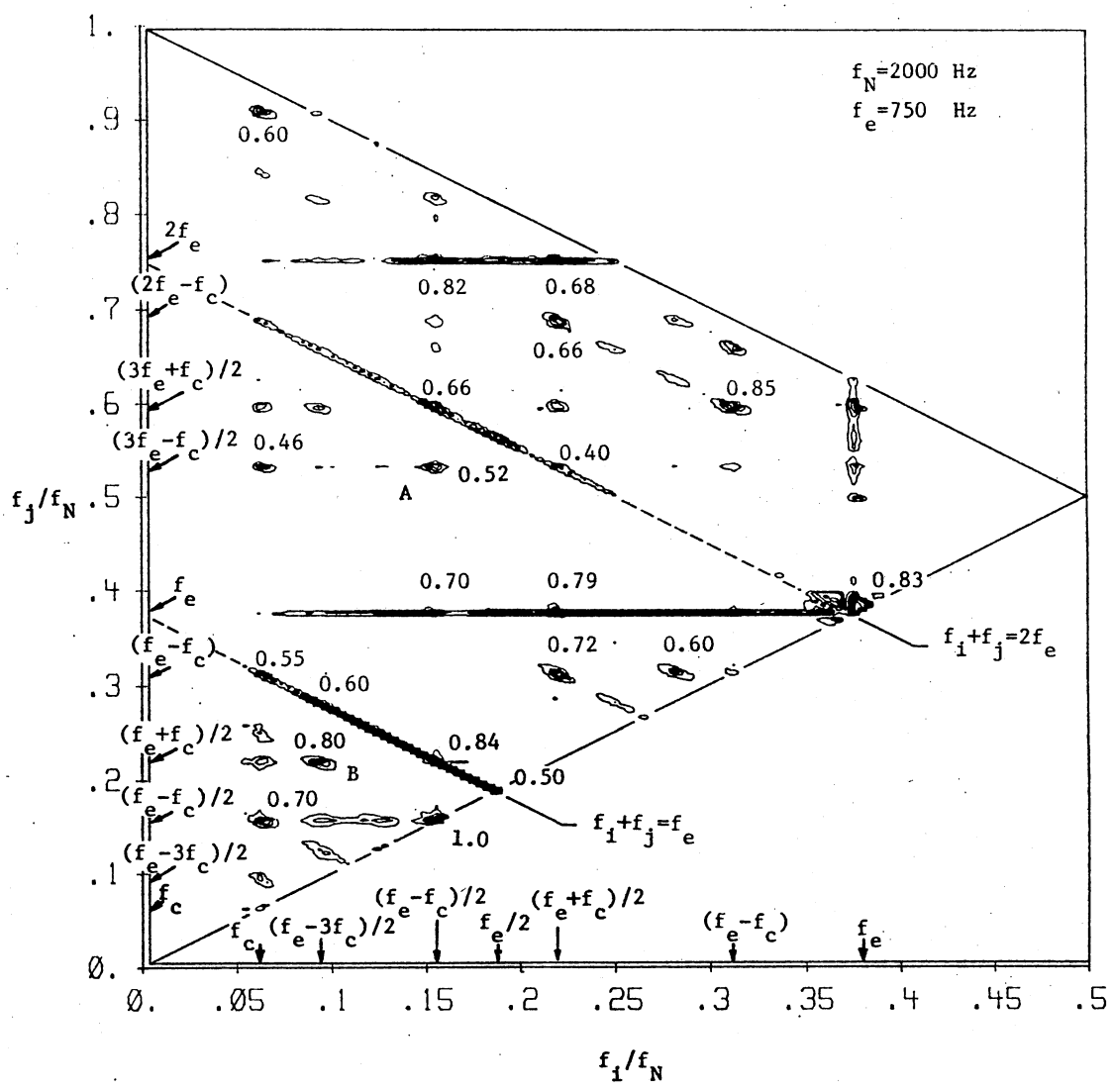

Figure 51. Excited Jet Shear Layer Bicoherence Spectrum at x/D = 1.25. Contours are from 0.1. The Contour Interval is 0.15.

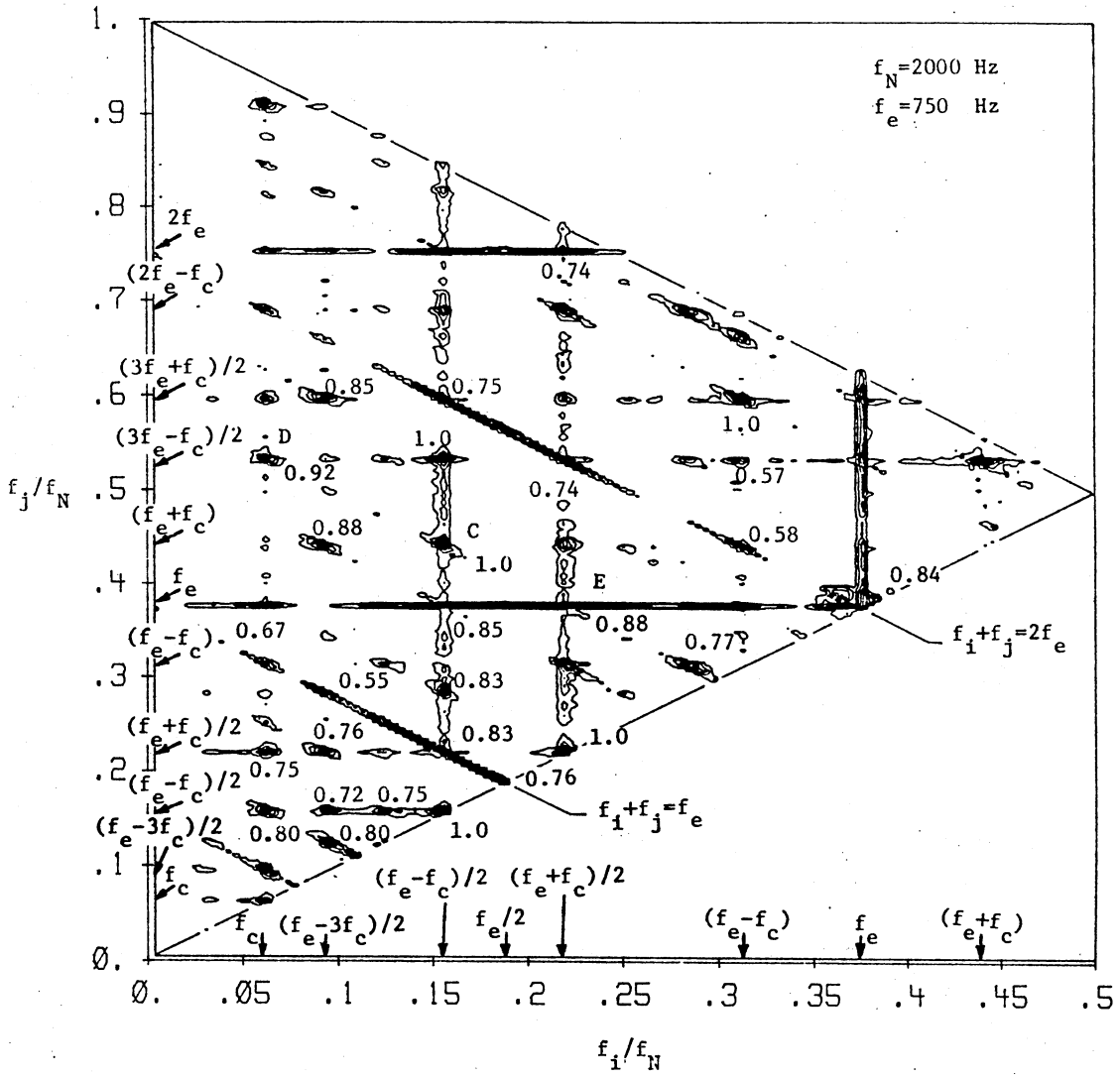

Figure 52. Excited Jet Shear Layer Bicoherence Spectrum at x/D = 1.5. Contours are from 0.1. The Contour Interval is 0.15.

peaks, $b^2((f_e-f_c)/2,(f_e-f_c)/2) = 1.0$ and $b^2((f_e+f_c)/2,(f_e+f_c)/2) = 1.0$, which demonstrate the strengthened interactions between the 312 Hz and 624 Hz modes and the 438 Hz and 876 Hz modes through the nonlinear interactions $(f_e-f_c)-(f_e-f_c)/2 \rightarrow (f_e-f_c)/2$ and $(f_e+f_c)-(f_e+f_c)/2 \rightarrow (f_e+f_c)/2$. At the same time, other interactions also exhibit growth behavior. Of particular interest in Figure 52 is the formation of the spectral contours along the discrete modes $f_i = f_c$, $(f_e-3f_c)/2$, $(f_e-f_c)/2$, $(f_e+f_c)/2$, f_e, and (f_e+f_c), and $f_j = (f_e-f_c)/2$, $(f_e+f_c)/2$, f_e, (f_e+f_c), $(3f_e-f_c)/2$, $(3f_e+f_c)/2$, $(2f_e-f_c)$, and $2f_e$ which indicate new multiple interactions and hence energy transfer between combinations of these f_i, f_j, f_k modes. As an example, consider the interaction labeled "C" for which the bicoherence contours extend in the $f_i = (f_e-f_c)/2$ and $f_k = (3f_e+f_c)/2$ directions from the interaction $b^2((f_e-f_c)/2,(f_e+f_c))$. These elongated contours suggest the existence of the nonlinear interactions between these dominant frequencies and nearby naturally occurring instabilities which result in the energy transfer from the dominant modes to the valley of the spectra. These phenomena also may be indicated by other interactions as labeled by "D" and "E" for example.

The data presented above for $x/D < 2.0$ indicate that interactions between the jet column mode f_c and the excitation frequency f_e play a crucial role in the energy redistribution process during the excited jet transition. Therefore, the energy transfer from the fundamental through the nonlinear generation of multiple modes provides an effective mechanism for spectral broadening. The formation of the multiple modes involving combinations of f_e and f_c is clearly seen in the excited shear layer power spectrum at $x/D = 1.5$ (see Figure 28).

The bicoherence spectrum at x/D = 2.0 is shown in Figure 53. Basically, the bicoherence contours exhibit the same interactions as in the previous case. It may be noted from Figure 31 of the previous section that the x/D = 2 shear layer spectrum demonstrates the growth of both the jet column mode f_c and the mode $(f_e-3f_c)/2$ simultaneous with the decay of the modes at $(f_e-f_c)/2$ and $(f_e+f_c)/2$. As shown in the bicoherence spectrum of Figure 53 for x/D = 2, the growth of the jet column mode f_c is related to several nonlinear interactions as evidenced by peaks at $b^2(f_c,(f_e-f_c)/2) = 0.48$, $b^2(f_c,(f_e-3f_c)/2) = 0.37$ and $b^2(f_c,(f_e-f_c) = 0.66$. The first of these interactions may be interpreted as $(f_e+f_c)/2-(f_e-f_c)/2 \rightarrow f_c$ which indicates the transfer of energy to f_c by a difference interaction between the decaying $(f_e+f_c)/2$ and $(f_e-f_c)/2$ modes. The second may be interpreted as an interaction of the form $(f_e-f_c)/2-(f_e-3f_c)/2 \rightarrow f_c$. In addition the interaction between the decaying mode at f_e and its lower sideband will enrich the mode at f_c through the difference interaction $f_e-(f_e-f_c) \rightarrow f_c$. Other dominant peaks are $b^2((f_e-3f_c)/2,(f_e+f_c)/2) = 0.38$ and $b^2((f_e-3f_c)/2,2f_c) = 0.37$ which indicate growth of the $(f_e-3f_c)/2$ spectral mode via the interactions $(f_e-f_c)-(f_e+f_c)/2 \rightarrow (f_e-3f_c)/2$ and $(f_e+f_c)/2-2f_c \rightarrow (f_e-3f_c)/2$. The harmonic of the jet column mode is produced from the interaction $f_c+f_c \rightarrow 2f_c$ as evidenced by the value $b^2(f_c,f_c) = 0.20$. The computed bicoherence interactions noted earlier as $b^2((f_e-f_c)/2,(f_e-f_c)/2)$ and $b^2((f_e+f_c)/2,(f_e+f_c)/2)$ (which were noted to be particularly strong at x/D = 1) weaken to values of 0.53 and 0.33, respectively for x/D = 2.0.

The shear layer power spectrum of Figure 33 indicated that the $(f_e+f_c)/2$ mode alone exhibited growth while other dominant modes f_e,

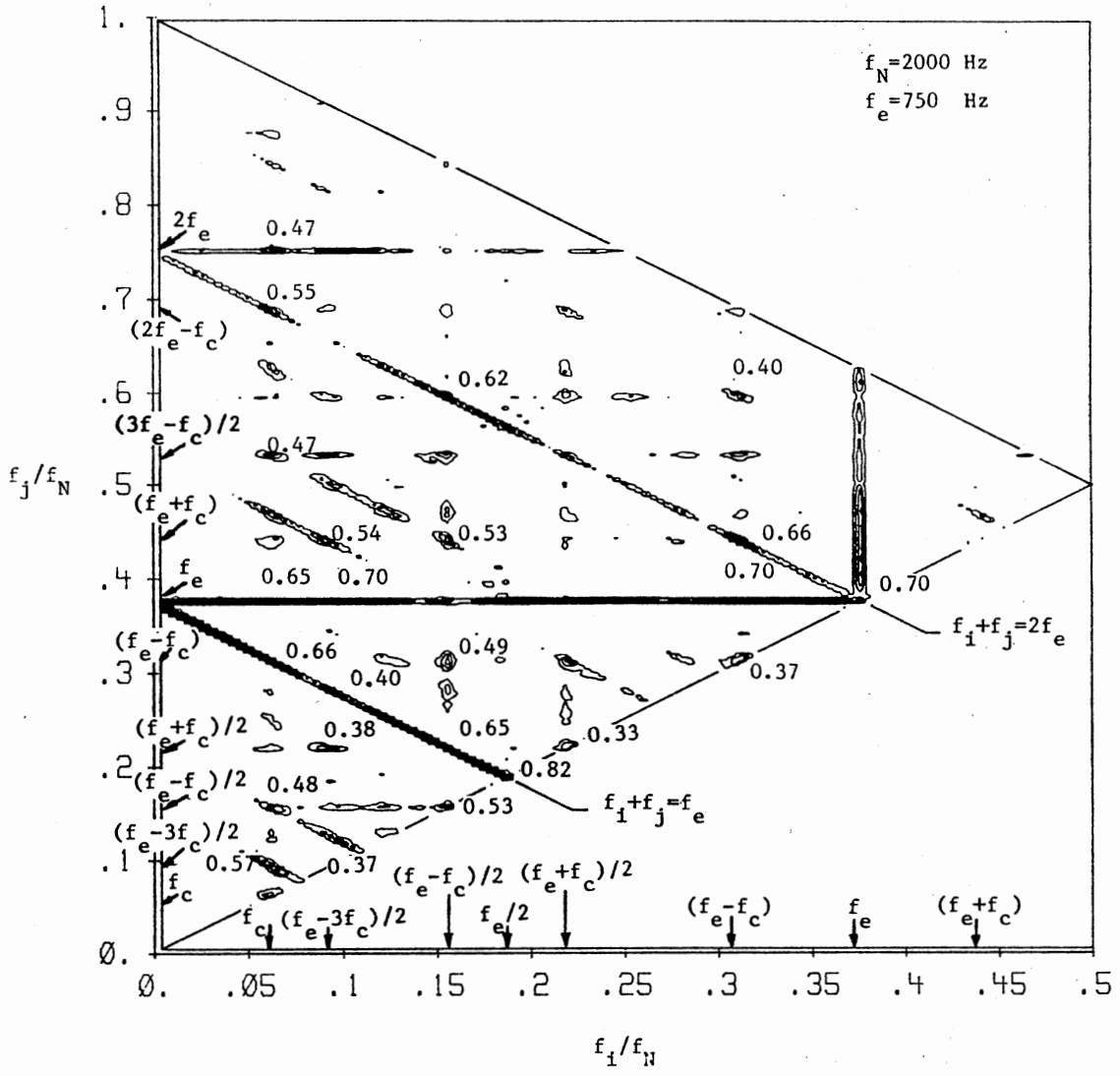

Figure 53. Excited Jet Shear Layer Bicoherence Spectrum at x/D = 2.0. Contours are from 0.1. The Contour Interval is 0.15.

$f_e/2$, and $(f_e-f_c)/2$ were in decay. The bicoherence spectrum at x/D = 2.5 is shown in Figure 54. Of particular interest in this figure are several interactions: $b^2((f_e+f_c)/2,(f_e+f_c)/2) = 0.32$, $b^2((f_e+f_c)/2,(f_e-f_c)) = 0.56$, $b^2((f_e+f_c)/2,f_e) = 0.30$, and $b^2((f_e+f_c)/2,(3f_e-f_c)/2) = 0.57$. These interactions are along the line of constant frequency $f_i = (f_e+f_c)/2$, which indicates nonlinear interactions between $(f_e+f_c)/2$ mode and several dominant instabilities. The growth of the $(f_e+f_c)/2$ may be contributed by the interactions of form $2f_e-(3f_e-f_c)/2 \rightarrow (f_e+f_c)/2$, $(3f_e+f_c)/2-f_e \rightarrow (f_e+f_c)/2$, $(3f_e-f_c)-(f_e-f_c) \rightarrow (f_e+f_c)/2$, and $(f_e+f_c)-(f_e+f_c)/2 \rightarrow (f_e+f_c)/2$.

As shown in the bicoherence spectrum of Figure 55 obtained at x/D = 3, the phase randomization of the instabilities that characterize the transition results in a decay of the time-averaged phase coherence which is measured by the bicoherence spectrum. For example, because of the lack of phase coherence, the computed bicoherence values $b^2((f_e-f_c)/2,(f_e-f_c)) = 0.12$, $b^2((f_e-f_c)/2,(f_e-f_c)/2) = 0.17$, and $b^2(f_e,f_e) = 0.17$ are substantially less than the values shown in the previous Figure 54 which were 0.20, 0.38, and 0.45, respectively. As the instability waves move downstream to x/D = 3.5 and 4 near the end of the potential core, as shown in Figures 56 and 57, the nonlinear interactions between the jet column mode and the excitation frequency still can be observed in these bispectral maps even though the contour levels are now quite low due to increased phase randomization. These interactions may be noted from the bicoherence contours in Figure 56 when $f_i = (f_e-f_c)$ and $f_j = (f_e-f_c)$ and (f_e+f_c). After x/D > 4, the high level of turbulence occurring at these locations make it impossible to discern the relevant nonlinear interactions.

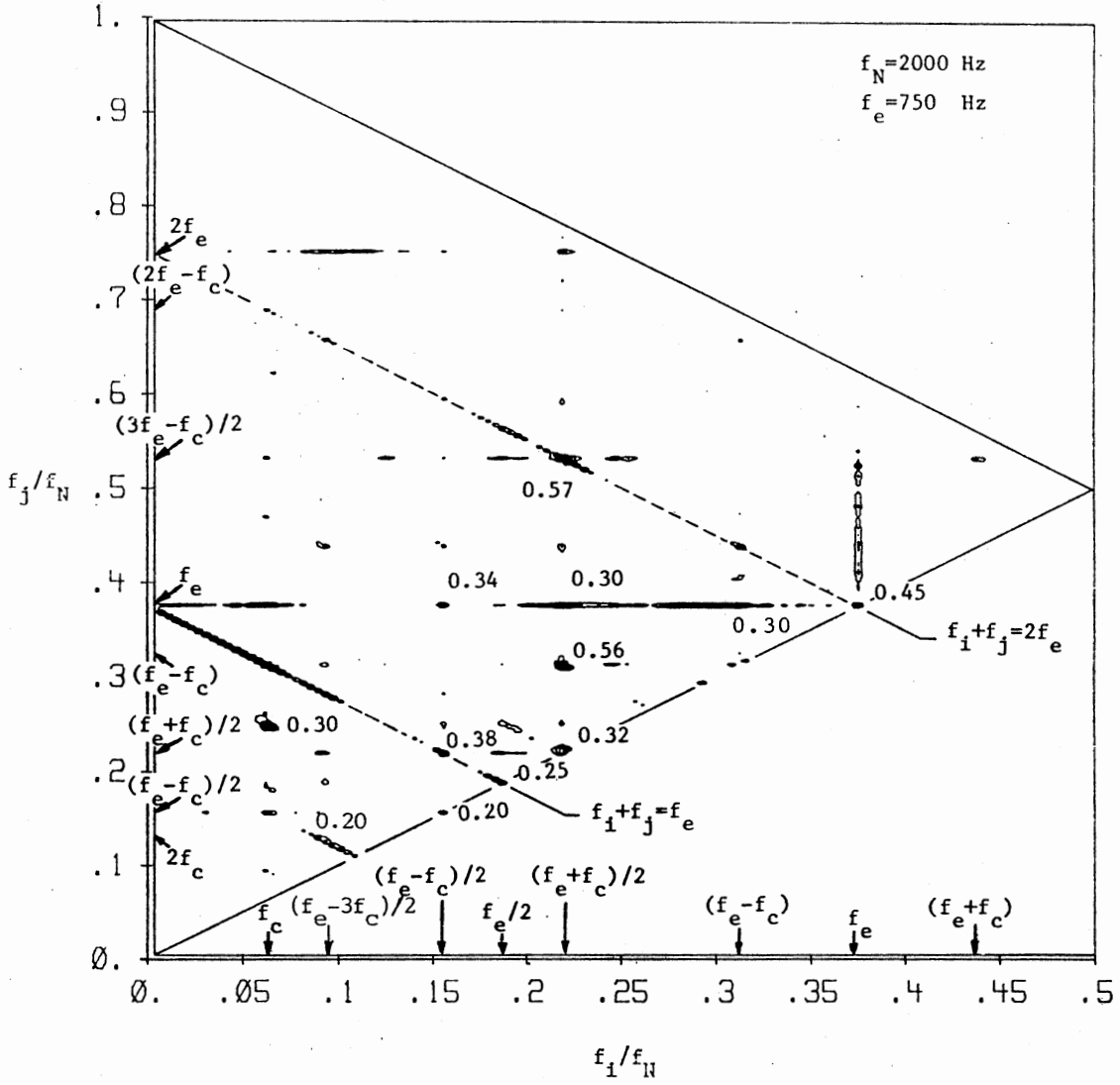

Figure 54. Excited Jet Shear Layer Bicoherence Spectrum at x/D = 2.5. Contours are from 0.1. The Contour Interval is 0.075.

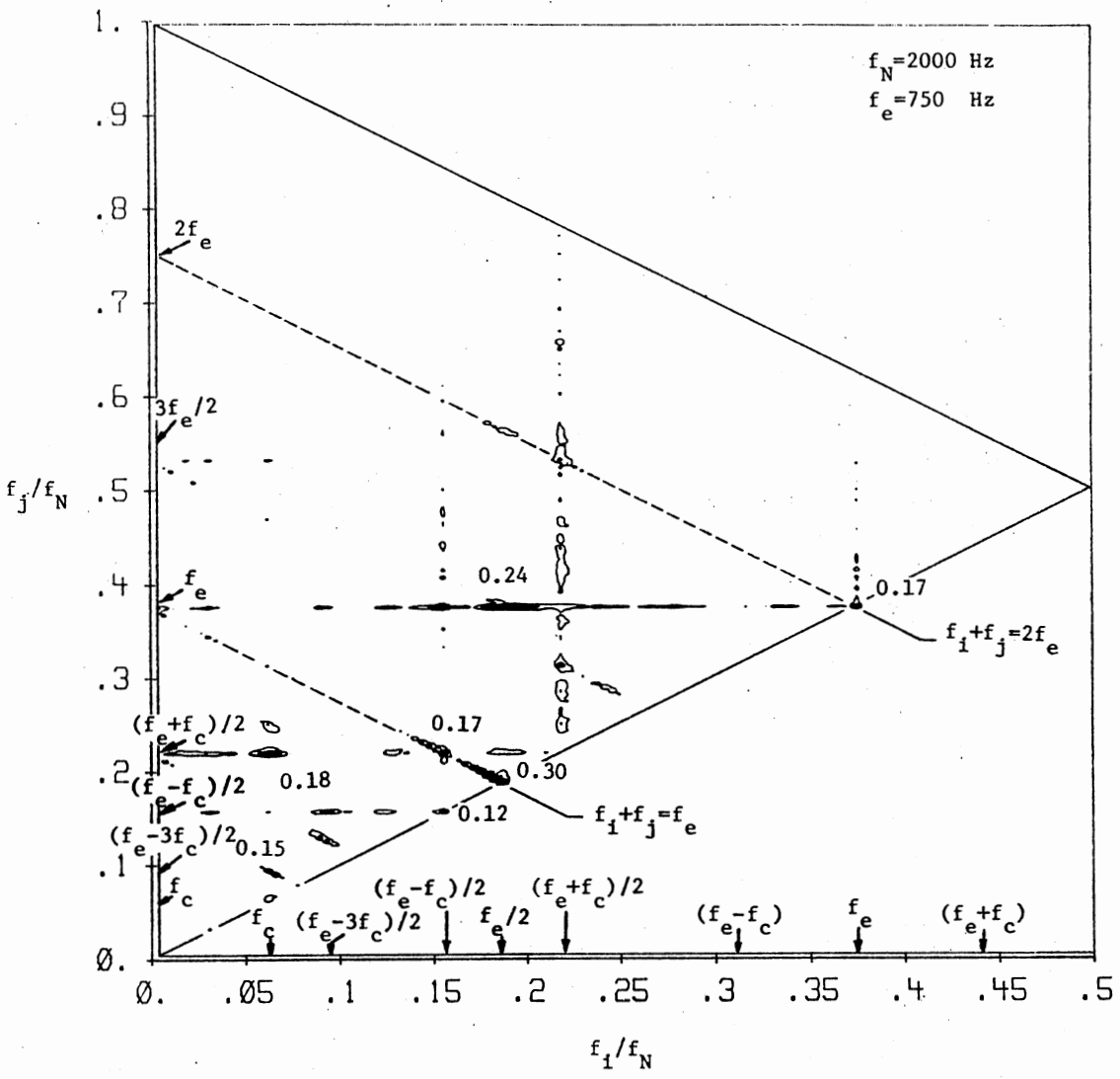

Figure 55. Excited Jet Shear Layer Bicoherence Spectrum at x/D = 3.0. Contours are from 0.05. The Contour Interval is 0.05.

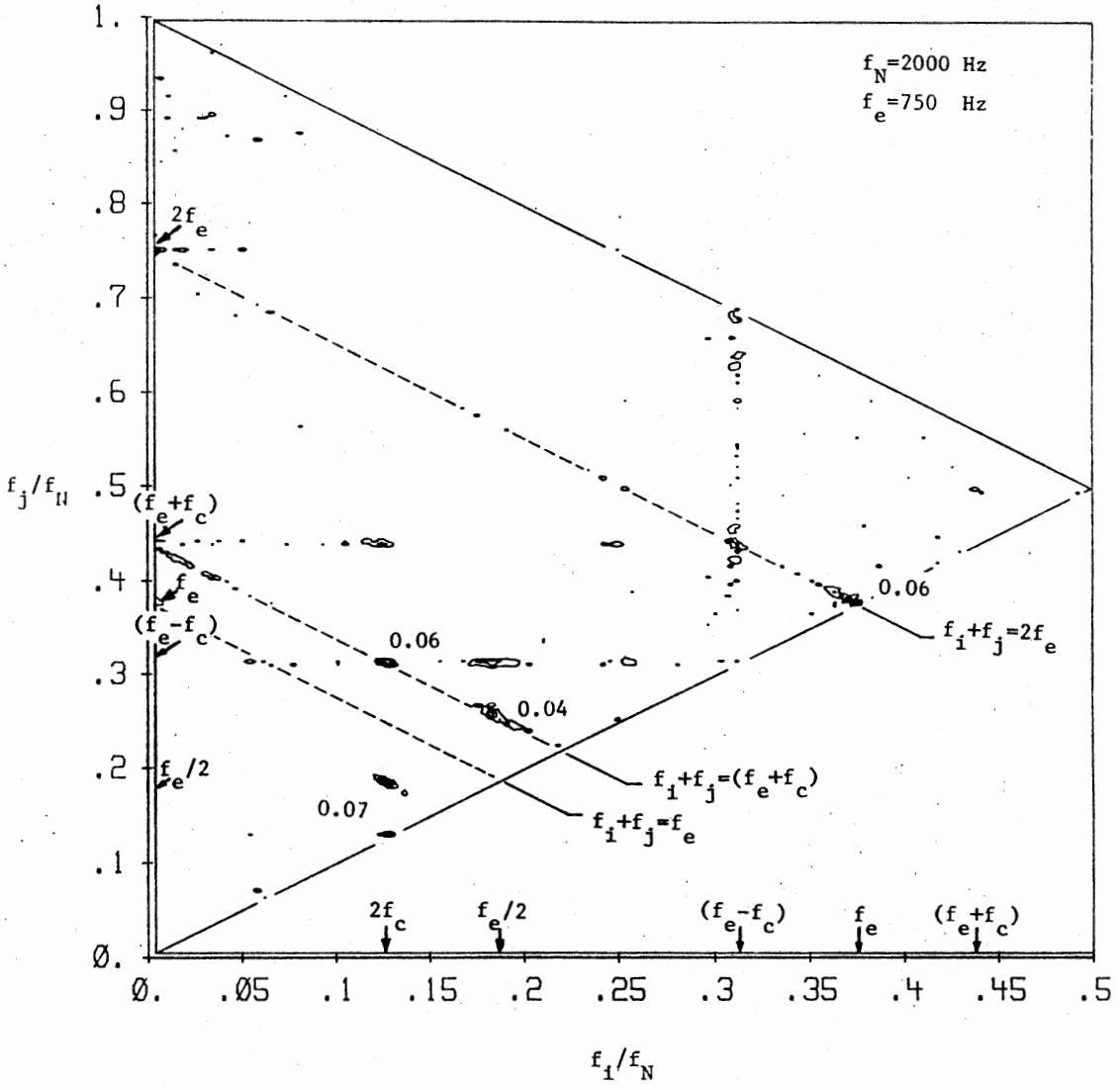

Figure 56. Excited Jet Shear Layer Bicoherence Spectrum at x/D = 3.5. Contours are from 0.015. The Contour Interval is 0.015.

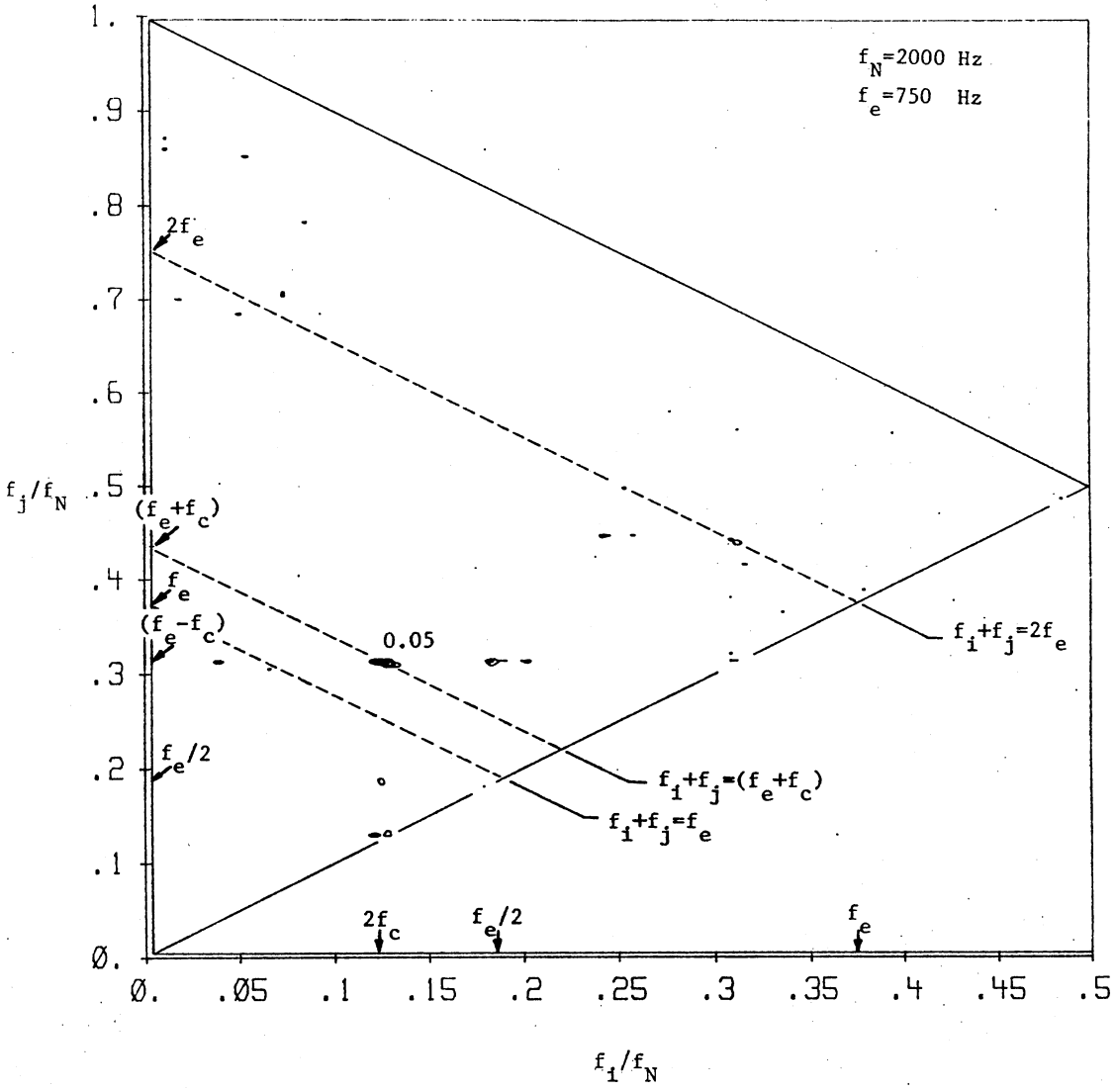

Figure 57. Excited Jet Shear Layer Bicoherence Spectrum at x/D = 4.0. Contours are from 0.015. The Contour Interval is 0.015.

In order to obtain more information regarding the developing jet transition, bicoherence spectra were measured on the jet centerline under excited conditions (f_e = 750 Hz) for x/D = 3 to 5 and are sequentially presented in Figures 58-60. Because of the reduced turbulence levels, it is expected that the bicoherence spectrum measured on the jet centerline will exhibit higher phase coherence compared to those obtained in the shear layer. It may be noted from Figure 58 at x/D = 3 that the bicoherence values at $b^2((f_e-f_c)/2,(f_e-f_c)/2)$ = 0.45, $b^2((f_e-f_c)/2,(f_e+f_c)/2)$ = 0.59, $b^2(f_e/2,f_e/2)$ = 0.52, and $b^2(f_e,f_e)$ = 0.17 do show significantly higher phase coherence than the corresponding bicoherence values obtained in the jet shear layer. The excited centerline bicoherence spectrum at x/D = 3 in Figure 58 indicates that the bicoherence contours basically lie on lines of constant frequencies $f_i = f_c$, $(f_e-3f_c)/2$, $2f_c$, $(f_e-f_c)/2$, $(f_e+f_c)/2$, and f_e. These bicoherence contours suggest the existence of the nonlinear interactions between these dominant modes and natural instabilities at multiple frequencies f_j. Also, there is a significant decrease in phase coherence with frequencies greater than f_k = 750 Hz and the strongest, most phase coherent interactions are noted to occur for $f_k < f_e$. Also, as noted in the centerline power spectrum of section 3.3.2 in Figure 41, the growth of the jet column mode f_c and $(f_e-3f_c)/2$ mode are significant for x/D > 4. The initial growth of the f_c mode may be demonstrated in the Figure 58 by the interactions $b^2(f_c,(f_e-f_c)/2)$ = 0.35, $b^2(f_c,(f_e-3f_c)/2)$ = 0.56 while the mode at $(f_e-3f_c)/2$ is contributed by the interaction $b^2((f_e-3f_c)/2,2f_c)$ = 0.40. These interactions may be written as $(f_e+f_c)/2-(f_e-f_c)/2 \rightarrow f_c$, $(f_e-f_c)/2-(f_e-3f_c)/2 \rightarrow f_c$, and $(f_e+f_c)/2-2f_c \rightarrow (f_e-3f_c)/2$, respectively. The first two interactions

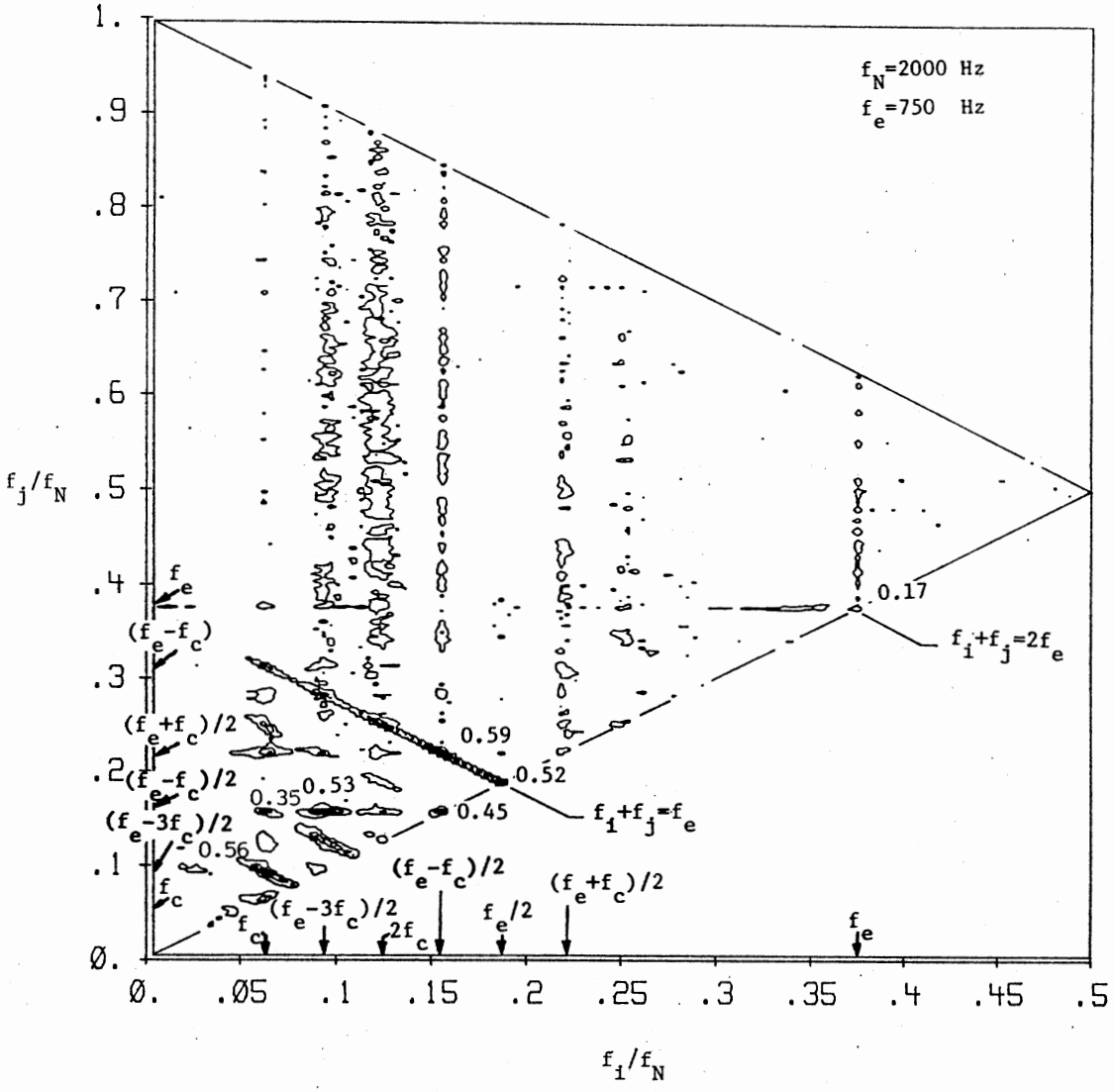

Figure 58. Excited Jet Centerline Bicoherence Spectrum at x/D = 3.0. Contours are from 0.075. The Contour Interval is 0.15.

indicate the production of the jet column mode f_c while the third interaction shows the production of the $(f_e-3f_c)/2$ mode. The growth of these discrete modes as shown above also may be noted in the centerline power spectrum Figure 40.

The centerline bicoherence spectrum at x/D = 4 is shown in Figure 59 clearly demonstrates the interactions of the modes $f_i = f_c$ and $f_i = (f_e-3f_c)/2$ mode with the natural instabilities at frequencies f_j. Also, in this figure the highest peak $b^2(f_c,(f_e-3f_c)/2) = 0.47$ indicates the interaction between $(f_e-f_c)/2$ and $(f_e-3f_c)/2$ modes which demonstrates the interaction $(f_e-f_c)/2-(f_e-3f_c)/2 \rightarrow f_c$. Other higher frequency modes presented at x/D = 3 have fully decayed which is due to the high turbulent level near the end of the potential core. With increasing downstream distances there is a gradual shift in energy to the subharmonic of the jet column mode as noted in Figure 60 at x/D = 5 by the interaction $b^2(f_c/2,f_c) = 0.25$ which indicates the interaction between the jet column mode and its subharmonic. The formation of a subharmonic of the jet column mode was also seen in the centerline power spectra of Figure 43 in section 3.3.2.

In order to obtain further information regarding the jet transition, the next section presents the coherence measurements between fluctuations in the two jet shear layers obtained for selected streamwise locations within the region $0.25 \leq x/D \leq 10$. These measurements will provide insight regarding the mechanism by which the jet column mode interacts with shear layer instabilities to configure the initial flow.

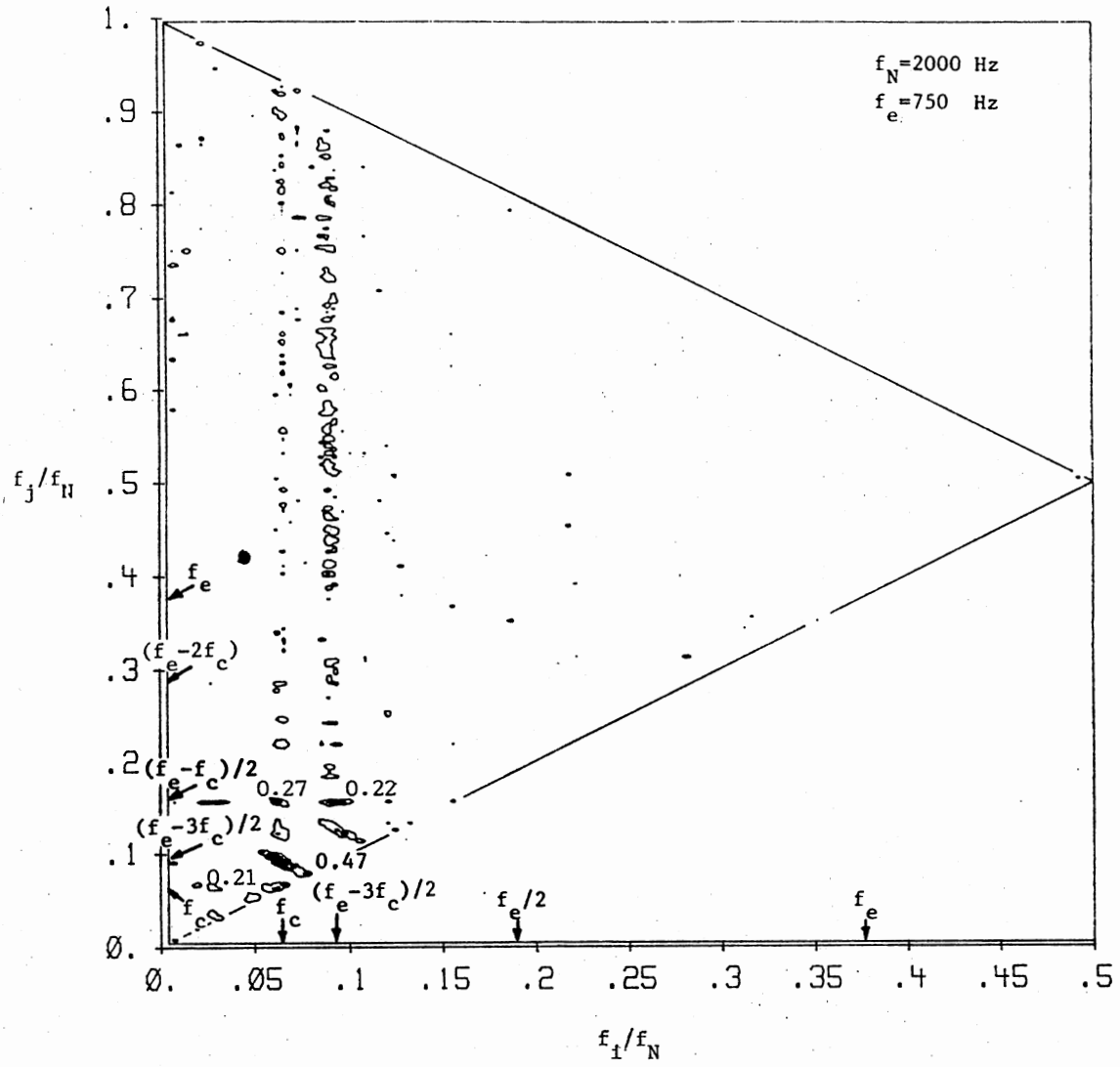

Figure 59. Excited Jet Centerline Bicoherence Spectrum at x/D = 4.0. Contours are from 0.075. The Contour Interval is 0.15.

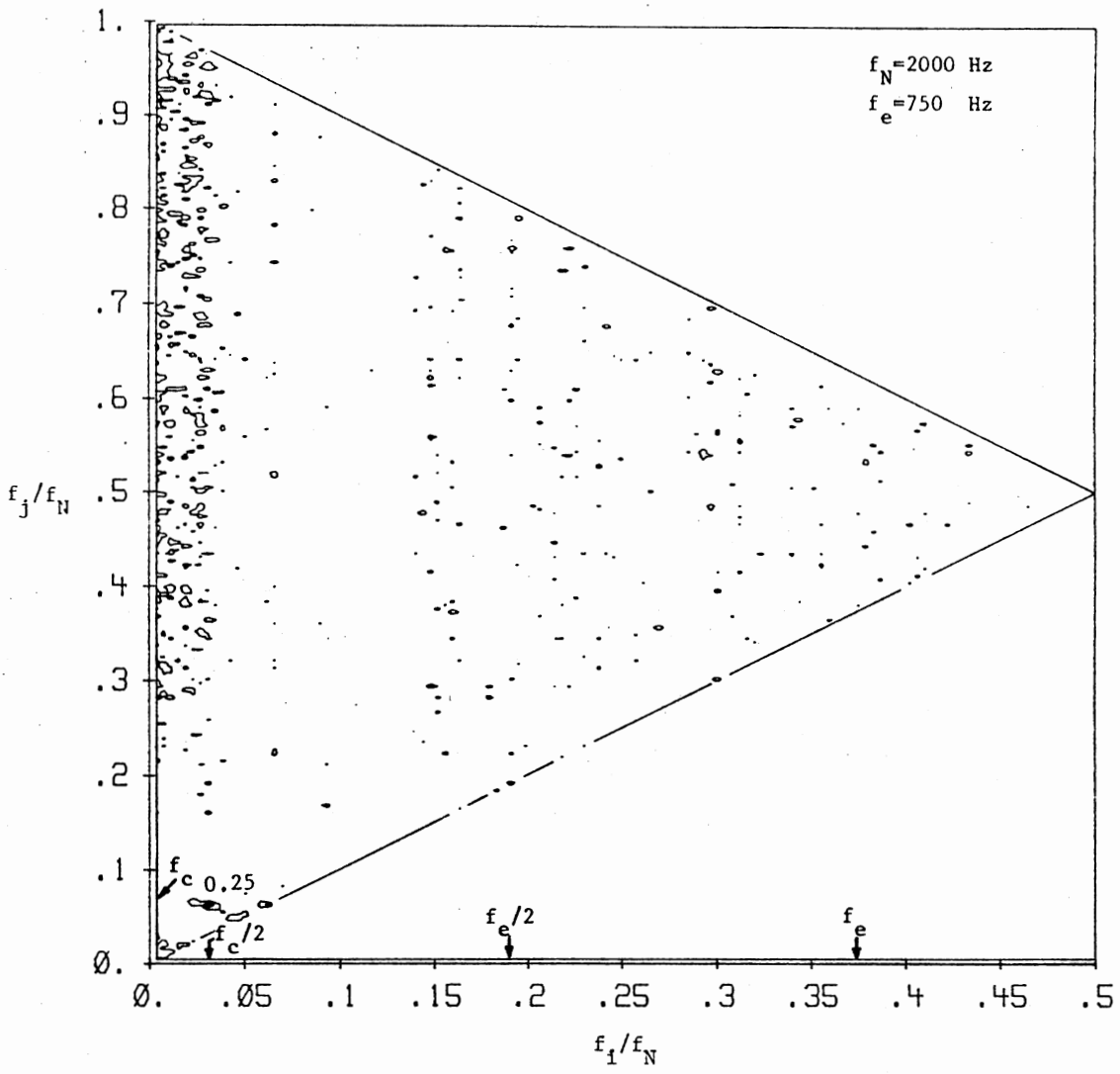

Figure 60. Excited Jet Centerline Bicoherence Spectrum at x/D = 5.0. Contours are from 0.05. The Contour Interval is 0.05.

3.5 Coherence and Phase Angle Measurements

The cross spectrum between the two signals x(t) and y(t) is a complex function of frequency such that

$$G_{xy}(f) = C_{xy}(f) - iQ_{xy}(f) \tag{3.1}$$

where the real part, $C_{xy}(f)$, is called the coincident spectral density function, and the imaginary part, $Q_{xy}(f)$, is called the quadrature spectral density function.

It is convenient to express the cross-spectral density function in complex polar notation such that

$$G_{xy}(f) = |G_{xy}(f)|e^{-i\theta_{xy}(f)} \tag{3.2}$$

$$|G_{xy}(f)| = \left(C_{xy}^{2}(f) + Q_{xy}^{2}(f)\right)^{1/2} \tag{3.3}$$

$$\theta_{xy}(f) = \tan^{-1}\left(Q_{xy}(f)/C_{xy}(f)\right) \tag{3.4}$$

where $|G_{xy}(f)|$ is the magnitude of the cross-spectral density function, and $\theta_{xy}(f)$ is the frequency dependent phase angle between the two signals x(t) and y(t). When applying cross-spectral density information to physical problems, it is often desirable to use a real-value quantity given by

$$\gamma^{2}_{xy}(f) = \frac{|G_{xy}(f)|^{2}}{\left(P_{x}(f)\ P_{y}(f)\right)} \tag{3.5}$$

where $\gamma^{2}_{xy}(f)$ is called the spectral coherence function, and $P_{x}(f)$ and

$P_y(f)$ are the power spectral density functions corresponding to two signals x(t) and y(t), respectively. When $\gamma^2_{xy}(f) = 0.0$, x(t) and y(t) are said to be incoherent at that frequency, and if $\gamma^2_{xy}(f) = 1$, then x(t) and y(t) are said to be fully coherent at that frequency. For values of coherence less than 1.0 the two signals are said to be partially coherent at that frequency.

Spectral coherence measurements were made in order to provide additional information concerning the relationship between corresponding frequency components in the two excited shear layers of the developing planar turbulent jet. In order to measure the longitudinal fluctuations in the shear layers, two standard hot-wire probes were used and positioned on opposite sides of the jet centerline at $y/b = \pm 1.0$ for selected x/D locations. The required cross spectra and autospectra were computed via the Fast Fourier Transform technique. Each spectral coherence and phase angle spectrum represents an ensemble average over 150 samples of 512 points each. The PASCAL program which was developed to perform these measurements is listed in Appendix A.

In the first set of measurements to be presented, two standard hot-wire probes were placed on opposite sides of the jet centerline at $y/b = \pm 1.0$ as shown schematically in Figure 61. The spectral coherence and phase angle spectra were both obtained at selected streamwise locations of the probe pair $0.25 \leq x/D \leq 5.0$. Representative data will next be presented and discussed.

Figure 62 presents the coherence function measured at $x/D = 0.75$. Figure 62 exhibits five distinct regions of elevated spectral coherence near 54-70 Hz, 289-335 Hz, 382-468 Hz, 656-674 Hz, and 800-828 Hz. Two of these peaks, 289-335 Hz and 382-468 Hz, are centered about the

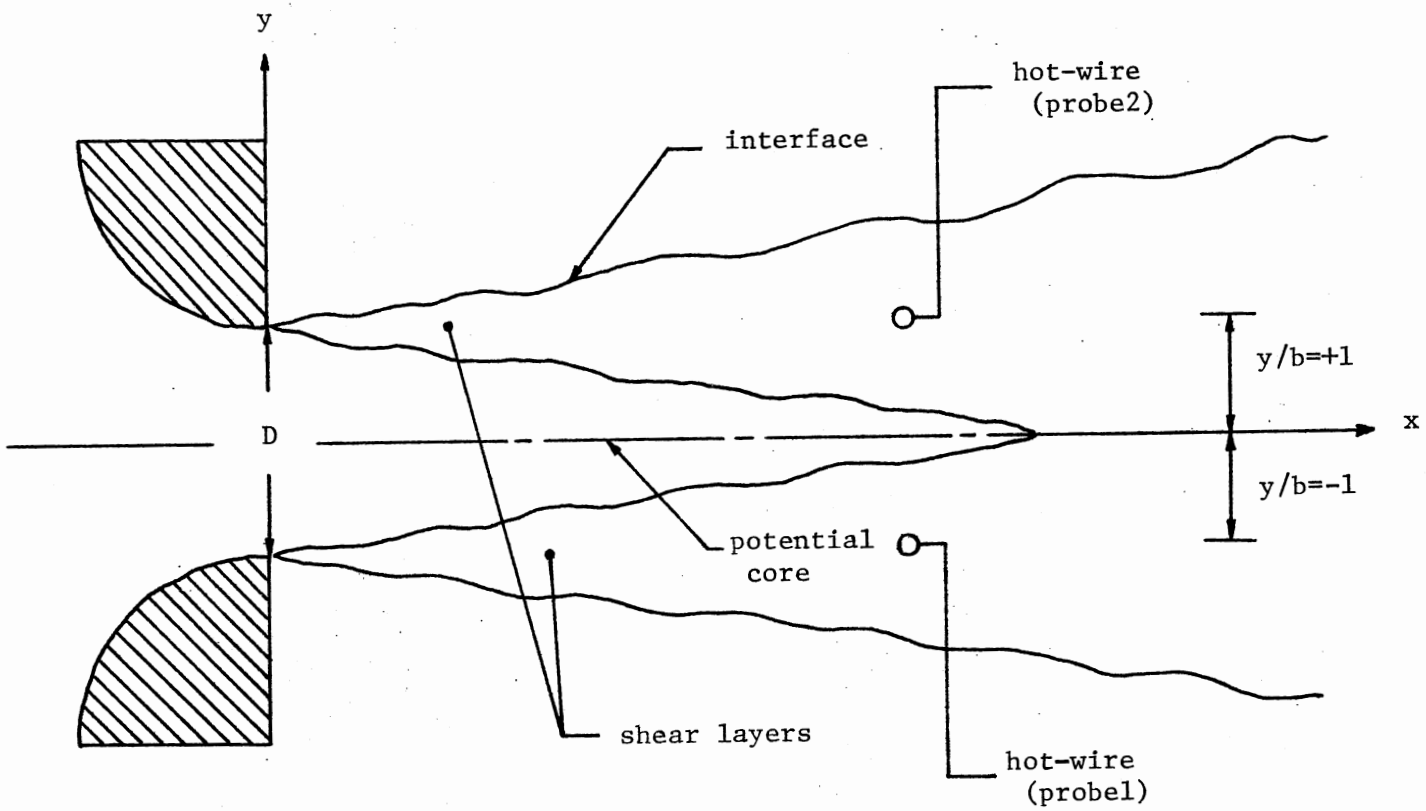

Figure 61. Probes Arrangement for Coherence Measurements

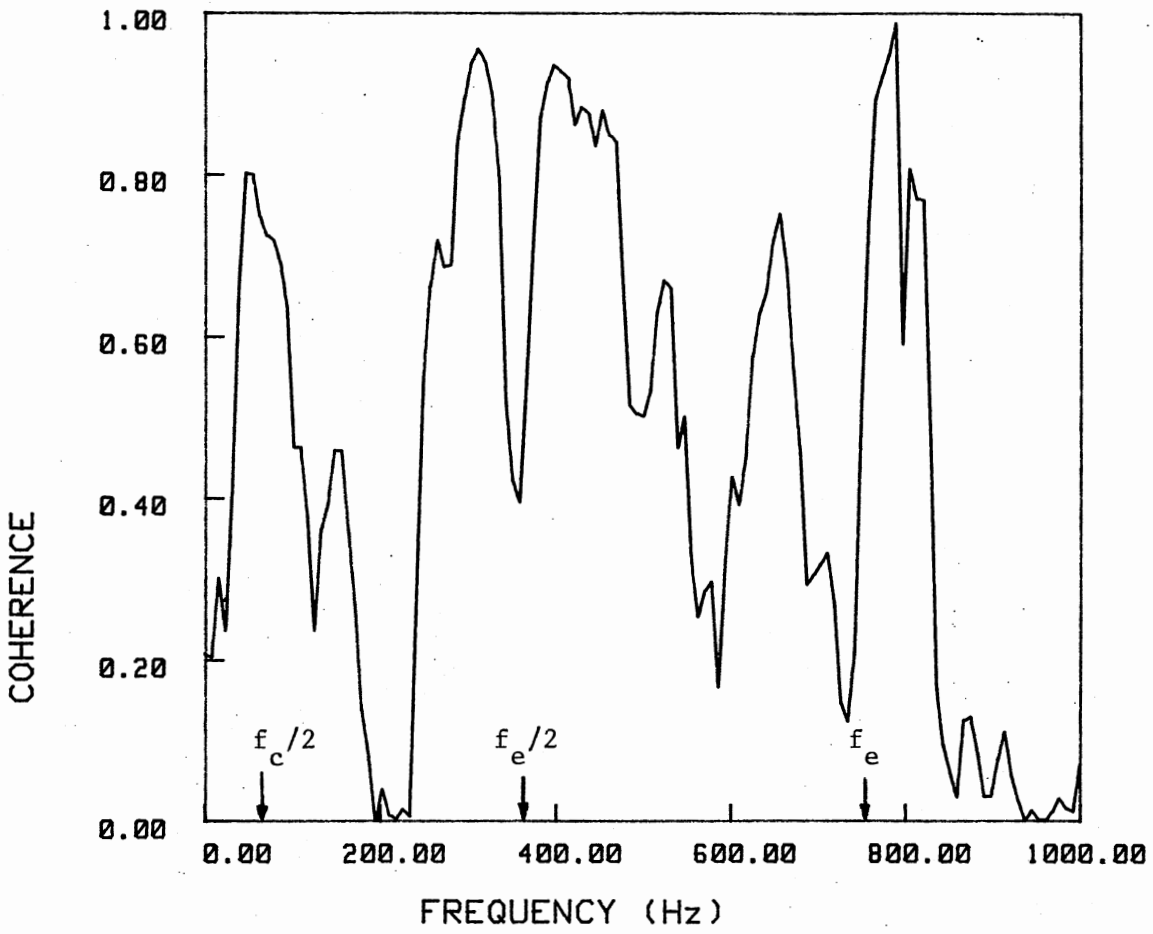

Figure 62. Excited Coherence Spectrum at x/D = 0.75
(probes placed side by side)

subharmonic frequency $f_e/2$ which exhibits a comparatively low coherence level. Two of the other peaks, 656-674 Hz and 800-828 Hz, are centered on the excitation frequency f_e which exhibits a much lower coherence level. Of particular interest in this figure is the spectral coherence peak at 54-63 Hz which suggests that the mode near $f_c/2$ is phase coupled on opposite sides of the near exit jet shear layers.

In order to investigate the implications of the spectral coherence measurements as shown in Figure 62, the coherence between two modeled complex waves was computed and used to duplicate certain features of the measured coherence functions. Based upon the results of the bicoherence measurements of the previous section, the two shear layer signals were modeled as involving two quadratic nonlinear interactions between the 375 Hz ($f_e/2$) mode and 63 Hz ($f_c/2$) mode and the 750 Hz (f_e) mode and 63 Hz ($f_c/2$) mode as shown below:

$$A_1 = a_o[\cos(\omega_1 t)+\cos(\omega_2 t)]\cos(\omega_3 t+\phi)+n(t) \qquad (3.6)$$

$$A_2 = a_o[\cos(\omega_1 t)+\cos(\omega_2 t)]\cos(\omega_3 t)+n(t) \qquad (3.7)$$

where $a_o = 1.0$, $\omega_1/2\pi = 375$ Hz $= (f_e/2)$, $\omega_2/2\pi = 750$ Hz $= (f_e)$, $\omega_3/2\pi = 63$ Hz $= (f_c/2)$, ϕ = arbitrary phase angle, and n(t) is small amplitude random noise. The range for the random noise n(t) is restricted between 0.0 and 0.1 which is never larger than $0.1a_o$. Certainly the actual shear layer anemometer signals are more complex than these. However, the bicoherence measurements indicate that the strongest interactions that occur in the developing jet shear layers involve the modes $f_e/2$ and $f_c/2$ so that certain dominant features (though not all) of the coherence

spectra may be duplicated. It may be noted from these equations that the ϕ phase shift on ω_3 mode was introduced to account for the possibility of asymmetry in the low frequency component. Also, these modeled shear layer signals suggest that the quadratic interactions in each shear layer are phase coherent across the jet.

For the purpose of comparison, several trials of phase shift of the low frequency mode were considered. The variation of phase shift of the low frequency mode was found to have no effect on the resulting coherence function. However, in the data to be presented, $\phi = \pi/4$ in order to obtain agreement with selected experimental phase spectra.

Figure 63 compares the coherence function for the experimental coherence function obtained at x/D = 0.75 and the modeled coherence function based upon the signals given by Equations 3.6 and 3.7. It is clearly seen from Figure 63 that the dominant features of the experimental measurement are in qualitative agreement with the coherence function based on the modeled signals. Note that two coherence peaks are centered on the subharmonic $f_e/2$ and two other peaks are centered on the excitation frequency f_e while the coherence of the subharmonic and excitation frequency are at very low levels.

Figure 64 presents the coherence spectrum obtained at x/D = 1.5. Based upon the comparison of Figures 62 and 63, this figure also suggests the presence of quadratic nonlinear interactions between primary jet shear layer modes and $f_c/2$ which are phase coherent across the jet. Figure 65 presents the coherence function obtained at x/D = 2.5. Though the overall coherence levels are reduced due to elevated turbulence, it may be noted that peaks occur at the same frequencies as seen upstream at x/D = 1.5 (compare with Figure 64). These figures both

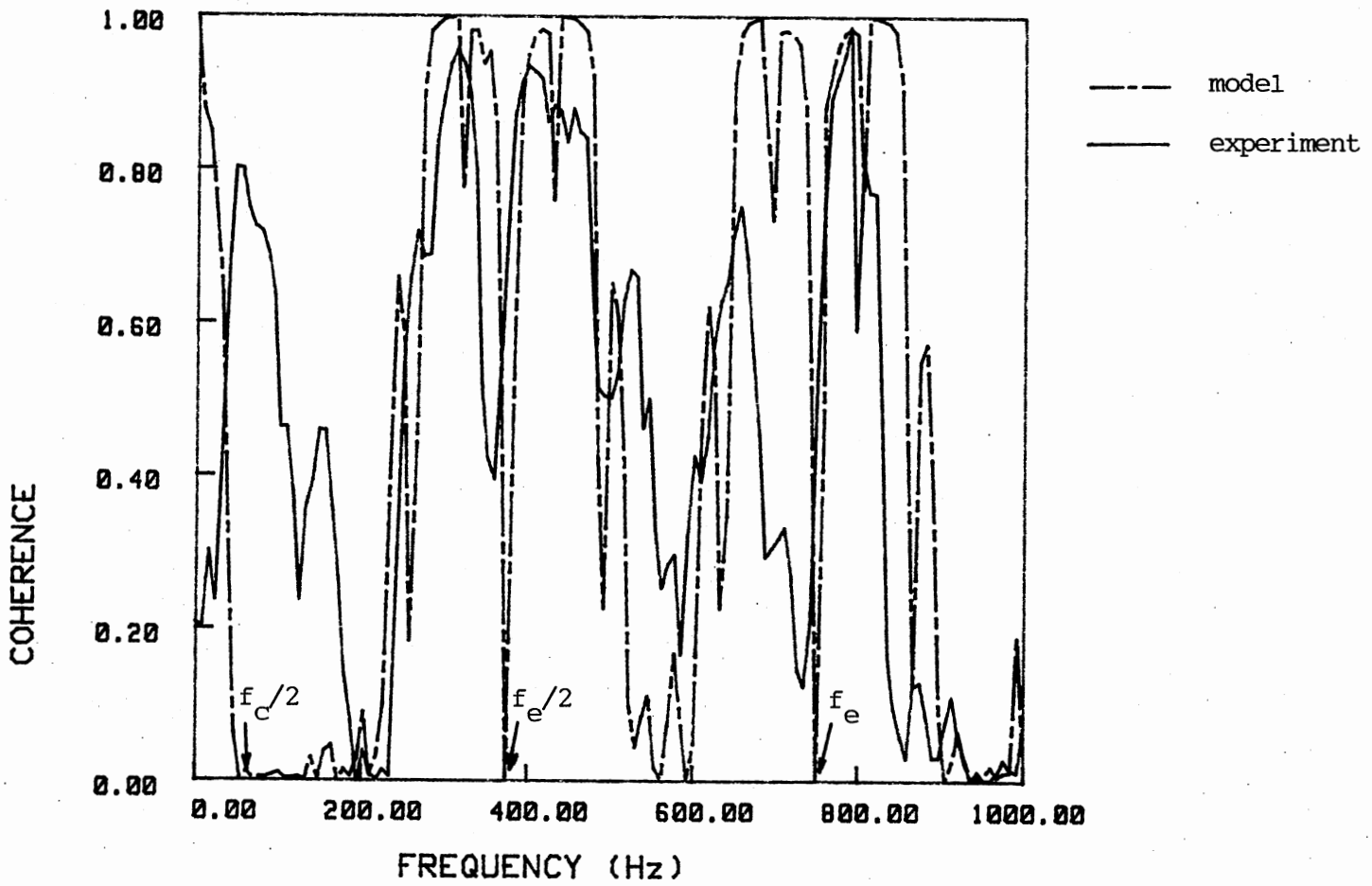

Figure 63. Comparison of Modeled Coherence Function and Experimental Coherence Function at x/D = 0.75

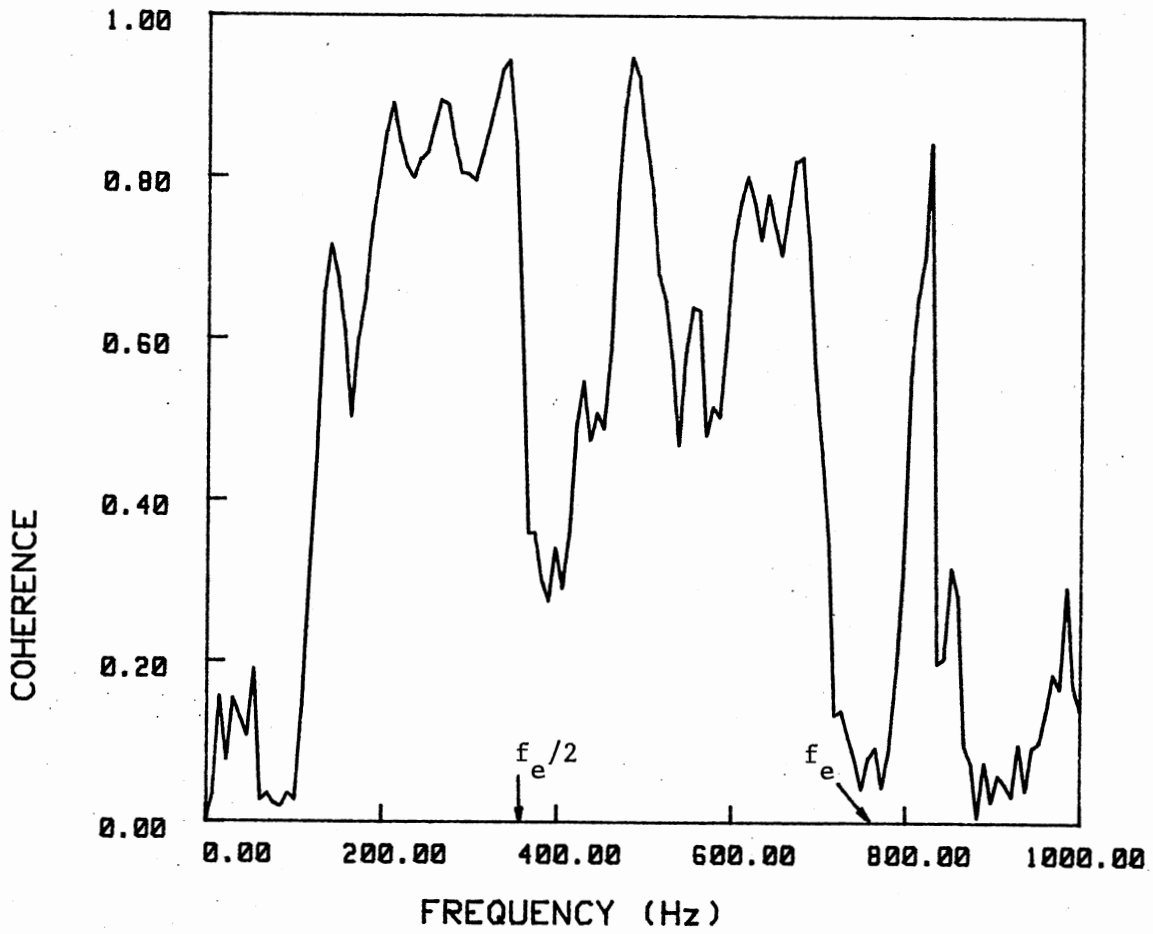

Figure 64. Excited Coherence Spectrum at x/D = 1.5 (probes placed side by side)

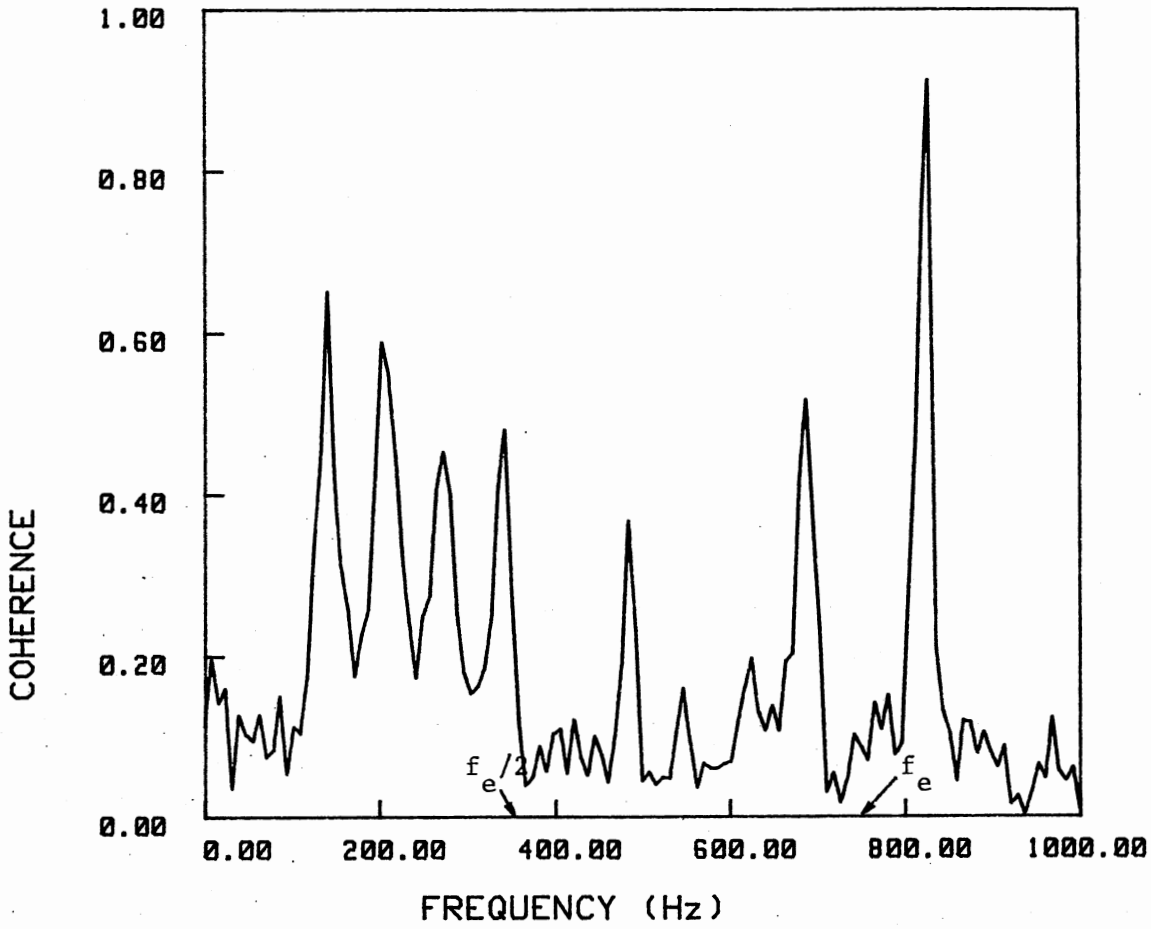

Figure 65. Excited Coherence Spectrum at x/D = 2.5
(probes placed side by side)

exhibit four distinct spectral peaks at 140 Hz, 203 Hz, 273 Hz, and 343 Hz. The separation between these discrete peaks is approximately 67 Hz which likely corresponds to the half of the jet column mode $f_c/2$. In addition, two spectral coherence peaks at 687 Hz and 828 Hz suggest quadratic nonlinear interaction between the excitation frequency f_e and the half of the jet column mode $f_c/2$ which is coherent across the jet. Certain features of these experimentally obtained coherence spectra shown in Figures 64 and 65 may be duplicated with modeled shear layer signals involving the linear combination of three simple waves and two quadratic nonlinear interactions. The model waveform is based upon examination of the power spectrum at x/D = 2.5 in Figure 34 and is given by below:

$$A_1 = a_o\{\cos(\omega_1 t)+\cos(\omega_2 t)+\cos(\omega_3 t) +[\cos(\omega_4 t)+\cos(\omega_5 t)]\cos(\omega_6 t+\phi)\} +n(t) \quad (3.8)$$

$$A_2 = a_o\{\cos(\omega_1 t)+\cos(\omega_2 t)+\cos(\omega_3 t) +[\cos(\omega_4 t)+\cos(\omega_5 t)]\cos(\omega_6 t)\} +n(t) \quad (3.9)$$

where $a_o = 1.0$, $\omega_1/2\pi = 126$ Hz $= (f_c)$, $\omega_2/2\pi = 186$ Hz $= ((f_e-3f_c)/2)$,

$\omega_3/2\pi$ = 252 Hz = $(2f_c)$, $\omega_4/2\pi$ = 375 Hz = $(f_e/2)$, $\omega_5/2\pi$ = 750 Hz = $(2f_e)$, $\omega_6/2\pi$ = 63 Hz = $(f_c/2)$, ϕ = the phase shift of low frequency mode $(\pi/4)$, and n(t) is small amplitude random noise. Figure 66 presents the comparison of the modeled coherence function corresponding to the two modeled shear layer signals given by Equations 3.8 and 3.9 and the experimental coherence function obtained at x/D = 2.5. In this figure the modeled function also exhibits seven coherence peaks at 126 Hz, 186 Hz, 252 Hz, 312 Hz, 438 Hz, 687 Hz, and 813 Hz. The existence of these modeled peaks are in qualitative agreement with the actual experimental results as shown in Figures 64 and 65. The separation between these peaks is 63 Hz. At the same time, the spectral coherence at subharmonic $f_e/2$ = 375 Hz and excitation frequency f_e = 750 Hz exhibit comparatively low coherence values which agree with the measured coherence functions as shown in Figures 64 and 65.

The phase spectrum based upon the modeled shear layer signals given by equations 3.8 and 3.9 was computed and is compared with the actual experimental phase spectrum obtained at x/D = 1.5 and 2.5 in Figures 67 and 68, respectively. The modeled phase spectrum in Figure 67 exhibits a sudden shift of phase angle at the subharmonic $f_e/2$ and excitation frequency f_e, and the absolute value of phase shift of their two side-bands located at $(f_e+f_c)/2$ and $(f_e-f_c)/2$ is $\pi/4$ which is identical to ϕ (eq. 3.8) of the low frequency mode. It may be noted from this figure that the experimental phase spectrum obtained at x/D = 1.5 also exhibits a shift of phase angle near the subharmonic $f_e/2$ and excitation frequency f_e. Basically, the variation of the phase shift of this experimentally obtained phase spectrum at $f_e/2$ and f_e are in qualitative agreement with the modeled phase spectrum though the values of the phase

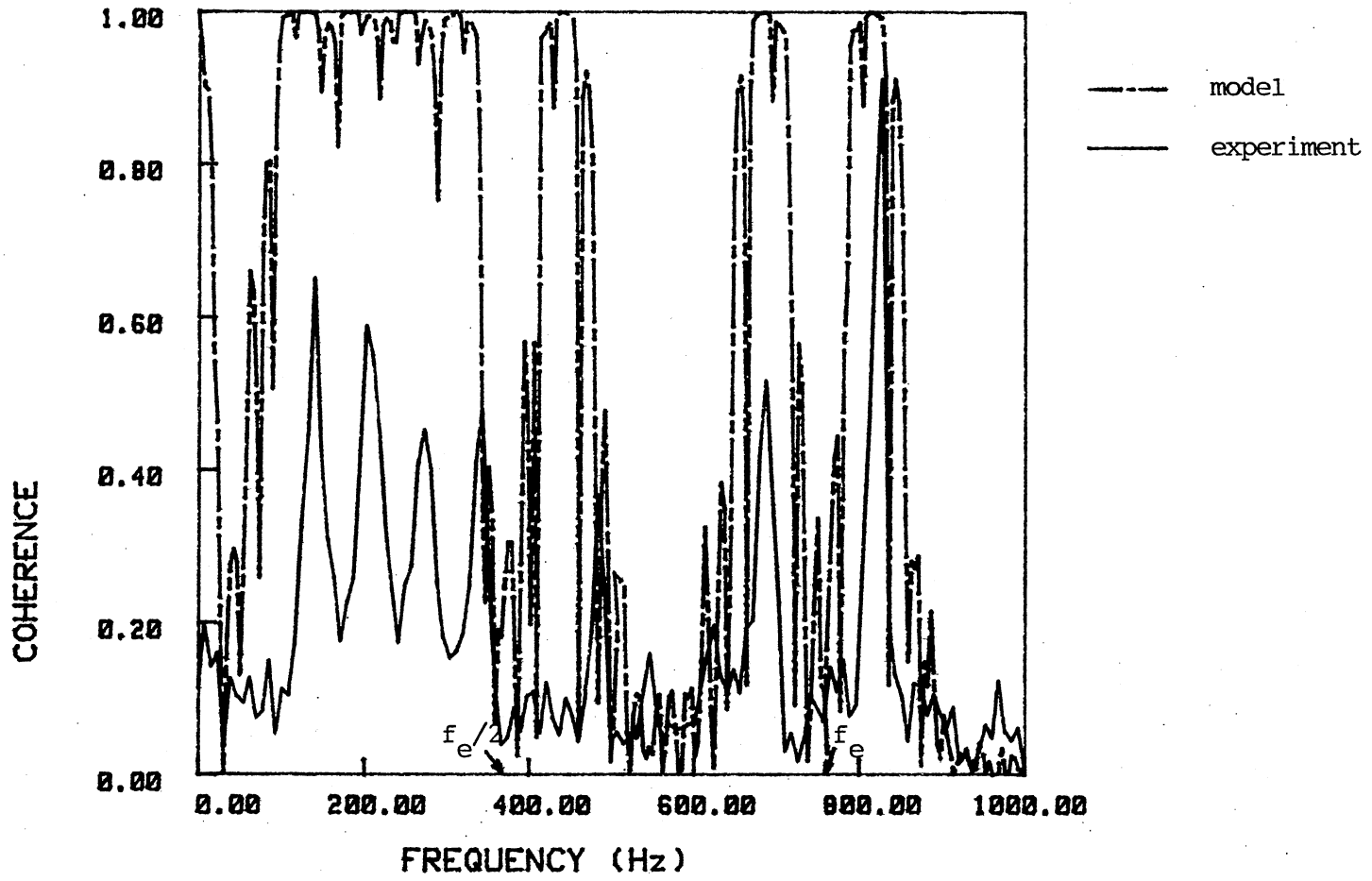

Figure 66. Comparison of Modeled Coherence Function and Experimental Coherence Function at x/D = 2.5

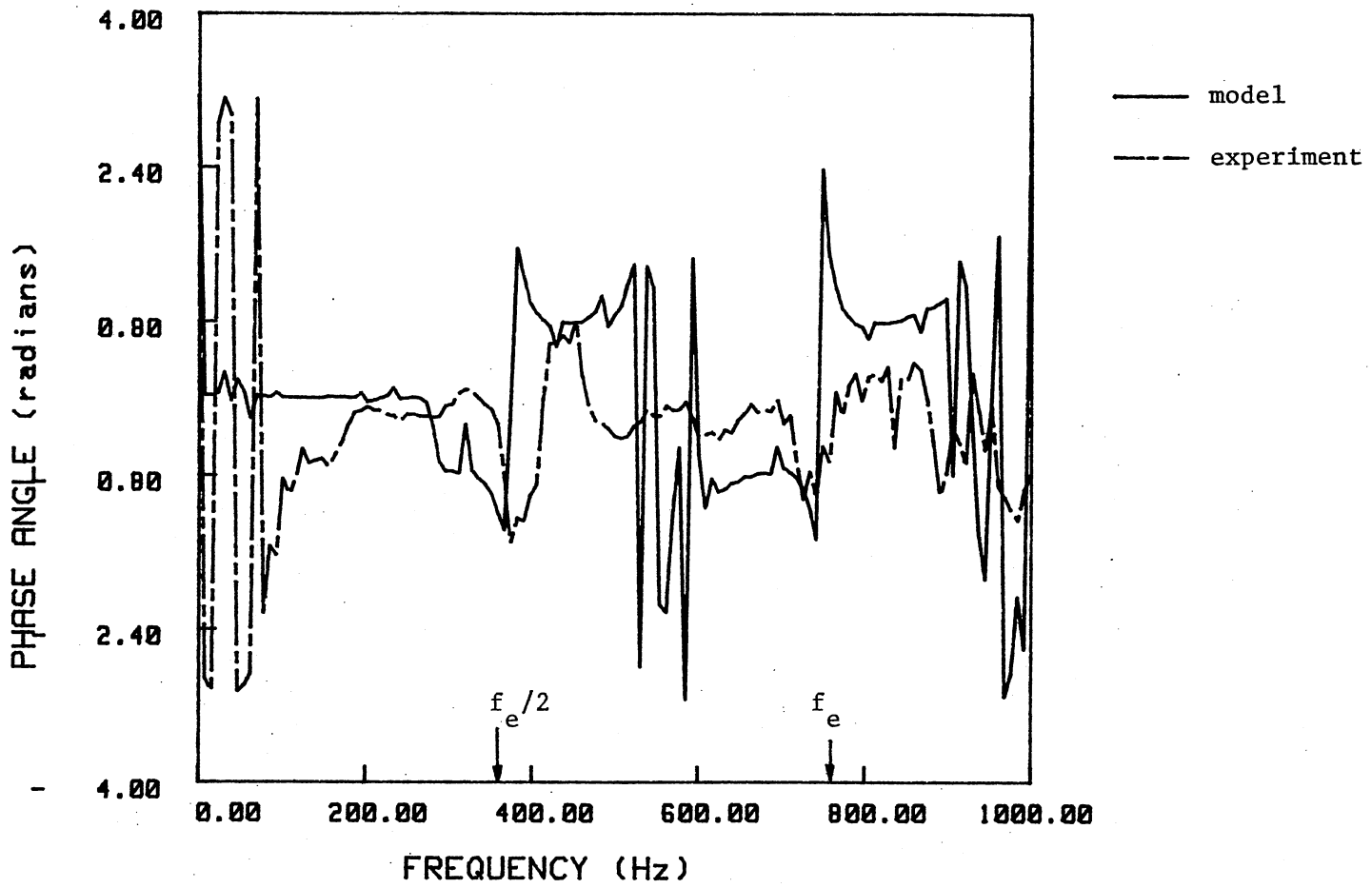

Figure 67. Comparison of Modeled Phase Spectrum and Excited Phase Spectrum at x/D = 1.5

shift at $f_e/2$ and f_e are not quite the same between both cases. The difference may be due to the increased phase randomness which characterizes the actual hot-wire signals. Figure 68 compares the modeled phase spectrum with the experimental phase spectrum obtained at x/D = 2.5. The experimental result shown in Figure 68 also displays significant phase shifts near $f_c/2$ and subharmonic $f_e/2$ while the phase angle spectrum at excitation frequency f_e exhibits negligible phase shift possibly due to the lower coherence of the quadratic interaction between f_e and $f_c/2$ suggested by Figure 65.

Based upon the results shown in Figures 67-68, it appears that the formation of the phase shift of the subharmonic $f_e/2$ and the excitation frequency f_e are related to the phase shift of $f_c/2$ through the quadratic nonlinear interaction during the jet transition.

Measurements made for x/D > 4.0 (not shown here) exhibit low coherence levels and random phase shifts between two shear layer signals due to the chaotic nature of the flow that characterizes this turbulent "breakdown" region. Therefore, these measurements do not seem capable of providing further information regarding the jet development occurring at locations near the end of the potential core.

The coherence spectra presented above were obtained with low level acoustic excitation at frequency f_e = 750 Hz which corresponds to the initially most unstable jet shear layer frequency. It is of interest to know how the coherence results obtained from the excited jet shear layers compare to the case of natural jet transition. The following data present a comparison of coherence functions obtained under excited and natural conditions for selected downstream locations. Figures 69-70 compare the coherence spectra under natural and excited conditions

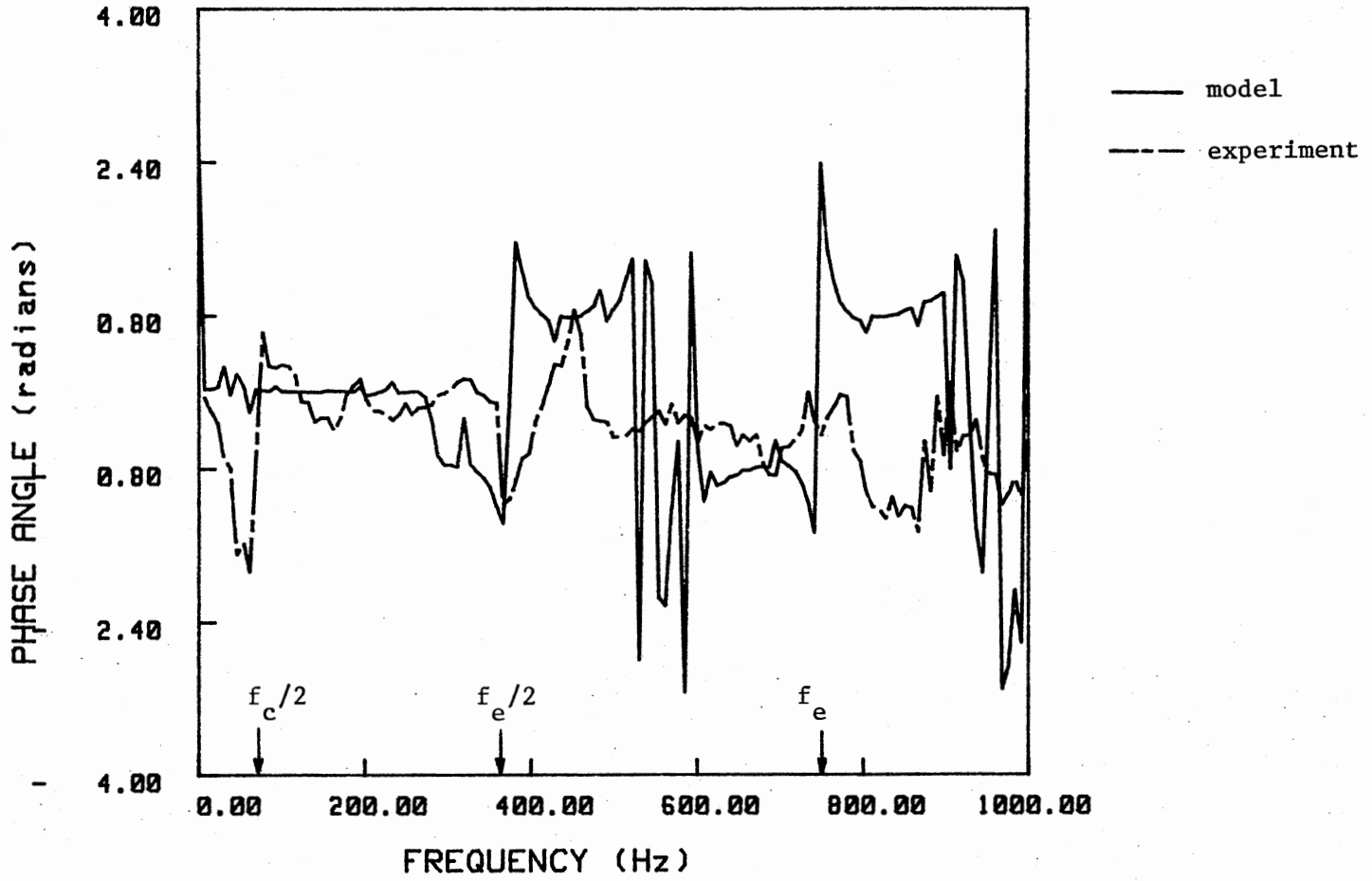

Figure 68. Comparison of Modeled Phase Spectrum and Excited Phase Spectrum at x/D = 2.5

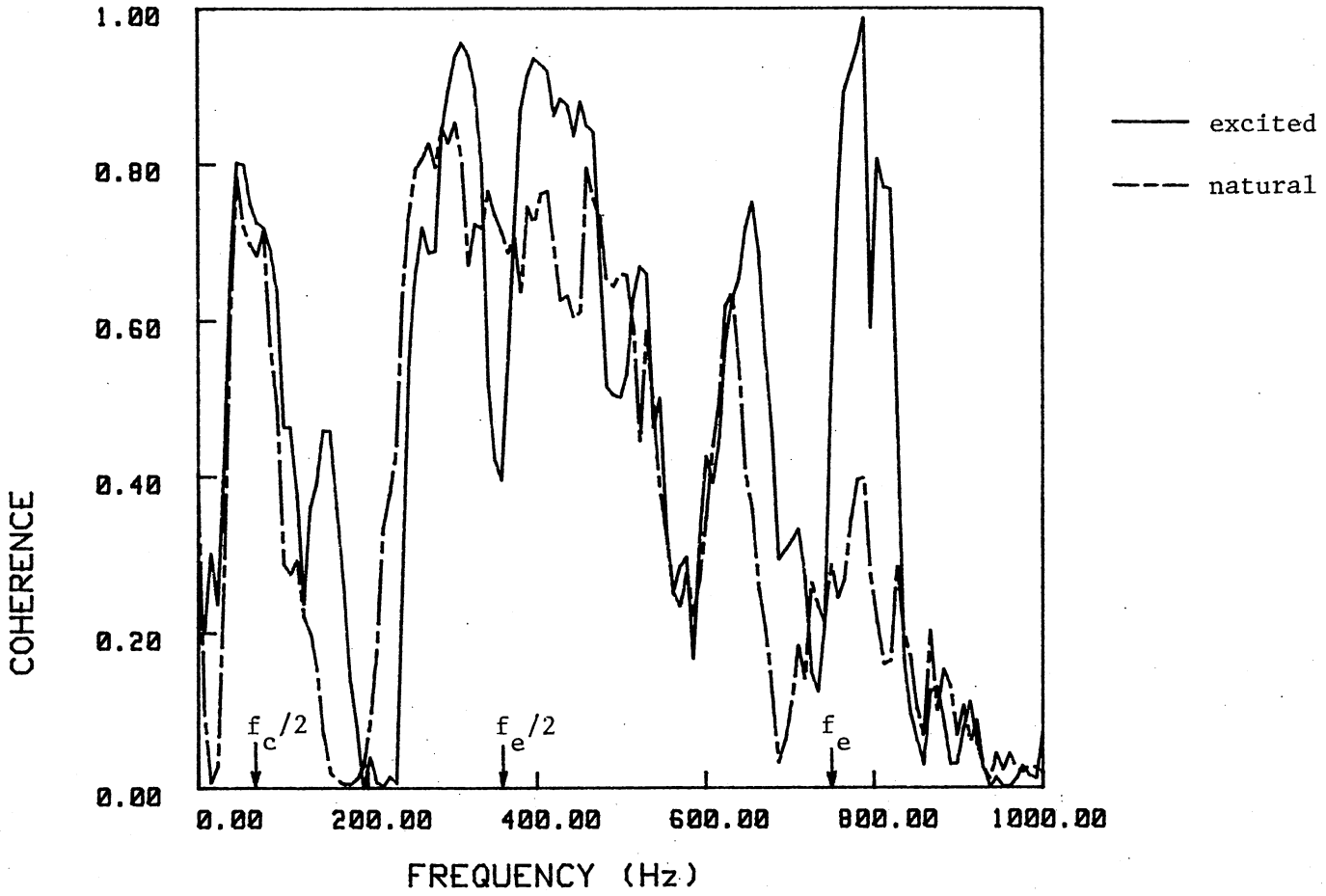

Figure 69. Comparison of natural and Excited Coherence Function at x/D = 0.75

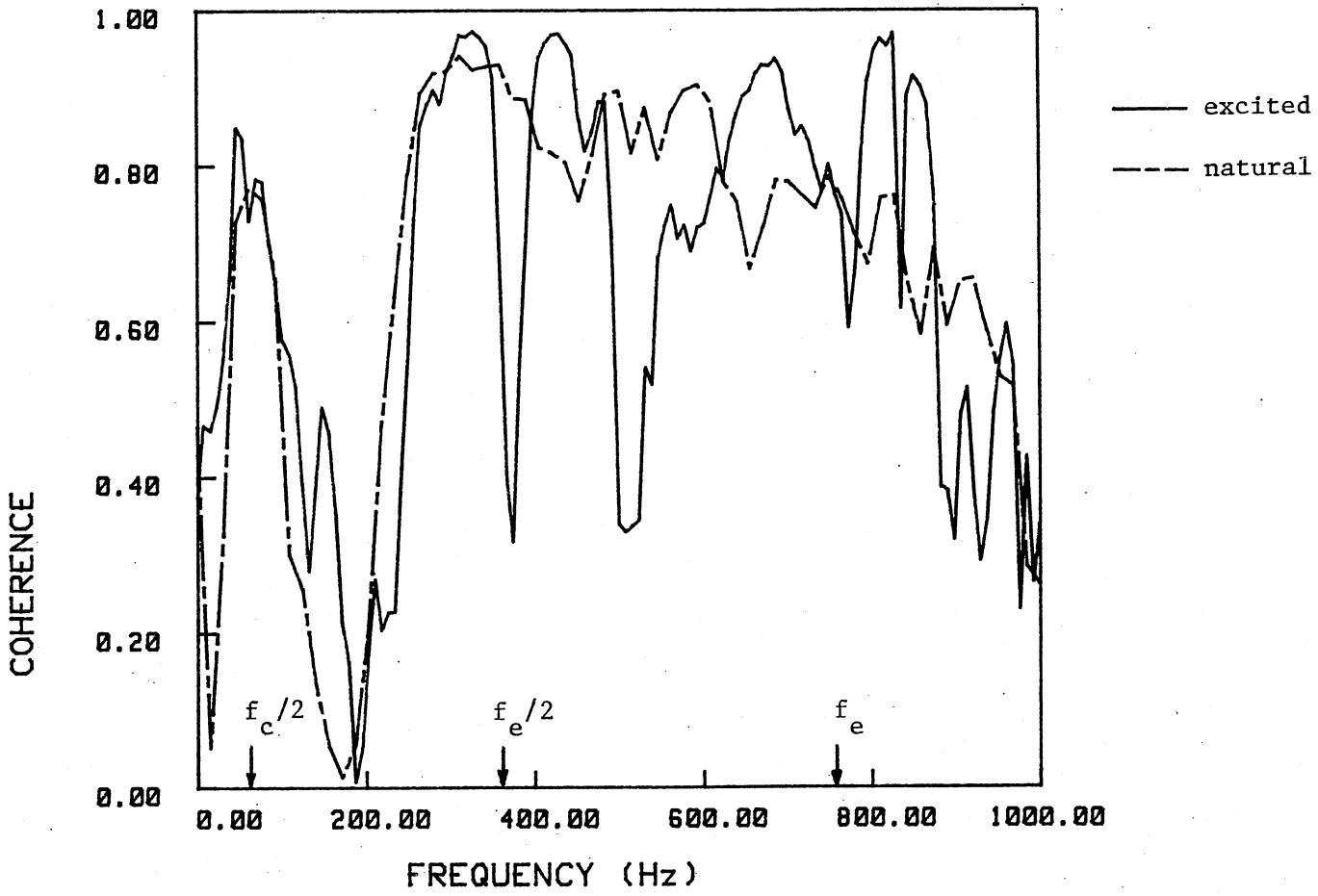

Figure 70. Comparison of Natural and Excited Coherence Function at x/D = 1.0

obtained at x/D = 0.75 and 1.0, respectively. It may be noted that the natural coherence spectra show similar trends as their excited counterparts with the exception of the absence of sharp peaks and valleys. In effect, the natural coherence spectra appear as "randomized" or "smoothed" versions of their excited case counterparts. This suggests that the interactions responsible for the appearance of the excited jet coherence spectra are also at work in the natural jet. As expected, the influence of the mode $f_c/2$ appears to be important in both natural and excited cases as both show a nearly identical coherence peak at half the jet column mode $f_c/2$.

Figure 71 compares natural and excited coherence spectra at x/D = 2.5. Due to the increased turbulence level, both coherence spectra exhibit lower coherence as compared to those made nearer to the nozzle exit. Again, the natural coherence spectrum can be viewed as a smoothed or randomized version of the excited case, with peaks at 140 Hz, 203 Hz, 273 Hz, and 343 Hz blending into a single broad peak in the natural case. In addition the peaks at 687 Hz and 828 Hz which appear in the excited case are absent in the corresponding natural case. This is not surprising since it has been shown that these coherence peaks are the results of interactions between the forcing frequency f_e and the mode $f_c/2$. Based on the comparison of the natural and excited cases, it appears that the excited jet should facilitate a better understanding of the results obtained from the natural jet transition.

In the next set of measurements to be presented, two standard hot-wire probes were placed on opposite sides of the jet centerline with one probe fixed in the jet shear layer near the nozzle exit at x/D = 0.25 (i.e. y/b = 1.0). The other probe was movable and was placed in the

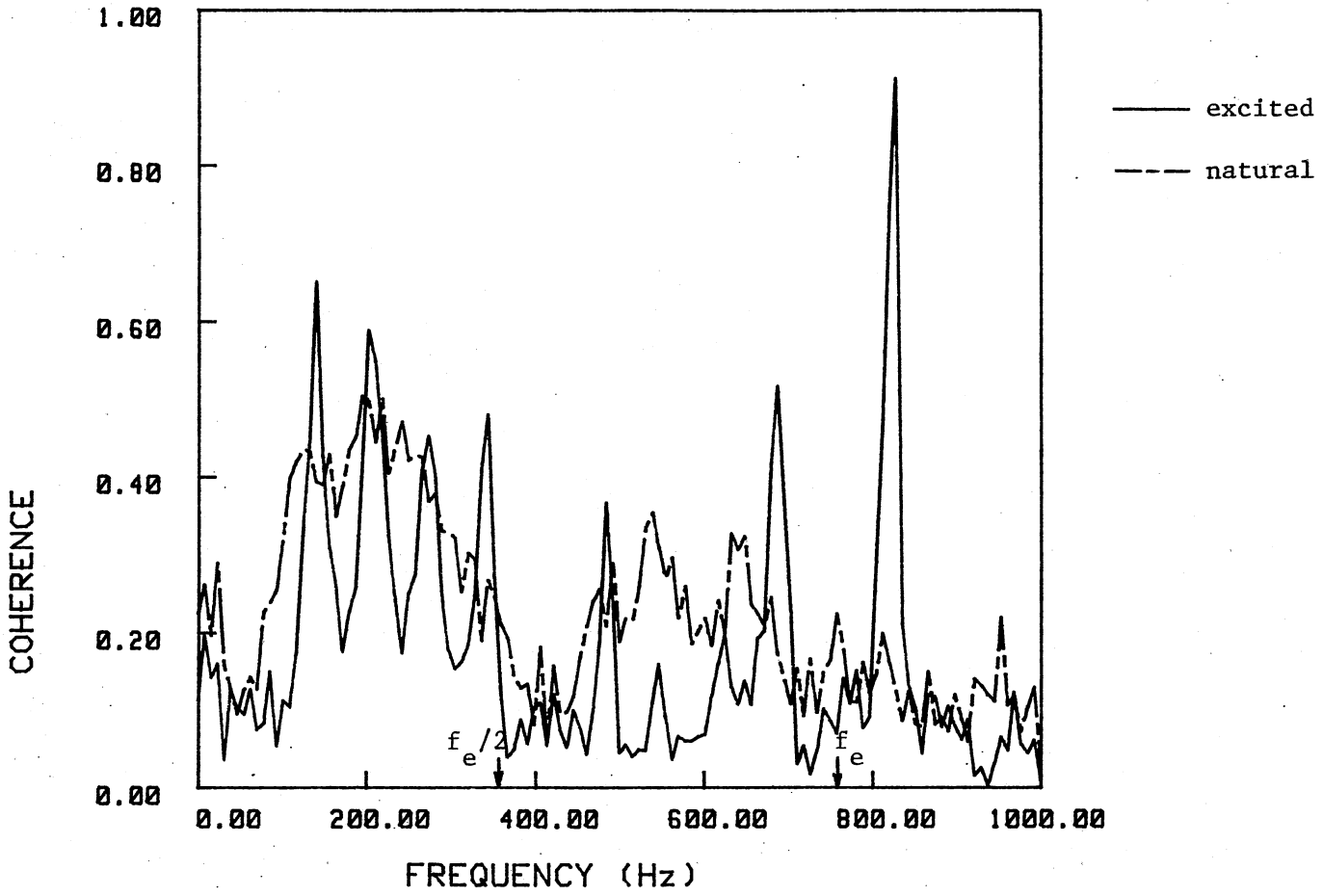

Figure 71. Comparison of Natural and Excited Coherence Function at x/D = 2.5

opposite jet shear layer over streamwise locations $0.25 \leq x/D \leq 10.0$. The probe positioning is shown schematically in Figure 72. In this manner the existence of a coupling between downstream spectral modes and the nascent shear layer flow could be investigated.

Figure 73 demonstrates experimentally measured modal frequencies corresponding to the maximum spectral coherence for various downstream locations of the movable probe in the excited jet. The results obtained from the natural jet shear layers by Prakash (1986) in the same setup and Reynolds number are also shown for comparison. The frequency variation with x/D is discontinuous and involves four levels of nearly constant frequency. As described by Prakash (1986) this phenomenon is consistent with the requirement for a global resonance mechanism to operate in the flow. It is clearly seen from this figure that for $0.25 \leq x/D \leq 2.5$, the spectral modes near 828 Hz and 63 Hz are most coherent with the nascent shear layer flow for the excited case. As described earlier in the first set of coherence measurements, the 828 Hz mode is produced by the quadratic nonlinear interaction between the excitation frequency f_e and the half of the jet column $f_c/2$ in the jet shear layers. The absence of the high coherence at 828 Hz for the natural flow is not surprising due to lack of coherent forcing at f_e. After $x/D > 2.5$, both cases basically exhibit the same behavior in order to satisfy global resonance requirements in the jet flow. Of particular importance in this figure is the elevated spectral coherence near 63 Hz ($f_c/2$) which indicates that for both natural and excited cases the nascent shear layers are coupled to the downstream flow at this frequency. This aspect is discussed later in this section.

Figure 74 demonstrates the variation of the spectral coherence

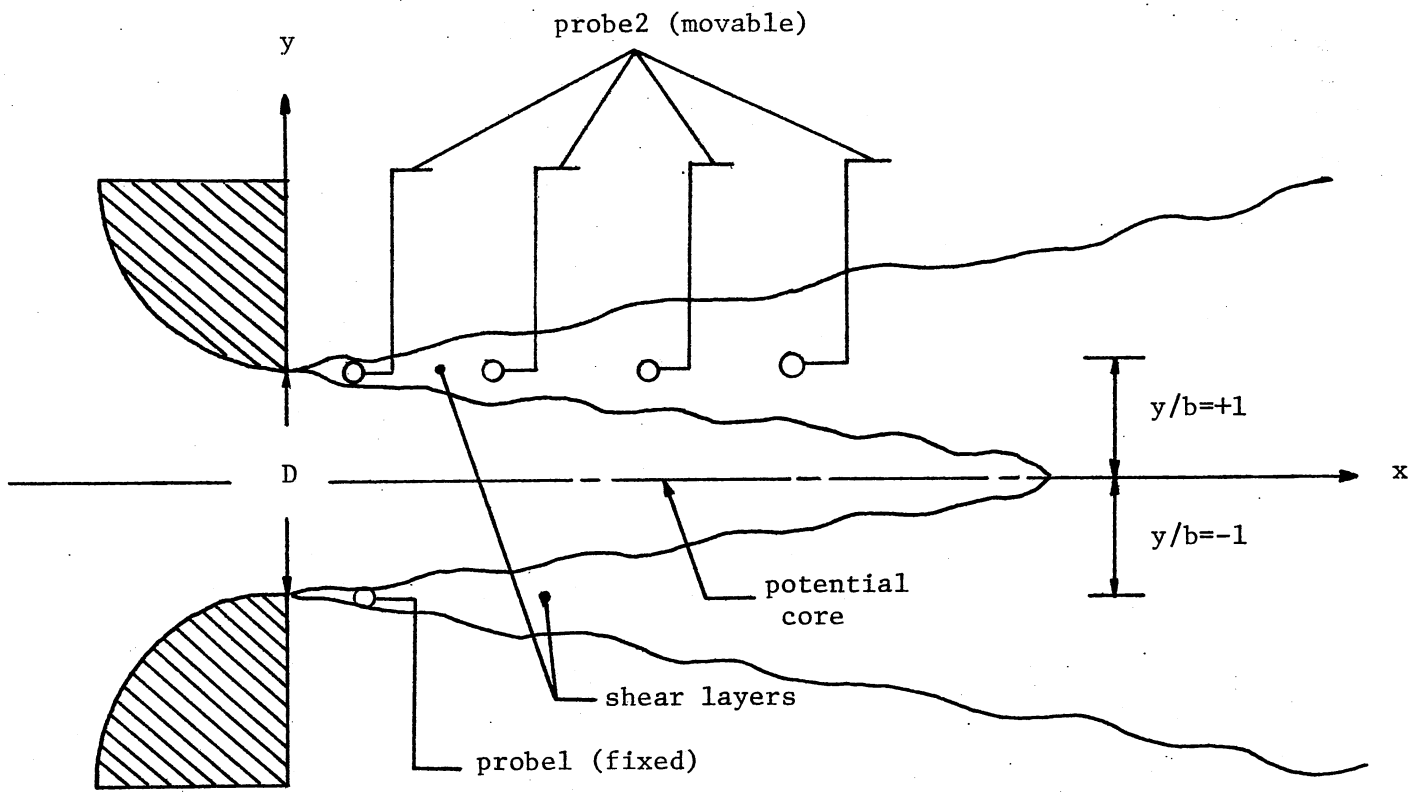

Figure 72. Probes Arrangement for Coherence Measurements

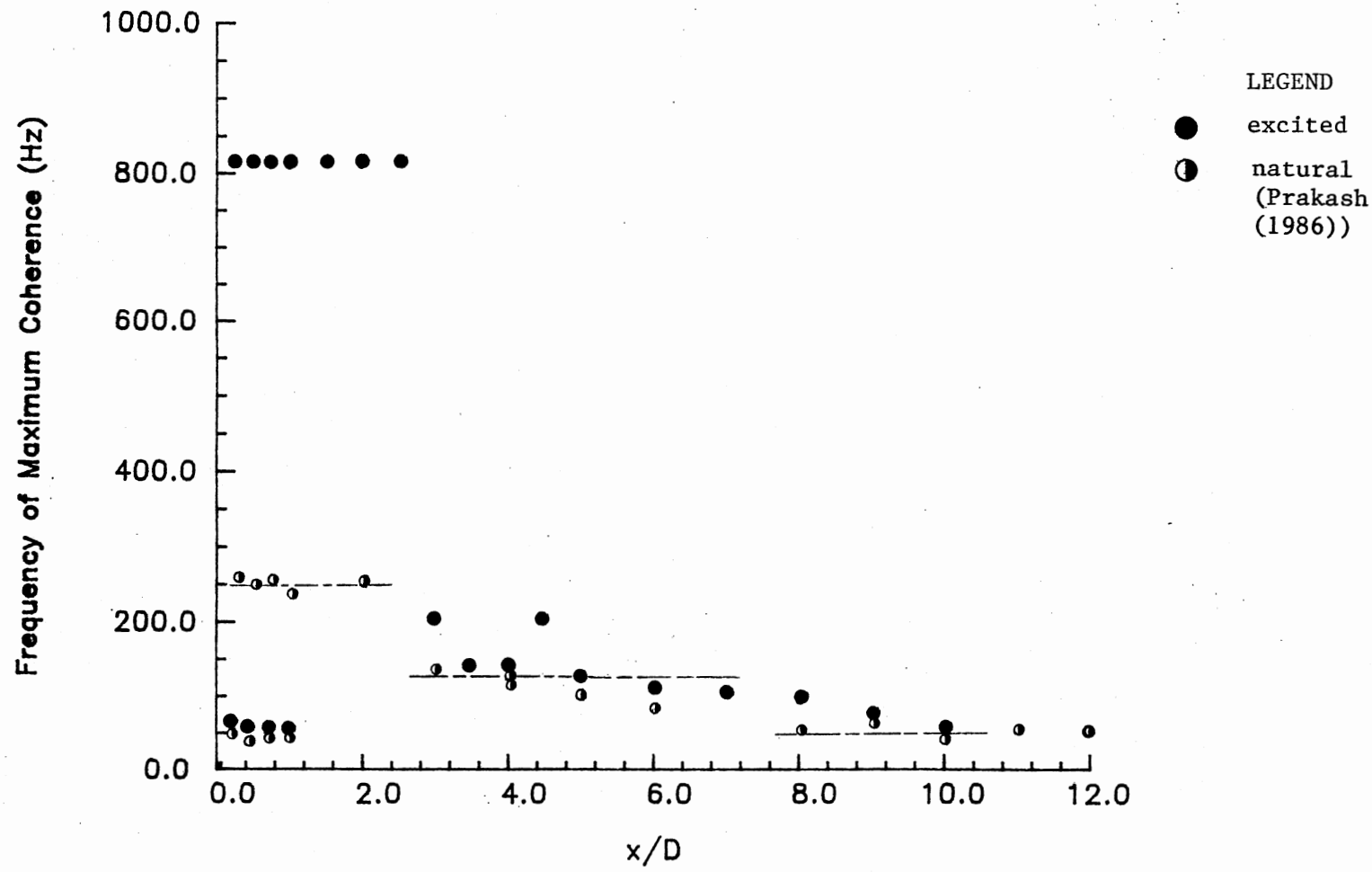

Figure 73. Comparison of Frequency of Maximum Coherence with Downstream Distance

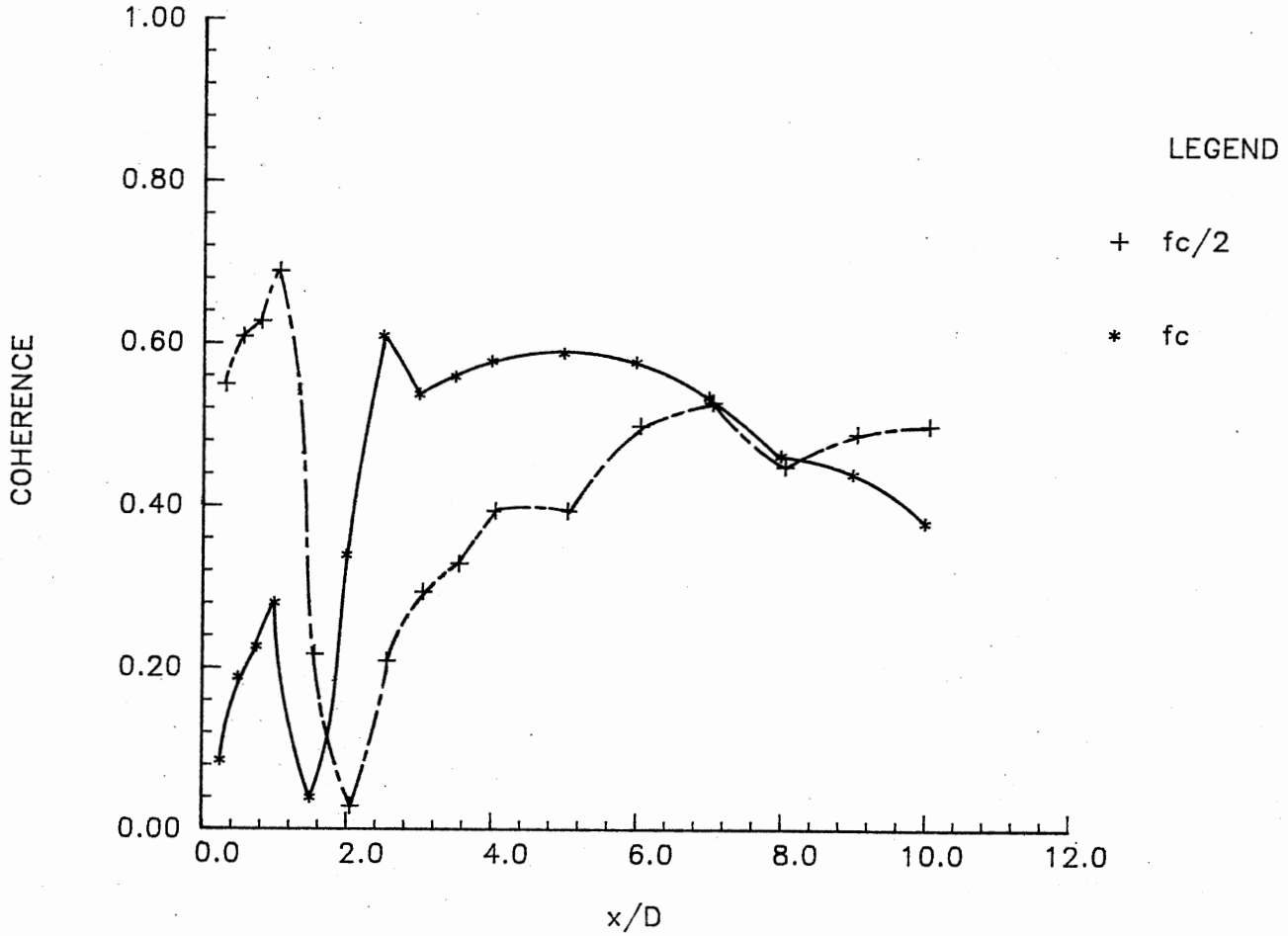

Figure 74. Variation of Coherence of the Modes near 63 ($f_c/2$) Hz and 125 (f_c) Hz with Downstream Distance

centered near the jet column mode f_c and $f_c/2$ with downstream distance. In order to interpret the variation of the spectral coherence as shown in Figure 74, a simple model involving the concept of resonant feedback may be postulated. The model (similar to that described by Prakash (1986)) is schematically illustrated in Figure 75. In this figure two large-scale vortical structures with vorticity of opposite sign exist in the two developing shear layers and are forced to interact with each other near the end of the potential core. They will generate a pressure field that propagates upstream and interacts with the initial inviscid shear layer instabilities. The interactions will subsequently generate the periodic structures that are convected to downstream locations to complete the feedback loop. Concerning the mechanism that is responsible for the phenomena observed from Figure 74, it may be seen that the coherence measurements exhibit higher values in region "A" since both shear layers are equally influenced by the "source" located at region "C". With increasing downstream distance to region "B", a sudden drop in coherence values was noted from Figure 74. It is expected that the streamwise evolution of the disturbance induced near the nozzle exit results in a loss of coherence between downstream shear layer and nozzle exit locations. This loss in coherence is also compounded by the random fluctuations that characterize the shear layers near $y/b = 1.0$. When the movable probe approaches the "Source" in region "C", the spectral coherence will regrow and reach the maximum coherence observed near $x/D = 7$. This is due to the fact that the source is responsible for the disturbance initiated at the nozzle exit and hence is coherent with respect to it. In effect, this indicates that the initial instability and the subsequent turbulent state of the

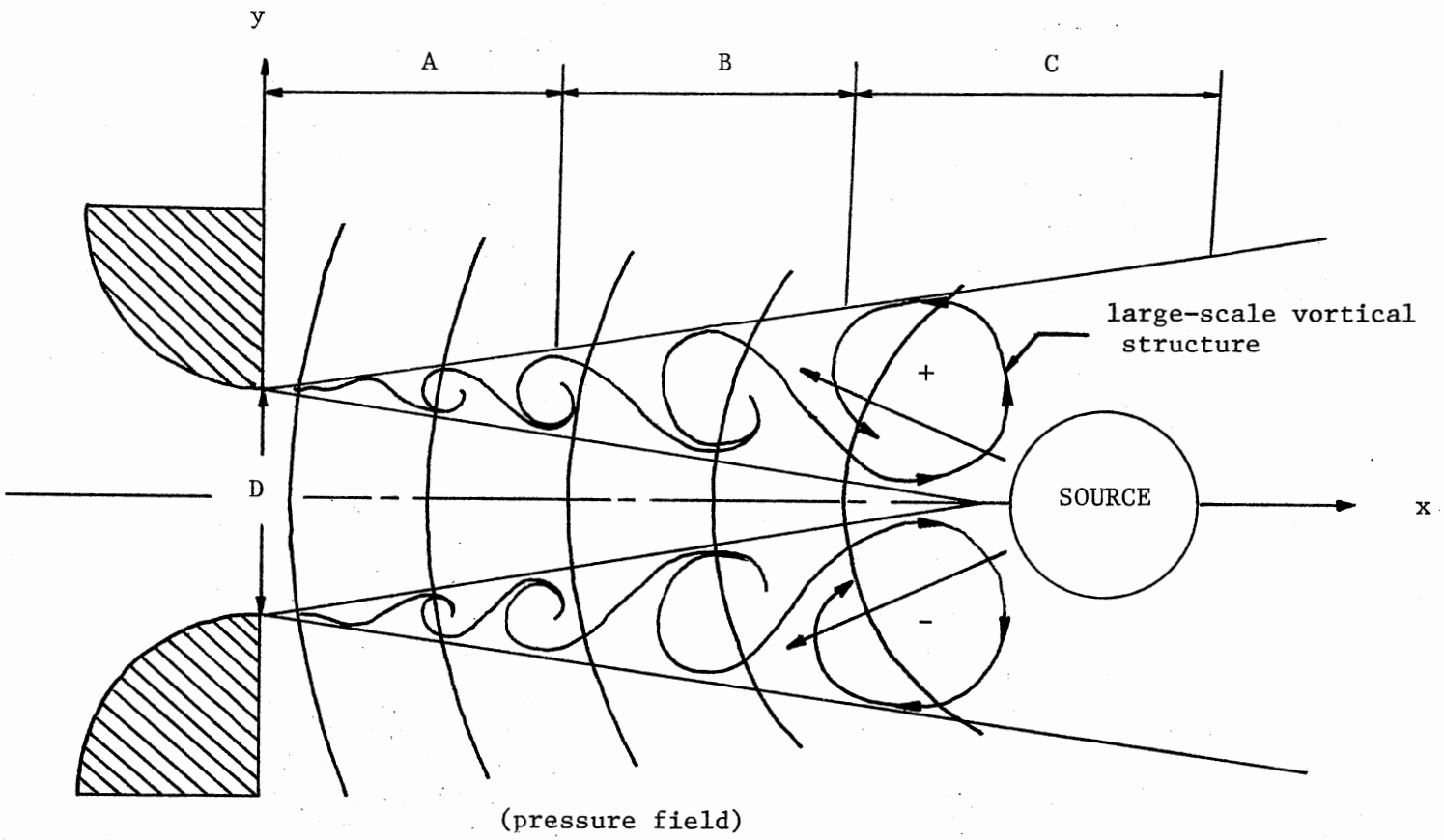

Figure 75. Schematic of Structural Patterns and Feedback Effects in the Jet Flow

flow are coupled.

Finally, of importance in this section is the recognition that the coherence measurements indicate that the initial excited jet shear layer development is strongly affected by downstream vortical interactions which couple the near exit flow with downstream locations. This has also been suggested from the power spectra and bicoherence measurements which together indicated the importance of the jet column mode, f_c, in the jet transition.

CHAPTER IV

CONCLUSIONS AND RECOMMENDATIONS

4.1 Conclusions

The conclusions based upon the experimental work presented are next summarized:

1. The power spectra and bicoherence spectra strongly indicate the importance of the jet column mode f_c in determining the initial spectral development and energy transfer which characterizes the excited jet transition. The formation of a dominant subharmonic mode $f_e/2$ does not necessarily occur in the excited jet shear layers as it does in the isolated planar mixing layer. Instead, quadratic nonlinear interaction of the acoustically induced instability mode f_e with the jet column mode f_c produces several modes. For $x/D < 2$, the most significant modes are located at frequencies $(f_e-f_c)/2$ and $(f_e+f_c)/2$, and the subharmonic $f_e/2$ is suppressed. The $(f_e-f_c)/2$ mode results from an interaction which is similar to the subharmonic resonance proposed by Kelly (1967) involving the (f_e-f_c) mode; the mode $(f_e+f_c)/2$ results from the nonlinear interaction of the form $f_e-(f_e-f_c)/2 \dashrightarrow (f_e+f_c)/2$. An additional source for the rapid growth of the spectral mode at $(f_e-f_c)/2$ is due to the quadratic nonlinear interaction of the form $(f_e+f_c)/2-f_c \dashrightarrow (f_e-f_c)/2$.

For $2 \leq x/D \leq 4$, it may be noted from the shear layer bicoherence spectra that there is a significant decrease in phase coherence for

interactions with frequencies greater than $f_k = 2f_e$, and the most phase coherent interactions are noted to occur for $f_k \leq 2f_e$. In this region several of the bicoherence contours lie on lines of constant frequencies $f_i = f_c$, $(f_e-3f_c)/2$, $2f_c$, $(f_e-f_c)/2$, $(f_e+f_c)/2$, (f_e-f_c), and f_e. This phenomenon indicates the existence of the quadratic nonlinear interactions between these dominant modes and multiple frequencies f_j which also involve combinations of f_e and f_c. The corresponding shear layer power spectra exhibit the same spectral modes as indicated in the bicoherence spectra and the valleys between the discrete spectral modes begin to be filled due to the increased random instabilities. For $x/D > 4$, the growth of the jet column mode f_c and $(f_e-3f_c)/2$ mode are significant. The production of these modes are attributed to the interactions $(f_e+f_c)/2-(f_e-f_c)/2 \rightarrow f_c$, $(f_e-f_c)/2-(f_e-3f_c)/2 \rightarrow f_c$, and $(f_e+f_c)/2-2f_c \rightarrow (f_e-3f_c)/2$, respectively. At $x/D = 6$, the dominant mode as noted from the centerline power spectrum is the jet column mode f_c which is defined as the structural passage frequency near the end of the potential core. Beyond this location the formation of a peak at half of the jet column mode $f_c/2$ is noted from the centerline power spectrum. Based upon the results from bicoherence spectra, the growth of the mode $f_c/2$ is produced by two quadratic nonlinear interactions which are $f_c-f_c/2 \rightarrow f_c/2$ and $(f_e-3f_c)/2-f_c \rightarrow (f_e-5f_c)/2$. The result of the second interaction, $(f_e-5f_c)/2$, is approximately 60 Hz which is also very near to the mode $f_c/2 \approx 63$ Hz.

Certain of the natural jet power spectra and bicoherence spectra were presented in this thesis for comparison with excited jet data. In effect, the natural cases resemble "smoothed" or "randomized" versions of the corresponding excited cases. These phenomena strongly suggest

corresponding to the maximum spectral coherence for various downstream locations of the movable probe in the excited jet are consistent with the requirement for a global resonance mechanism to operate in the jet flow as described by Prakash (1986) in natural jet transition. Therefore, the near exit interactions which have been noted to involve f_c and $f_c/2$ indicate that the jet column mode and the half of the jet column mode exert an upstream influence on the nascent flow field.

4.2 Recommendations

1. An additional measurement technique, digital complex demodulation, allows the instantaneous amplitude and phase modulation to be extracted from raw time-series data. Certain of the quadratic nonlinear interaction described in this thesis may be interpreted as modulation effects. The complex digital demodulation technique could provide a powerful tool for the analysis of such modulation effects in the planar jet flow and permit the interpretation of the experimental results in terms of theoretical framework.

2. A similar experimental measurement could be made by using two artifically excited instabilities from upstream of the nozzle exit. The interaction of two artifically induced waves would result in a difference mode, and the effect of such difference interactions on the jet transition could be studied. Of particular interest would be the interaction between the artifically induced difference mode and the modes near f_c and $f_c/2$. This work should clearly demonstrate the importance of such difference interactions in producing the continuous distribution of sideband fluctuations which are responsible for spectral broadening.

that conclusions from the experiments involving low level acoustic excitation are also valid for the natural jet transition. In particular, this suggests that the nonlinear interactions which occur in the excited jet are also at work in the natural jet transition. This is to be expected since the primary function of the low level excitation at the most unstable jet shear layer frequency is to organize the initial instabilities. Therefore, the presented results regarding the excited jet shear layers facilitate a better understanding of the natural jet transition.

2. As indicated from coherence measurements, the nonlinear interactions noted from power spectra and bicoherence spectra were coherent across the jet indicating that phase coherence exists between similar frequencies in the two developing jet shear layers. In order to obtain further information concerning the quadratic nonlinear interactions in the jet flow, shear layer fluctuations were modeled in terms of quadratic nonlinear interactions suggested in the bicoherence data and the coherence function was computed based on the modeled fluctuations. The dominant features observed from both modeled coherence functions and experimental coherence functions are in qualitative agreement with each other. This supports conclusions regarding the quadratic nonlinear interactions occurring in the jet shear layers as noted from bicoherence data and coherence functions and indicates that such interactions are coherent across the jet.

3. The results of the coherence measurements suggest that the initial excited jet shear layer development is strongly affected by downstream vortical interactions which couple the near exit flow with downstream locations. Also, the measured modal frequencies

3. The bicoherence spectrum has been employed to discriminate between nonlinearly coupled waves and simultaneously excited independent waves. In addition to these, a new quantitative measure called the cross-bispectrum could be a very powerful tool in providing new quantitative insights regarding the phase coherence between two developing jet shear layers with different frequency modes. Also, this technique could be used to measure the growth of three-dimensional effects which characterize the large-scale vortical structures in the shear layer.

4. A new technique for the experimental determination of transfer functions which characterize turbulence transition has been presented by Ritz and Powers (1986). This work presents a method by which linear and quadratically nonlinear transfer functions are to be computed based on the measurement of the fluctuations at two points in space or time. This method is attractive in that it is capable of providing quantitative insight regarding the dynamic mechanisms involved in the spectral energy redistribution that characterizes the transition process. Of particular interest is that the nonlinear transfer function eliminates the need for physical interpretation of bicoherence by reference to power spectra. That is the interactions f_i+f_j --> f_k, f_k-f_j --> f_i, and f_k-f_i --> f_j are each mapped into three different regions when the nonlinear transfer function is computed.

5. Experimental measurements similar to those reported also could be done but with different nozzle contours, nozzle slot widths (D), and different Reynolds numbers to see how these parameters affect the characteristics of the planar turbulent jet.

REFERENCES

Bradbury, L. J. S., "The Structure of a Self-Preserving Turbulent PLane Jet," J. Fluid Mech., 23, Part 1, pp. 31-63, 1965.

Cervantes De Gortari, J. G., "An Experimental Study of the Flapping Motion of a Turbulent Plane Jet," Ph.D. dissertation, Purdue University, 1978.

Chambers, F. W., "Acoustic Interaction With a Turbulent Plane Jet," Ph.D. dissertation, Purdue University, 1977.

Dimotakis, P. G. and Brown, G. L., "The Mixing Layer at High Reynolds Number: Large-Structure Dynamics and Entrainment," J. Fluid Mech. 78, pp. 535-60, 1976.

Everitt, K. W. and Robins, A. G., "The Development and Structure of Turbulent Plane Jets," J. Fluid Mech., 88, 3, pp. 563-568, 1978.

Flora, J. J. Jr., and Goldschmidt, V. W., "Virtual Origins of a Free Plane Turbulent Jet," AIAA Journal, 7, 12, pp. 2344-2346, 1969.

Foss, F. J., "A Study of Incompressible Bounded Turbulent Jets," Ph.D. dissertatoin, Purdue University, 1965.

Gutmark, E. and Wygnanski, I., "The Planar Turbulent Jet," J. Fluid Mech., 73, pp. 465-495,1976.

Ho, C. M. and Huang, L. S., "Subharmonics and Vortex Merging in Mixing Layers." J. Fluid Mech. 119, pp. 443-73, 1982.

Ho, C. M. and Nosseir, N. S., "Dynamics of an Impinging Jet. Part 1. The Feedback Phenomenon." J. Fluid Mech. 105, pp. 119-42, 1981.

Jenkins, P. E. and Goldschmidt, V. M., "Study of the Intermittent Region of a Two-Dimensional Plane Jet," Herrick Lab Report, HL 74-75, Purdue University, 1974.

Jordinson, R., "Design of Wind Tunnel Contractions," Aircraft Eng., 33, 392, pp. 294-297, 1961.

Kaiser, K. F., "An Experimental Investigation of Interaction of an Acoustic Field and a Plane Turbulent Jet," M.S. Thesis, Purdue University, 1971.

Kelly, R. E., "On the Stability of an Inviscid Shear Layer which is Periodic In Space And Time," J. Fluid Mech. 31, pp. 789-99, 1967.

Kim, Y. K. and Powers, E. J., "Digital Bispectral Analysis and Its Application to Nonlinear Wave Interactions," IEEE Trans. on Plasma Sci., PS-7, pp. 120-131, 1979.

Kim, Y. C., Khadra, L. and Powers, J., "Wave Modulation in a Nonlinear Dispersive Medium," Phys. Fluids, 23, pp. 2250-2257, 1980.

Kline, S. J., and McClintock, F. A., "Describing Uncertainties in Single Sample Experiments," Mech. Eng., 75, pp. 3-8, 1953.

Knisely, C. and Rockwell, D., "Self-Sustained Low-Frequency Components in an Impinging Shear Layer," J. Fluid Mech., 116, pp. 157-186, 1982.

Laufer, J., Monkewitz, P. A., "On Turbulent Jet Flow In A New Perspective." AIAA Pap. No. 80-0962, 1980.

Laufer, J., "Instability and Turbulence in Jets," In Transition and Turbulence , pp. 63-76, New York: Academic, 1981.

Lii, K. S., Rosenblatt, M. and Van Atta, C., "Bispectral Measurements in Turbulence," J. Fluid Mech., 77, pp. 45-62, 1976.

Michalke, A., "On Spatially Growing Disturbances in an Inviscid Shear Layer," J. Fluid Mech., 23, pp. 521-544, 1965.

Miksad, R. W. , "Experiments on the Nonlinear Stages of Free Shear Layer Transition," J. Fluid Mech., 56, 4, pp. 695-719, 1972.

Miksad, R. W. , "Experiments on Nonlinear Interactions in the Transition of a Free Shear Layer," J. Fluid Mech. , 3, 1, pp. 1-21, 1973.

Miksad, R. W., Jones, F. L., Powers, E. J., Kim, Y. C., and Khadra, L., "Experiments on the Role of Amplitude and Phase Modulations During Transition to Turbulence," J. Fluid Mech., 123, pp. 1-29, 1982.

Miksad, R. W., Jones, F. L. and Powers, E. J. "Measurement of Nonlinear Interactions During Natural Transition of a Symmetric Wake," Phys. Fluids, 26, 1402-1409, 1983.

Monkewitz, P. A., "On the Nautre of Amplitude Modulation of Jet Shear Layer Instability Waves," Phys. Fluids, 26, 3180-3184, 1983.

Mulej, D. J., "The Velocity of the Interface," M. S. Thesis, Purdue University, 1975.

Ott, E. S., "Convective Velocities in a Turbulent Plane Jet," M.S. Thesis, Purdue University, 1972.

Prakash, K. M. K., "Influence of a Global Resonance Mechanism on the Structural Development of a Planar Turbulent Jet," M.S. Thesis, Oklahoma State University, 1986.

Ritz, Ch. P. and Powers, E. J., "Estimation of Nonlinear Transfer Functions for Fully Developed Turbulence," Physica 20D, pp. 320-334, 1986.

Sato, H., "An Experimental Study of Non-linear Interaction of Velocity Fluctuations in the Transition Region of a Two-Dimensional Wake," J. Fluid Mech. 44, pp. 741-765, 1970.

Sato, H. and Saito, H., "Fine Structure of Energy Spectra of Velocity Fluctuations in the Transition Region of a Two-Dimensional Wake," J. Fluid Mech. 67, pp. 539-559, 1975.

Solis, R. S., Miksad, R. W. and Powers, E. J., "Experiments on the Influence of Mean Flow Unsteadiness on the Laminar-Turbulent Transition of a Wake," Presented at the 10th Symposium on Turbulence, University of Missouri-Rolla, Sept. 1986.

Thomas, F. O., "Effect of Nozzle Geometry of Acoustic Interaction With a Turbulent Jet," M.S. Thesis, Purdue University, 1980.

Thomas, F. O., "Development of a Two-Dimensional Turbulent Jet Under Natural and Excited Conditions," Ph.D. dissertation, Purdue University, 1983.

Thomas, F. O. and Goldschmidt, V. W., "The Possibility of a Resonance Mechanism in the Developing Two-Dimensional Jet," Phys. of Fluids, 28, pp. 3510-3514, 1985.

Thomas, F. O. and Goldschmidt, V. W., "Structural Characteristics of a Developing Turbulent Planar Jet," J. Fluid Mech., 163, pp. 227-256, 1986.

Thomas, F. O., and Brehob, E. G., "An Investigation of Large-Scale Strucuture in the Similarity Region of a Two-Dimensional Turbulent Jet," Phys. of Fluids, 29, pp. 1788-1795, 1986.

Thomas, F. O., and Prakash, K. M. K., "Influence of a Global Resonance Mechanism on the Structural Development of a Planar Turbulent Jet," J. Fluid Mech., Submitted for Publication, 1986.

Van Atta, C. W. and Yeh, T. T., "The Structure of Internal Intermittency in Turbulent Flows at Large Reynolds Numbers: Experimental Scale Similarity," J. Fluid Mech., 59, pp. 537-559, 1973.

Van Der Hegge Zijnen, B. G., "Measurments of Turbulence in a Plane Jet of Air by the Diffusion Method and by the Hot-Wire Method," Applied Science Rec., Section A, 7, pp. 256-276, 1958.

Winant, C. D. and Browand, F. K., "Vortex Pairing: The Mechanism of Turbulent Mixing Layer Growth at Moderate Reynolds Number," J. Fluid Mech., 63, pp. 237-255, 1974.

APPENDIXES

APPENDIX A

COMPUTER PROGRAM LISTING

BICOHERENCE PROGRAM LISTING

```
PROGRAM BIAB(INPUT,OUTPUT);

{THIS PROGRAM SAMPLES A TIME VARYING VOLTAGE & COMPUTES
 THE BICOHERENCE SPECTRUM BY THE FFT METHOD.
 THE BICOHERENCE SPECTRUM IS WRITTEN TO DISK AS "V15:BSQUARED.TXET"}

    IMPORT IODECLARATIONS;
    IMPORT GENERAL_2;
    IMPORT MEASUREMENT_LIB;

    CONST
                NAME = 'ADC';
               MODEL = '98640A';
         SELECT_CODE = 18;
               ERROR = 'NO';
               UNITS = 'STANDARD';
          MULTIPLIER = 1.0;
              OFFSET = 0.0;
              P_SIZE = 1;
              G_SIZE = 1;
              C_SIZE = 1;
                   N = 512;
                  N1 = 511;
                  N2 = 256;
                  N4 = 128;
                   R = 9;
                  PI = 3.14159265;

   TYPE
              R_ARRAY = ARRAY[1..512] OF REAL;
              R_PTR = ^R_ARRAY;
              I_ARRAY = ARRAY[1..7] OF SHORTINT;
              I_PTR = ^I_ARRAY;
              COMPLEX = RECORD X,Y: REAL END;
              DATTA = ARRAY[0..N1] OF COMPLEX;
              C_PTR = ^DATTA;
              A_ARRAY = ARRAY[0..N1] OF REAL;
              B_ARRAY = ARRAY[1..N4,1..N2] OF COMPLEX;
              B_PTR   = ^B_ARRAY;

  VAR
            CHANNEL : I_PTR;
            GAIN : I_PTR;
            PACE : R_PTR;
            DATA : R_PTR;
            GANE,D_SIZE,REPT,I,II,J,K,
            L,M,C,T,MSAMP,NSAMP,NN            :INTEGER;
            GAN,FMAX,FL,FK,DELTAF,TIME,
            NUMSAMP,PASE,SC,DELTA,SUMV,MEANV :REAL;
            B:B_PTR;
            P:COMPLEX;
            W,A,D: C_PTR;
            TXT1,TXT2,TXT3:TEXT;
            AMP: A_ARRAY;
            FILENAME :STRING[15];


procedure reord(var a:c_ptr);
var
   i,j,k,l:integer;
        q:complex;
begin
  for i:=1 to n1 do begin
   l:=i;
```

```
  k:=0;
  for j:=0 to (r-1) do begin
    k:=(2*k)+l mod 2;
    l:=l div 2
    end;
  if i<k then begin
    q:=a^[i];
    a^[i]:=a^[k];
    a^[k]:=q
    end
  end
end;  {reord}

procedure sum(z,w:complex; var s:complex);
begin
with s do begin
  x:=z.x+w.x;
  y:=z.y+w.y
  end
end;

procedure dif(z,w:complex; var s:complex);
begin
with s do begin
  x:=z.x-w.x;
  y:=z.y-w.y
  end
end;

procedure prod(z,w:complex; var s:complex);
begin
with s do begin
  x:=z.x*w.x-z.y*w.y;
  y:=z.x*w.y+z.y*w.x
  end
end;

procedure neg(u:complex; var w:complex);
begin
  w.x:=-u.x;
  w.y:=-u.y
end;

procedure conj(u:complex; var w:complex);
begin
  w.x :=u.x;
  w.y :=-u.y;
end;


procedure trf(var x:c_ptr);

var
   lvl,tl,tll,expon,t,i,j,k:integer;
   s,z:complex;

{tl = 2^lvl}
{tll=2^(lvl-1)}
{p=2^(r-lvl)}
{expon=j*p}

begin
tl:=2; tll:=1;
for lvl:=1 to r do
   begin
   t:=n div tl;  expon:=0;
```

```
    for j:=0 to tll-1 do
       begin
       i:=j;  s:=w^[expon];
       while i<n do
          begin
          k:=i+tll;
          if j=0 then z:=a^[k]
          else prod(a^[k],s,z);
          dif(a^[i],z,a^[k]);
          sum(a^[i],z,a^[i]);
          i:=i+tl
          end;
       expon:=expon+t
       end;
   tl:=2*tl;  tll:=2*tll
   end
end; {trf}

function mag(z:complex):real;
begin
 with z do
   mag:=sqr(x)+sqr(y)
end;
      BEGIN {MAIN PROGRAM}
        NEW(W);
        NEW(A);
        new(B);
        NEW(D);
        WRITELN('ENTER THE MAXIMUM FREQUENCY COMPONENT OF THE SIGNAL');
        READNUMBER(1,FMAX);
        WRITELN;
        PASE:= (1.0/(2.0*FMAX));
        IF (PASE<0.000018) THEN
        BEGIN
    WRITELN('THE PACE VALUE IS TOO SMALL FOR THE HP-98640A!!');
    WRITELN('**********************************************');
    WRITELN('IF ALLOWED TO CONTINUE PACE WILL BE SET TO THE VALUE');
    WRITELN('0.000018');
          PASE:= 0.000018;
        END;
        IF (PASE>0.0393336) THEN
        BEGIN
          WRITELN('THE PACE VALUE IS TOO LARGE FOR THE HP-98640A!!');
          WRITELN('**********************************************');
          WRITELN('IF ALLOWED TO CONTINUE PACE WILL BE SET TO THE VALUE');
          WRITELN('0.0393336');
          PASE:= 0.0393336;
        END;
        WRITELN(' THE PACE RATE ON THE HP-98640A WILL BE SET TO:',PASE:9:7);
        WRITELN;
        D_SIZE:=N;
        WRITELN('THE NUMBER OF ELEMENTS STORED IS ',D_SIZE:5);
        REPT:= D_SIZE;
        WRITELN;
        DELTAF:=(2*FMAX)/N;
        WRITELN('THE FREQUENCY RESOLUTION WILL BE ',DELTAF:6:4,' HZ ');
        WRITELN;
        WRITELN('ENTER THE NUMBER OF SAMPLES TO FORM THE BISPECTRAL');
        WRITELN('MEASUREMENT');
        WRITELN;
        READNUMBER(1,NUMSAMP);
        NSAMP:=ROUND(NUMSAMP);
     NEW(CHANNEL);
     CHANNEL^[1]:=1;
     NEW(PACE);
     PACE^[1]:=PASE;
```

```
NEW(GAIN);
WRITELN('ENTER THE GAIN SETTING FOR HP-98640A ADC BOARD');
WRITELN('THE AVAILABLE CHOICES ARE 1, 8, 64, 512');
WRITELN;
READNUMBER(1,GAN);
GANE:=ROUND(GAN);
GAIN^[1]:=GANE;
MEAS_LIB_INIT;
CONFIG_0(NAME,MODEL,SELECT_CODE,1,0.02,ERROR,UNITS,MULTIPLIER,OFFSET);
INIT(NAME);

SC:=(8*ARCTAN(1)/N);

  FOR I:= 0 TO N1 DO
  WITH W^[I] DO BEGIN
   X:= COS(SC*I);
   Y:= SIN(SC*I)
   END;

  FOR I:= 0 TO N1 DO BEGIN
   AMP[I]:=0
   END;

   FOR I:= 0 TO N1 DO BEGIN
    WITH D^[I] DO BEGIN
     X:=0.0;
     Y:=0.0;
    END;
    END;

   CALIBRATE(NAME,3,0.0001,1000);
   NEW(DATA);
   WRITELN('NOW CALCULATING THE MEAN VOLTAGE TO BE SUBTRACTED FROM ALL');
   WRITELN('TIME SERIES DATA ELEMENTS');
   WRITELN;
   WRITELN('ENTER SAMPLE TIME FOR MEAN VOLTAGE CALCULATION');
   READNUMBER(1,TIME);
   MSAMP:= ROUND(TIME/(PASE*D_SIZE));
   SUMV:=0.0;

   {******** INITIALIZE ALL B[I,J] = 0 ********}
   FOR I := 1 TO ROUND(N/4) DO BEGIN
     FOR J := 1 TO ROUND(N/2) DO BEGIN
       WITH B^[I,J] DO BEGIN
         X := 0.0;
         Y := 0.0;
       END;
     END;
   END;
   {*****************************************}

   {1111111111111111111111111111111111111111}
   FOR I:= 1 TO MSAMP DO BEGIN
     WRITELN(CHR(12));
     WRITELN;
   WRITELN('MEAN VOLT CALCULATION IN PROGRESS...REPETITION ',I:3,' OF ',
          MSAMP:3);
   RANDOM_SCAN(NAME,C_SIZE,CHANNEL,D_SIZE,DATA,REPT,P_SIZE,PACE,G_SIZE,
          GAIN);
   FOR J:=1 TO D_SIZE DO BEGIN
      SUMV:=SUMV+DATA^[J];
      END;
   END;
   {1111111111111111111111111111111111111111}
   WRITELN;
   MEANV:= SUMV/(D_SIZE*MSAMP);
```

```
        WRITELN('******** MEAN VOLTAGE = ',MEANV:10:6);
        WRITELN;

        {2222222 BEGIN MAIN CALCULATION LOOP 2222222}

      FOR T:= 1 TO NSAMP DO BEGIN
        WRITELN(CHR(12));
WRITELN('FFT DATA SAMPLING IN PROGRESS*******SAMPLE ',T:3,' OF ',NSAMP:4);
        RANDOM_SCAN(NAME,C_SIZE,CHANNEL,D_SIZE,DATA,REPT,P_SIZE,PACE,
              G_SIZE,GAIN);
       {SUBTRACT MEAN VOLTAGE FROM EACH TIME SERIES ELEMENT}
             FOR I:= 1 TO D_SIZE DO BEGIN
             DATA^[I]:= DATA^[I]-MEANV;
             END;
        {APPLY COSINE WINDOWING}
            FOR I:=1 TO ROUND (D_SIZE/10) DO BEGIN
                DATA^[I]:=DATA^[I]*(1-COS(5*PI*(I-1)/D_SIZE));
                END;
            FOR I:=ROUND(9*D_SIZE/10) TO D_SIZE DO BEGIN
                DATA^[I]:=DATA^[I]*(1+COS(5*PI*I/D_SIZE));
                END;
                {END DATA WINDOWING}

            FOR I:= 0 TO N1 DO
            WITH A^[I] DO BEGIN X:=DATA^[I+1]; Y:=0.0 END;

            REORD(A);
             TRF(A);

            FOR I:= 0 TO N1 DO BEGIN
                AMP[I]:= AMP[I]+MAG(A^[I])
                END;

            WRITELN(CHR(12));
            WRITELN('SET ',T:3,' OF ',NSAMP:3,' SETS OF FOURIER );
            WRITELN;
            FOR L := 1 TO ROUND(N/4) DO BEGIN
              FOR K := L TO (ROUND(N/2)-L) DO BEGIN
               PROD(A^[K],A^[L],P);
               CONJ(A^[K+L],D^[K+L]);
               PROD(P,D^[K+L],P);
               SUM(P,B^[L,K],B^[L,K]);
              END;
              END;
            END;
            {22222222222222222222222222222222222222}

            {33333333333333333333333333333333333333}
            FOR L := 1 TO ROUND(N/4) DO BEGIN
             FOR K := L TO (ROUND(N/2)-L) DO BEGIN
              WITH B^[L,K] DO BEGIN
               X := SQRT(MAG(B^[L,K]));
              END;
             END;
            END;
            FOR L := 1 TO ROUND(N/4) DO BEGIN
             FOR K := L TO (ROUND(N/2)-L) DO BEGIN
              WITH B^[L,K] DO BEGIN
               X := X*SQR(1.0/N)*PASE*1.14286/NSAMP;
               Y := 0.0;
              END;
             END;
            END;
            {33333333333333333333333333333333333333}

            NN:= ROUND(N/2);
```

```
 FOR I:=0 TO N1 DO BEGIN
 AMP[I]:=AMP[I]*(2*PASE/N)*1.14286;
 AMP[I]:=AMP[I]/NSAMP;
 END;
 {4444444444444444444444444444444444444444}
 FOR L := 1 TO ROUND(N/4) DO BEGIN
  FOR K := L TO (ROUND(N/2)-L) DO BEGIN
   WITH B^[L,K] DO BEGIN
    X := SQR(X)/(AMP[L]*AMP[K]*AMP[L+K]);
   END;
  END;
 END;
{4444444444444444444444444444444444444444}

 {5555555555555555555555555555555555555555}
 II := 1;
 REWRITE(TXT3,'V15:BSQUARED.TEXT');
 FOR L := 1 TO ROUND(N/4) DO BEGIN
  FOR K := L TO (ROUND(N/2)-L) DO BEGIN
   IF (II <= 9) THEN BEGIN
     WITH B^[L,K] DO BEGIN
     WRITE(TXT3,' ',X:7:5);
    END;
   END
 ELSE
  BEGIN
   WITH B^[L,K] DO BEGIN
    WRITELN(TXT3);
    WRITE(TXT3,' ',X:7:5);
   END;
   II := 1;
  END;
 II := II+1;
 END;
 END;
 CLOSE(TXT3,'SAVE');
 {5555555555555555555555555555555555555555}
 END.
```

COHERENCE PROGRAM LISTING

```
program COHERENCE(input,output);

{This program uses the FFT method to compute the coherence}
{function between two sampled anemometer signals}

import iodeclarations;
import general_2;
import measurement_lib;

const
            name = 'ADC';
           model = '98640A';
     select_code = 18;
           error = 'NO';
           units = 'STANDARD';
      multiplier = 1.0;
          offset = 0.0;
          p_size = 2;
          g_size =1;
          c_size =2;
                n=256;
                n1=255;
                 r=8;
                pi=3.14159265;
type
          r_array = ARRAY[1..2*n] of real;
          r_ptr = ^r_array;
          i_array = ARRAY[1..7] of shortint;
          i_ptr = ^i_array;
          complex=record x,y: real end;
          datta = ARRAY[0..(2*n)-1] of complex;
          c_ptr = ^datta;
          a_array=ARRAY[0..n1] of real;
          l_array=ARRAY[1..n] of real;
var

          channel: i_ptr;
          gain: i_ptr;
          pace: r_ptr;
          data: r_ptr;
          d_size,rept,i,j,m,c,p,msamp,k          :integer;
          fmax,time,nsamp,pase1,pase2,sc,
          sumv1,sumv2,meanv1,meanv2,temp,tau,f :real;
          w,a,b,g:c_ptr;
          txt:text;
          theta,sumx,sumy,gxy,gx,gy,gamma:a_array;
          q,qq:complex;
          v:l_array;


procedure reord1(var a:c_ptr);
var
   i,j,k,l:integer;
          q:complex;
begin
  for i:=1 to n1 do begin
    l:=i;
    k:=0;
    for j:=0 to (r-1) do begin
      k:=(2*k)+l mod 2;
      l:=l div 2
      end;
    if i<k then begin
      q:=a^[i];
```

```
      a^[i]:=a^[k];
      a^[k]:=q
      end
    end
  end;  {reord1}


 procedure reord2(var b:c_ptr);
var
   i,j,k,l:integer;
         q:complex;
begin
  for i:=1 to n1 do begin
   l:=i;
   k:=0;
   for j:=0 to (r-1) do begin
     k:=(2*k)+l mod 2;
     l:=l div 2
     end;
   if i<k then begin
     q:=b^[i];
     b^[i]:=b^[k];
     b^[k]:=q
     end
   end
 end;  {reord2}

 procedure sum(z,w:complex; var s:complex);
 begin
 with s do begin
   x:=z.x+w.x;
   y:=z.y+w.y
   end
 end;

 procedure dif(z,w:complex; var s:complex);
 begin
 with s do begin
   x:=z.x-w.x;
   y:=z.y-w.y
   end
 end;

 procedure prod(z,w:complex; var s:complex);
 begin
 with s do begin
   x:=z.x*w.x-z.y*w.y;
   y:=z.x*w.y+z.y*w.x
   end
 end;

 procedure neg(u:complex; var w:complex);
 begin
   w.x:=-u.x;
   w.y:=-u.y
 end;

 procedure trf1(var x:c_ptr);

 var
    lvl,tl,tl1,expon,p,i,j,k:integer;
    s,z:complex;

 {tl = 2^lvl}
 {tl1=2^(lvl-1)}
 {p=2^(r-lvl)}
```

```
 {expon=j*p}

 begin
 tl:=2; tll:=1;
 for lvl:=1 to r do
    begin
    p:=n div tl;  expon:=0;
    for j:=0 to tll-1 do
       begin
       i:=j;  s:=w^[expon];
       while i<n do
          begin
          k:=i+tll;
          if j=0 then z:=a^[k]
          else prod(a^[k],s,z);
          dif(a^[i],z,a^[k]);
          sum(a^[i],z,a^[i]);
          i:=i+tl
          end;
       expon:=expon+p
       end;
   tl:=2*tl;  tll:=2*tll
   end
end; {trf1}

 procedure trf2(var x:c_ptr);

 var
    lvl,tl,tll,expon,p,i,j,k:integer;
    s,z:complex;

 {tl = 2^lvl}
 {tll=2^(lvl-1)}
 {p=2^(r-lvl)}
 {expon=j*p}

 begin
 tl:=2; tll:=1;
 for lvl:=1 to r do
    begin
    p:=n div tl;  expon:=0;
    for j:=0 to tll-1 do
       begin
       i:=j;  s:=w^[expon];
       while i<n do
          begin
          k:=i+tll;
          if j=0 then z:=b^[k]
          else prod(b^[k],s,z);
          dif(b^[i],z,b^[k]);
          sum(b^[i],z,b^[i]);
          i:=i+tl
          end;
       expon:=expon+p
       end;
   tl:=2*tl;  tll:=2*tll
   end
end; {trf2}

procedure conj(u:complex; var w:complex);
begin
    w.x:=u.x;
    w.y:=-u.y
end;

function mag(z:complex):real;
```

```
begin
 with z do
   mag:=sqr(x)+sqr(y)
end;

function phase(y1,x1:real):real;
begin
 if (x1=0.0) and (y1>0.0) then phase:=1.570796327;
 if (x1=0.0) and (y1<0.0) then phase:=-1.570796327;
 if (x1>0.0) and (y1>0.0) then phase:=arctan(y1/x1);
 if (x1<0.0) and (y1>0.0) then phase:=pi+arctan(y1/x1);
 if (x1>0.0) and (y1<0.0) then phase:=arctan(y1/x1);
 if (x1<0.0) and (y1<0.0) then phase:=arctan(y1/x1)-pi;
 if (x1<0.0) and (y1=0.0) then phase:=pi;
end;

 begin {MAIN PROGRAM}
   new(w);
   new(a);
   new(data);
   new(b);
   new(g);
   writeln('ENTER THE MAXIMUM FREQUENCY COMPONENT OF THE DATA (HZ)');
   writeln;
   readnumber(1,fmax);
   writeln;
   pase1:=0.000025;
   pase2:=1.0/(2.0*fmax);
   d_size:=2*n;
   writeln('THE TOTAL NUMBER OF ELEMENTS STORED IS ',d_size:5);
   writeln;
   rept:=n;
   writeln('ENTER THE NUMBER OF SAMPLES TO FORM THE AVERAGE COHERENCE');
   writeln;
   readnumber(1,nsamp);
new(channel);
for i:= 1 to 2 do
begin
   channel^[i]:=i
end;
new(pace);
pace^[1]:=pase2;
pace^[2]:=pase1;
new(gain);
gain^[1]:=8;
meas_lib_init;
config_0(name,model,select_code,1,0.02,error,units,multiplier,offset);
init(name);
calibrate(name,3,0.0001,1000);
sc:=(8*arctan(1)/n);
for i:=0 to n1 do
  with w^[i] do begin
    x:=cos(sc*i);
    y:=sin(sc*i)
    end;
writeln('* * * * * * * * * * * * * * * * * * * * * * * * * * * * * * * * * ');
writeln('NOW CALCULATING THE MEAN VOLTAGE TO BE SUBTRACTED FROM ALL');
writeln('TIME SERIES DATA ELEMENTS');
writeln('* * * * * * * * * * * * * * * * * * * * * * * * * * * * * * * * * ');
writeln;
writeln('ENTER THE AVERAGING TIME FOR COMPUTING THE MEAN VOLTAGE');
writeln;
readnumber(1,time);
msamp:=round((2*time)/((pase1+pase2)*d_size));
sumv1:=0.0;
sumv2:=0.0;
```

```
for i:= 1 to msamp do begin
    writeln(chr(12));
  writeln;
writeln('MEAN VOLT CALCULATION IN PROGRESS...REPETITION ',i:3,' OF',msamp:3)
random_scan(name,c_size,channel,d_size,data,rept,p_size,pace,g_size,gain);
for j:=1 to (d_size-1) do begin
   sumv1:=sumv1+data^[j];
   sumv2:=sumv2+data^[j+1];
   j:=j+1;
   end;
end;
  meanv1:=(2.0*sumv1)/(d_size*msamp);
  meanv2:=(2.0*sumv2)/(d_size*msamp);
  {* * * * * * * * * * * * * * * * * * * * * * * * * * * * * * * * * * * * *}
for k:=0 to n1 do begin
 gxy[k]:=0.0;
 gx[k]:=0.0;
 gy[k]:=0.0;
 theta[k]:=0.0;
 gamma[k]:=0.0;
 end;
for p:=1 to round(nsamp) do begin
writeln(chr(12));
writeln('************************************************');
writeln('COHERENCE MEASUREMENT IN PROGRESS.............');
writeln('SAMPLE ',p:3,' OF ',nsamp:4:0);
writeln('************************************************');
writeln;
random_scan(name,c_size,channel,d_size,data,rept,p_size,pace,g_size,gain);
     for i:=1 to (d_size-1) do begin
     data^[i]:=data^[i]-meanv1;
     data^[i+1]:=data^[i+1]-meanv2;
     i:=i+1;
     end;

i:=1;
for j:=1 to round(d_size/2) do begin
v[j]:=data^[i];
i:=i+2;
end;
for i:=1 to round(d_size/20) do begin
v[i]:=v[i]*(1-cos(10*pi*(i-1)/d_size));
end;
for i:=round(9*d_size/20) to round(d_size/2) do begin
v[i]:=v[i]*(1+cos(10*pi*i/d_size));
end;
i:=1;
for j:=1 to round(d_size/2) do begin
data^[i]:=v[j];
i:=i+2
end;
i:=1;
for j:=1 to round(d_size/2) do begin
v[j]:=data^[i+1];
i:=i+2
end;
for i:=1 to round(d_size/20) do begin
v[i]:=v[i]*(1-cos(10*pi*(i-1)/d_size));
end;
for i:=round(9*d_size/20) to round(d_size/2) do begin
v[i]:=v[i]*(1+cos(10*pi*i/d_size));
end;
i:=1;
for j:=1 to round(d_size/2) do begin
data^[i+1]:=v[j];
i:=i+2
```

```
end;

 j:=1;
 for i:=0 to n1 do begin
 with a^[i] do begin x:=data^[j]; y:=0.0; j:=j+2 end;
 end;

 j:=1;
 for i:=0 to n1 do begin
 with b^[i] do begin x:=data^[j+1]; y:=0.0; j:=j+2 end;
 end;

 reord1(a);
 trf1(a);
 reord2(b);
 trf2(b);
 for k:=0 to n1 do begin
  gx[k]:=gx[k]+mag(a^[k]);
  gy[k]:=gy[k]+mag(b^[k]);
  end;
  for i:=0 to n1 do begin
  conj(a^[i],q);
  prod(q,b^[i],g^[i]);
  with g^[i] do begin sumx[i]:=sumx[i]+x;
  sumy[i]:=sumy[i]+y end;
  end;
  end;
  for i:=0 to n1 do begin
  gxy[i]:=sqrt(sqr(sumx[i])+sqr(sumy[i]));
  theta[i]:=phase(sumy[i],sumx[i]);
  end;
writeln;
for k:=0 to n1 do begin
gx[k]:=gx[k]*(2*pase2/n)*1.14286*1/nsamp;
gy[k]:=gy[k]*(2*pase2/n)*1.14286*1/nsamp;
gxy[k]:=gxy[k]*(2*pase2/n)*1.14286*1/nsamp;
gamma[k]:=sqr(gxy[k])/(gx[k]*gy[k]);
 end;

   rewrite(txt,'V20:COHERENCE.TEXT');
   for j:=0 to round(n/2) do begin
   f:=j/(n*pase2);
   writeln(txt,f:9:6,'  ',gamma[j]:9:6);
   end;
   close(txt,'SAVE');
   rewrite(txt,'V20:FAZE.TEXT');
   for j:=0 to round(n/2) do begin
   f:=j/(n*pase2);
   writeln(txt,f:9:6,'  ',theta[j]:9:6);
   end;
   close(txt,'SAVE');
   end.
```

CONTOUR PLOTTING PROGRAM LISTING

```
C234567
      COMMON X(128), Y(255), Z(128,255), WORK(128,255)
      REAL   LOWEST,HIGHEST,XTICVAL,YTICVAL,SMOO,ADJ,DD,FRE,PASE
      REAL   FX, FY,XWINMIN,XWINMAX,YWINMIN,YWINMAX,AUTO
      INTEGER FXX,FYY,N,N1,N2,N3,N4
      REAL PENS(7),INCRE
      CHARACTER NAME*20,XTITLE*20,YTITLE*20,TITLE*20
      DATA PENS/ 1.0,2.0,3.0,4.0,3.0,2.0,1.0/
C*************************************************************************
C     THIS PROGRAM IS USING X AND Y ONE-DIMENSIONAL ARRAY TO DRAW
C     THE CONTOURS OF A FUNCTION OF TWO VARIABLES Z = F(X,Y), WHERE
C     Z IS DEFINED ON A RECTANGULAR MESH
C*************************************************************************
C
C     DEFINITION OF INPUT VARIABLES:
C     X[ ]        ONE-DIMENSIONAL ARRAY READ FROM DATAFILE
C     Y[ ]        ONE-DIMENSIONAL ARRAY READ FROM DATAFILE
C     NAME        DATAFILE NAME (USER INPUT)
C     FX          THE NUMBER OF "COLUMN" OF POINTS IN THE X DIRECTION
C                 AS WELL AS THE LEADING DIMENSION OF Z FUNCTION.(REAL)
C     FY          THE NUMBER OF "ROW" OF POINTS IN THE Y DIRECTION AS
C                 WELL AS THE SECOND DIMENSION OF Z FUNCTION.(REAL)
C     XWINMIN     USERS DEFINE THE X-AXIS MINIMUM WINDOW VALUE
C     XWINMAX     USERS DEFINE THE X-AXIS MAXIMUM WINDOW VALUE
C     YWINMIN     USERS DEFINE THE Y-AXIS MINIMUM WINDOW VALUE
C     YWINMAX     USERS DEFINE THE Y-AXIS MAXIMUM WINDOW VALUE
C     LOWEST      LOWEST CONTOUR LEVEL
C     HIGHEST     HIGHEST CONTOUR LEVEL
C     INCRE       CONTOUR INCREMENT VALUE
C     N           THE NUMBER OF CONTOUR LABEL INCREMENT
C     XTITLE      X AXIS LABEL
C     YTITLE      Y AXIS LABEL
C     TITLE       THE PLOT TITLE
C*************************************************************************
C234567
      PRINT*,'*****************************************************'
      PRINT*,'THIS PROGRAM IS USING TEMPLATE PACKAGE ROUTINE (UPCNTR)'
      PRINT*,'TO DRAW TWO-DIMENSIONAL CONTOUR LINES'
      PRINT*,'*****************************************************'
      PRINT*,'PLEASE ENTER DATA FILENAME'
      READ(3,'(A20)') NAME
      PRINT*,'ENTER THE MAX FREQUENCY'
      READ(3,*)FRE
      PASE=1.0/(2.0*FRE)
      OPEN(UNIT=122,FILE=NAME)
C
      N=512
      N1=N-1
      N2=N/2
      N4=N/4
C
      DO 1400 I=1,N4
      X(I)=0.0
      DO 1400 J=1,(N2-1)
      Y(J)=0.0
      Z(I,J)=0.0
 1400 CONTINUE
C
```

```
      DO 1510 I=1,N4
      X(I)=I/(N*PASE)
 1510 CONTINUE
      DO 1520 J=1,(N2-1)
      Y(J)=J/(N*PASE)
 1520 CONTINUE
      READ(122,*)((Z(I,J),J=I,(N2-I)),I=1,N4)

C
      PRINT*,'AUTO CALCULATION OF THE CONTOUR LEVEL OR NOT'
      PRINT*,'.1. FOR YES   ;  .2. FOR NO'
      READ(3,*)ADJ
C
      IF (ADJ .EQ. 2) THEN
      PRINT*,'ENTER THE LOWEST CONTOUR LEVEL'
      READ(3,*)LOWEST
      PRINT*,'ENTER THE HIGHEST CONTOUR LEVEL'
      READ(3,*)HIGHEST
      PRINT*,'ENTER THE CONTOUR INCREMENT VALUE'
      READ(3,*)INCRE
      PRINT*,'ENTER THE NUMBER OF CONTOUR LABEL INCREMENT'
      READ(3,*)N
      ELSE
      ENDIF
C     PRINT*,'ENTER THE PLOT TITLE'
C     READ(3,'(A20)')TITLE
C     PRINT*,'ENTER X-AXIS TITLE'
C     READ(3,'(A20)')XTITLE
C     PRINT*,'ENTER Y-AXIS TITLE'
C     READ(3,'(A20)')YTITLE
C     PRINT*,'DO YOU WANT TO USE THE DEFAULT DEVICE VIEWPORT'
C     PRINT*,'ENTER  .1. FOR YES  .2. FOR NO  '
C     READ(3,*)ADJ
      PRINT*,'USING AUTOSCALING OR NONAUTOSCALING FOR X-Y AXES'
      PRINT*,'ENTER  .1. FOR AUTO ;  .2. FOR NON AUTO'
      READ(3,*)AUTO
      IF (AUTO .EQ. 2.) THEN
       PRINT*,'PLEASE ENTER X-AXIS MINIMUM AND MAXIMUM WINDOW VALUE'
       READ(3,*)XWINMIN,XWINMAX
       PRINT*,'PLEASE ENTER Y-AXIS MINIMUM AND MAXIMUM WINDOW VALUES'
       READ(3,*)YWINMIN,YWINMAX
       PRINT*,'PLEASE ENTER  X AND Y AXES TICVALUES'
       READ(3,*)XTICVAL,YTICVAL
      ELSE
      ENDIF
C
      PRINT*,'DO YOU WANT CONTOUR LINES ARE SMOOTHED OR NOT'
      PRINT*,'.1. FOR YES ;  .2. FOR NO'
      READ(3,*)SMOO
C
      PRINT*,'DO YOU WANT CONTOUR PLOT IN 2-D OR 3-D'
      PRINT*,'.1. FOR 2-D ; .2.  FOR 3-D'
      READ(3,*)DD
C
      FX = N4 * 1.0
      FY = (N2-1)*1.0
C
      DO 10 I =1,N4
      DO 10 J = 1,(N2-1)
      WORK(I,J) = 0.0
 10   CONTINUE
C
```

```
      XMIN = X(1)
      XMAX = X(1)
      YMIN = Y(1)
      YMAX = Y(1)
      ZMIN =Z(1,1)
      ZMAX =Z(1,1)
C234567
      DO 20 I = 2, N4
       IF (X(I) .GT. XMAX) XMAX = X(I)
       IF (X(I) .LT. XMIN) XMIN = X(I)
 20   CONTINUE
C
      DO 30 J = 2, (N2-1)
       IF (Y(J) .GT. YMAX) YMAX = Y(J)
       IF (Y(J) .LT. YMIN) YMIN = Y(J)
 30   CONTINUE
C
      DO 32 I=1,N4
      X(I)=X(I)/FRE
 32   CONTINUE
C
      DO 35 I=1,(N2-1)
      Y(I)=Y(I)/FRE
 35   CONTINUE
C
      DO 40 I=1,N4
      DO 40 J=1,(N2-1)
      IF(Z(I,J) .GT. ZMAX) ZMAX=Z(I,J)
      IF(Z(I,J) .LT. ZMIN) ZMIN=Z(I,J)
 40   CONTINUE
C
C*********************************************
C
C     START TO USE TEMPLATE GRAPHICS
C
C*********************************************

C
      CALL USTART
C
C
C*********************************************
C     ADJUST AND OUTLINE THE DEVICE VIEWPORT
C*********************************************
      CALL UOUTLN
C
C*********************************************
C     PLOT THE X-Y AXES AND LABEL
C*********************************************
      CALL USET('ERROR')
      CALL USET('LARGE')
C
C
      CALL UPSET('XLABEL','X-Fx/FN\')
      CALL UPSET('YLABEL','Y-Fy/FN\')
      CALL USET('XBOTH')
      CALL USET('YBOTH')
C*********************************************
C
C     USING AUTOSCAL(1) OR OWNSCALE(2)
C
C************************************ 1
      CALL USET('XYAXES')
```

```
      IF (AUTO .EQ. 1.) THEN
      CALL USET('AUTOSCALE')
      CALL USET('BESTFORMAT')
C ---------------------------------- 2
      ELSE
      CALL USET('OWNSCALE')
      CALL UPSET('TICX',XTICVAL)
      CALL UPSET('TICY',YTICVAL)
      CALL UWINDO(XWINMIN,XWINMAX,YWINMIN,YWINMAX)
      ENDIF
C**************************************

C**** DRAW THE CONTOUR LINS FROM THE ORIGIN
      CALL USET('ORIGIN')


C**** CONTOUR SMOOTHING
      IF(SMOO .EQ. 1) THEN
      CALL USET('SMOOTH')
      ELSE
      CALL USET('NOSMOOTH')
      ENDIF
C**** MINMAX LABELS
      CALL USET('MINMAX')

C**** CONTOUR DIMENSION
      IF (DD .EQ. 1) THEN
      CALL UPOINT(0.0,0.0,1.0)
      CALL USET('2DOCNTOURS')
      ELSE
      CALL USET('3DOCNTOURS')
      ENDIF
C     CALL UPOINT(X,Y,Z)
C**** UNIFORMITY
      CALL USET('UNIFORM')

C**** VIEWING RESET OR NOT
      CALL USET('RESET')
C
C*****************************************
C     CONTOUR GENERATION AUTO OR USERS GIVE
C*****************************************
C
      IF(ADJ .EQ. 1) THEN
      CALL USET('CCONTOURS')
C +++++++++++++++++++++++++++++++++
      ELSE
      CALL UPSET('CLOW',LOWEST)
      CALL UPSET('CHIG',HIGHEST)
      CALL UPSET('CINC',INCRE)
      ENDIF

C**** CONTOUR LABEL INCREMENT
      CALL UPSET('CBOT', 0.0)
      CALL UPSET('CTOP', 0.5)
      CALL UPSET('CLABEL',FLOAT(N))
C
C***** CONTOUR ROUTINE ******************
C
      CALL UPCNTR(Z,X,Y,WORK,FX,FY,PENS)
C
C*****************************************
C
      CALL UEND
C ***************************************
      STOP
      END
```

APPENDIX B

UNCERTAINTY ANALYSIS

In order to determine the experimental uncertainties associated with measurements performed in this investigation, an analysis based on the method of Kline and McClintock (1953) was used. The following results were obtained

1. Uncertainty in setting the Reynolds Number

$$Re_b = \pm 3.6\%$$

2. Uncertainty in Mean Velocity Measurements

$$U = U \pm 2.5\%$$

3. Uncertainty in RMS Velocity Measurements

$$\sqrt{\overline{u^2}} = \pm 5\%$$

VITA

Huan-Chang Chu

Candidate for the degree of

Master of Science

Thesis: QUANTITATIVE MEASUREMENT OF NONLINEAR WAVE INTERACTIONS CHARACTERIZING THE TRANSITION OF A PLANAR TURBULENT JET

Major Field: Mechanical Engineering

Biographical:

Personal Data: Born in Taijung, Taiwan, August 11, 1958, the son of Chu Kaw-Fai and Fu Won-Chin.

Education: Graduated from National Fu Jung High School, Taipei, Taiwan, in May, 1978; received Bachelor of Science Degree in Mechanical Engineering from Chung Yuang Christian University in May, 1982; completed requirements for the Master of Science degree at Oklahoma State University in December, 1987.

Professional Experience: Assistant Engineer, Pacific Cable & Wire Company, Taipei, Taiwan, August, 1984 to December, 1984; Teaching Assistant, School of Mechanical and Aerospace Engineering, Oklahoma State University, January, 1986 to May, 1987; Research Assistant, School of Mechanical and Aerospace Engineering, Oklahoma State University, January, 1987 to June, 1987.